SOIL GEOGRAPHY AND LANDSCAPE GROUP

Department of ENVIRONMENTAL SCIENCES
WAGENINGEN UNIVERSITY AND RESEARCH

MSc thesis:
The effect of tools with different lithologies on erosion efficiency in Bedrock rivers

---

Author:
BSc. T.M.M. Koelewijn
930615452130

Supervisors:
prof. dr. D. Scherler
dr. J.M. Schoorl
MSc. R. van Dongen

Abstract

Digital elevation models of a mountain range in Parque Nacional Pan d'Azúcar (Chile) are used to examine the influence of tools with different lithologies and sizes on erosion efficiency. The slope-drainage area power scaling is investigated to see if channel incision is different in areas with dike intrusions that experience the same rate of uplift. The tools provided by the andesite-basalt dike intrusions are larger on average and less weathered compared to the granitic host rock. Plots of drainage area versus slope are difficult to analyze due to the large scatter of the data points. The CRS algorithm is used to smoothen the channels and this resulted in a significantly better slope-drainage area power scaling. On Average, trunk channel slopes are steeper at locations where dikes occur and the average channel steepness index is also significantly higher over the total length of trunk channels in areas where dikes are present. Mainly straight slope-drainage area relationships, inconsistent upstream channel head areas and relatively small catchment sizes in all areas are indicators that these channels might not be called alluvial bedrock channels. Instead, hillslope processes (debris flows and landslides) in combination with extreme precipitation events are more likely causes of forming the present channels. Hence, it is important to know on what spatial scale tools could have a significant effect on erosion processes.

Keywords: Tools, slope-drainage area, alluvial bedrock channel, hillslope processes

Table of Contents

1. Introduction

1.1. Problem Description

Landscapes are continuously changing by tectonically driven uplift and climate-modulation driven erosion processes. River incision is the driving force behind this continuously changing landscape (Howard, Dietrich et al. 1994). Important feedback mechanisms are involved in the dynamic system of tectonics and erosion that force the orogenic system toward a steady state (Willett and Brandon 2002). Rivers respond to changes in climate (e.g. stream discharge, hillslope sediment production), by changes in tectonics (e.g. changing gradients, base level changes) and also to variations in substrate (e.g. rock tensile strength), (Hancock, Anderson et al. 1998). The equilibrium between the rate of rock uplift and the erosion at every point in the landscape results in the adjustment of rivers to attain a certain geometry in space and time (Lavé and Avouac 2001, Wobus, Whipple et al. 2006, Kirby and Whipple 2012). The most well-known mathematical formulation of how people think bedrock rivers incise is the stream power incision model (Howard and Kerby 1983, Howard, Dietrich et al. 1994, Whipple and Tucker 2002). The steam power model (SPM) is a mathematical erosion rule that does not capture all the physical details of individual incision processes like abrasion, plucking, cavitation and corrosion. Instead, it combines these processes to end up with a lumped model that represents the overall dependence of river incision rate on local bed shear stress, metrics of rock strength and flood frequency (Whipple, DiBiase et al. 2013). In the past, research has been done to find correlations between drainage area and channel slope, but the effect of climate, sediment production rate and rock properties to predict the rate of river incision are studied less in field experiments. Sklar and Dietrich (1998) found problems when implementing a mechanistic theory for the effect of sediment supply in the stream power river incision law. They found that constant parameters are unlikely to be appropriate for the entire river network. Channels steeper than 20% are probably dominated by debris flows, while on gentle slopes the incision is inhibited because of the burial of bedrock by sediments. The latter, also known as the 'cover effect' was validated e.g in a field experiment in the Henry Mountains, Utah by Johnson et al. (2009). Future models require a cover term, since they found that alluvial transport and deposition can greatly reduce the efficiency of river incision into bedrock. Moreover, Sklar and Dietrich (2004) and Turowski et al. (2007) imply that there is an optimum bedload sediment flux, providing the tools for erosion by abrasion. If the sediment flux is too low, than the erosion is inhibited by a lack of tools and if the sediment flux is too high again the erosion is inhibited by too many tools, the mentioned cover effect. Interestingly, this dual role of sediment in river incision processes has already been recognized by Gilbert in 1877. However, the parameterization in models appears to be difficult and also little fieldwork has been done to measure and analyze this cover and tools effect. Sklar and Dietrich (1998, 2004) postulated that the tools effect could be captured with a linear dependence on sediment flux per unit width and the cover effect by a linear dependence on the ratio of sediment flux to transport capacity. The SPM predicts that rivers in steady-state landscapes (the uplift rate at every point in the landscape equals the erosion rate at that point) display "concave-up" longitudinal river profiles. From empirical data these river profiles can be described with a power-law relationship that relates local slope to the upstream drainage area, also known as Flint's law (Flint 1974).

The focus in this research will be on the possible change of erosional efficiency when tools are present in an unique setting that is formed by dike intrusions. Emphasis will be put on the delivery, size and lithology of the tools originating from these characteristic dikes. The expected difference in the presence of tools between the study areas and the effect this factor could have on river profiles will be investigated. Tectonic driven and climate-modulation driven erosion processes are assumed to be invariant over a sufficiently long time. Therefore, it is expected to find a power law relationship between slope and drainage area of the channels in the study areas. Possible differences in this power law scaling relationship could be found due to the supply of tools with a different lithology from the dike intrusions. Understanding the role these tools could have in erosion processes from this field experiment, combined with prior knowledge might be very useful in future landscape evolution

models to predict more precisely the rate and location of abrasion processes.

1.2. Background information

1.2.1. Bedrock Rivers

Bedrock rivers are actively incising channels through in-place rock over millennial to geologic timescales (Montgomery, Abbe et al. 1996). Bedrock channels are highly coupled to hillslopes, because the amount of sediments in a channel is dictated by hillslope processes that strongly influences channel slope, bed state morphology and also the rate of river incision (Sklar and Dietrich 1998, Sklar and Dietrich 2004, Johnson and Whipple 2007, Turowski, Lague et al. 2007). According to Howard (1998) bedrock rivers have a semi-continuous cover of coarse sediment that is alternated by pure bedrock. A subclass of bedrock rivers are mountainous channels with steep slopes, spatially limited floodplains and a direct connection with hillslopes (Wohl 2000). Since in mountainous channels slopes are steeper, episodic debris flows are a common occurrence. More specific, it has been found that channels steeper than 10%, with catchment sizes < 1-10 km^2, are traversed by debris flows more often (Montgomery and Foufoula-Georgiou 1993, Stock and Dietrich 2003). Due to these debris flows, channels normally covered by a thin layer of alluvium are swept clean and fresh rock is exposed which again can be weathered more rapidly (Whipple, DiBiase et al. 2013).

1.2.2. Topographic Steady State

To understand what the influence of lithology and the possible cover and tools effect could be on bedrock river incision and the evolvement of hillslope evolution during steady state, it is important to know what steady state really is. According to Montgomery (2001) there are several definitions of steady state. The relation between rock uplift and erosion determines whether a mountain range gains or loses elevation. Erosional steady state means no change in storage of material from the landscape. Tectonic steady state is the state in which the long-term rock uplift rate is constant. In literature the term 'steady state' is often used as the combination of both states described above and known as the topographic steady state. Accordingly, the topographic steady state means no net change in surface elevation due to a balance between rock uplift and erosion. The erosion is caused by the response of stream power to uplift. The stream power is the change in potential energy of flowing water over a given distance. The stream power [Ω] is the product of density [ρ_w] times gravity [g], discharge [Q_w] and the slope [S] and given by the following formula:

$$\Omega = \rho_w g Q_w S \qquad (1)$$

Dividing equation (1) by the width of the channel results in the unit stream power [ω]. The unit stream power is the energy available for entrainment and transport of sediment according to Bagnold (1973, 1977). The potential energy [E] is the driving force for erosion to occur and therefore incorporated in the generalized erosion rule. The generalized erosion rule is the product of the erodibility [k_e], a function of the sediment flux [q_s] and the function of the unit stream power [ω] and given by:

$$E = k_e f(q_s) f(\omega) \qquad (2)$$

The function of [q_s] describes the influence of tools and cover (eq. 3). Sklar and Dietrich (1998, 2004) postulated a formula that describes the dual role sediments have in river incision. The tools effect could be captured with a linear dependence on sediment flux per unit width [qs] and the cover effect by a linear dependence on the ratio of sediment flux to transport capacity [qs/qc] given by equation (3):

$$f(q_s) = q_s[1 - (q_s/q_c)] \qquad (3)$$

In a topographic steady state where the uplift equals the erosion rate and consecutively results in an unchanged surface level, the general formula is:

$$\frac{dz}{dt} = Uplift - Erosion = 0 \qquad (4)$$

A change in surface level [dz] is equal to zero over a period of time [dt]. Therefore, in topographic steady state the incision matches rock uplift or in other words erosion is equal to incision. Equation (4) becomes:

$$\frac{dz}{dt} = Uplift - Incision = 0 \qquad (5)$$

The general formula for incision [I] is:

$$I = KA^m S^n \qquad (6)$$

Equation (6) is known as the stream power incision model with (Howard, Dietrich et al. 1994); (Whipple

and Tucker 1999) in which [*K*] is the erodibility and a measure for erosion efficiency, [*A*] is the upstream area, [*S*] the topographic slope and [*m*], [*n*] are exponents.

If the surface topography does not change:

$$\frac{dz}{dt} = 0 \quad \rightarrow \quad U = I \quad ,$$

than equation (6) becomes:

$$KA^m S^n = U \qquad (7)$$

And can be rewritten to;

$$S = \left(\frac{U}{K}\right)^{\frac{1}{n}} A^{-\frac{m}{n}} \qquad (8)$$

The SPM predicts that rivers should obey a power-law scaling in a topographic steady state landscape. With $k = \left(\frac{U}{K}\right)^{\frac{1}{n}}$ and $\theta = \frac{m}{n}$ equation 7 is similar with scaling observations from empirical data for well-adjusted fluvial systems around the globe that yield the following slope-drainage area scaling (Flint 1974):

$$S = k_s A^{-\theta} \qquad (9)$$

Where $[k_s]$ is known as the channel steepness index and $[\theta]$ as the concavity index. According to Gilbert (1877) concave rivers are the general form in an erosional steady state landscape because of the compensating behavior of the slope when the discharge increases moving downstream. If the effective rainfall is uniform in the catchment, the area is a proxy for the discharge. For well-adjusted fluvial systems around the globe the concave rivers yield the stream power law scaling assuming uniform uplift rates and erodibility. It is stated that a lot of factors are hidden in this simplified scaling of the slope against the drainage area. The k_s is composed of the erodibility k_e (lithology, weathering, jointing, bedding etc.), ρ_w (density of water), g (gravity), the sediment flux function $f(q_s)$ (equation 3), k_q, k_w (basin hydrology, climate), *n* (erosion processes on channel bed, *U* (rock uplift). Moreover, the θ is composed of *m* (basin hydrology, climate) and *n* (erosion processes on channel bed). When for a catchment the slope of the channel is plotted against the drainage area, in a topographically steady state landscape, a hypothetical linear relation exist on a loglog scale. The slope of the line represents the profile concavity index (θ) and the y-intercept the channel steepness [k_s]. If the cover or tools effect has a significant effect on erosion processes, how would this be visible in the slope-area relationship? It could be that this effect is visible by a different slope of the slope-area relation, indicating a higher or lower value of the concavity index, resulting in faster or slower erosion. On the other hand, the line might shift in its total up- or downwards, indicating a change in channel steepness, resulting in a change in erosion.

1.3. Research Objectives

The objective of this research is to investigate the effect of tools on erosion processes using data from a field site in the south of Pan d'Azucar, Chile. Knowledge about the role of sediments from field observations will contribute to the understanding of landscape evolution and how models can be validated or even improved. The power-law scaling will be used to see if the cover or tools effect is visible in the slope area graphs of incising channels in an assumed topographic steady state landscape. An extensive approach to actually measure the erosion rates and uplift in the field between the different areas lies beyond the scope of this research project. Instead, the approach of this research is to make aerial photographs to create Digital Elevation Models (DEM) that will be used to compare areas that are provided by different amounts and lithologies of tools. By comparing the effect of tools on slope-area relationships from a DEM, useful information can be found about sediment control on the bedrock erosion rate.

1.4. Research Questions

What is the effect of tools on the erosion efficiency in an arid climate and can this effect be derived from the slope-drainage area power-law scaling?

In order to answer this main question the following sub-questions are identified:

1. What are the grain sizes and lithologies of the tools in the areas with abundant dikes and no dikes?
2. Does the size of the dikes influence the provision of tools and consequently the relationship between slope and drainage area?
3. If a difference in erosional efficiency caused by the presence of dikes exist, how is this effect reflected in the start of channel incision i.e. the upstream areas?

2. Description of the case study areas

2.1. Location and Field Observations

The study area is located south of Parque Nacional Pan de Azúcar, 10 km land inwards of the city Chañaral, Chile (26°19'52.83"S, 70°29'16.31"W). The area, geologically known as the Cerros del Vetado pluton, is formed by a S-type Permo-triassic intrusion into the Paleozoic Chañaral metamorphic complex (Berg and Baumann 1985). Nowadays this is visible as whitish to reddish granitic mountains in which dark andesite-basaltic dike swarms crisscross through the landscape, figure 1. According to Bell (1987) the dike swarms intrude the Vetado pluton, see Appendix I. The granitic Vetado pluton is formed in late Triassic and the dikes are formed in Jurassic 155 Ma years ago. The total Vetado pluton is about 10 km² with the highest point at 996 m above sea level (Berg and Baumann 1985). Small channels are present in the areas as well as numerous of the aforementioned dike intrusions. To investigate if there is a link between these two characteristic features, we chose to select four areas that are assumed to be representative for the total study area. The four selected areas consist of; A) an area without dike swarms and small boulders B) an area with dike swarms and large boulders C) an area without dike swarms, but with large boulders and D) an area with dike swarms and large boulders, see figure 1. Area A and C are comparable in having no dikes, but differ in the presence of large boulders. Area B and D are similar in having dike intrusions and large boulders in the channels. Area B and C are closer to the sea, with their mountain top at a lower altitude and with some of the mountain slopes covered by aeolian sand deposits. In Appendix II the wind rose of Chañaral is given and shows the yearly windspeed and -direction based on historical archived and calculated weather data (Meteoblue). The data shows that most often the wind has an ENE and SWS orientation with the heaviest wind speeds reaching 28 km/h on average in July. These areas are selected to investigate if rock size and lithology of rocks found in the channels affect the channel erosion. Field observations about the effect of floodings in due to extreme precipitation events in the Salado River basin the made by Wilcox et al. (2016) are comparable to the channels that were found in the investigated study areas for this research. Though the very small rills were absent, the small linear gullies that faded near the foot slope are common features especially found in study area 2 with dikes, see figure 1B. Almost no vegetation was present, only some individual shrubs were growing in the gullies and in the valley fills. The dike intrusions were most often found at the higher locations in the landscape.

Figure 1. Study area A: No Dike 1, B: Dike 2, C: No-Dike 3, D: Dike 4.

2.2. Climate

The region of the studied areas has a desert climate with an annual rainfall of only 15mm. The average annual temperature is 20.1 °C which varies by 7.5 °C. According to Köppen and Geiger this climate is classified as BWh (climate-data.org). The study areas are located close to the sea and aeolian deposits are found in the valleys and on mountain slopes. For this research, areas with these aeolian cover sands are excluded, because that would influence the bedrock channel profiles.

2.3. High Precipitation Event

In March 2015 an unusual high precipitation event over a period of only 48 h from March 24 to 26 resulted in a catastrophic flooding (Wilcox, Escauriaza et al. 2016). The nearby city of Chañaral was covered by several meters thick mud deposit. Heavy precipitation events, such as the one that occurred in March 2015, are presumably very rare, as it was the largest one that has ever been recorded in this area (Wilcox et al., 2016). The cause for this extreme precipitation event is a cutoff low-pressure system that moved inland (Barrett, Campos et al. 2016). The high precipitation resulted in high sediment concentration flows due to sediment delivery by landslides and debris flows. Similar sediment rich flows have been investigated in the past for less extreme precipitation events in the Atacama region, (Sepúlveda, Rebolledo et al. 2014).

In figure 2 the Salado river basin is shown with the satellite based spatial distribution of the precipitation measured during the March event and shows that the study area (red box in figure 2) lies into the Salado river basin. Though the highest precipitation intensity was measured more land inwards, the area might also have been hit by this event. Observations by Wilcox et al. (2016) showed widespread rilling and gullying initiated by overland flow on hillslopes: “The rills were shallow, linear features showing no consistent spacing or a clear initiation threshold. Sediment from these sources did not reach valley bottoms; rills and gullies typically faded near the base of the hillslopes (i.e., at the footslope).” They concluded that the mass wasting from these rills and gullies appeared to be a negligible source of sediment to the fluvial sediment flux and that most sediments came from the valley fills. The last large flood occurred on the Salado River in 1972 (Desinventar.org), unfortunately little is known about other past flood events. Though little is known about these intensive precipitation events in our study area, it is known that in other regions in the Atacama desert these events occur more often. According to Zhou and Lau (1998) and Magiligan et al. (2008) most flooding events are associated with the South American summer monsoon and with El Niño.

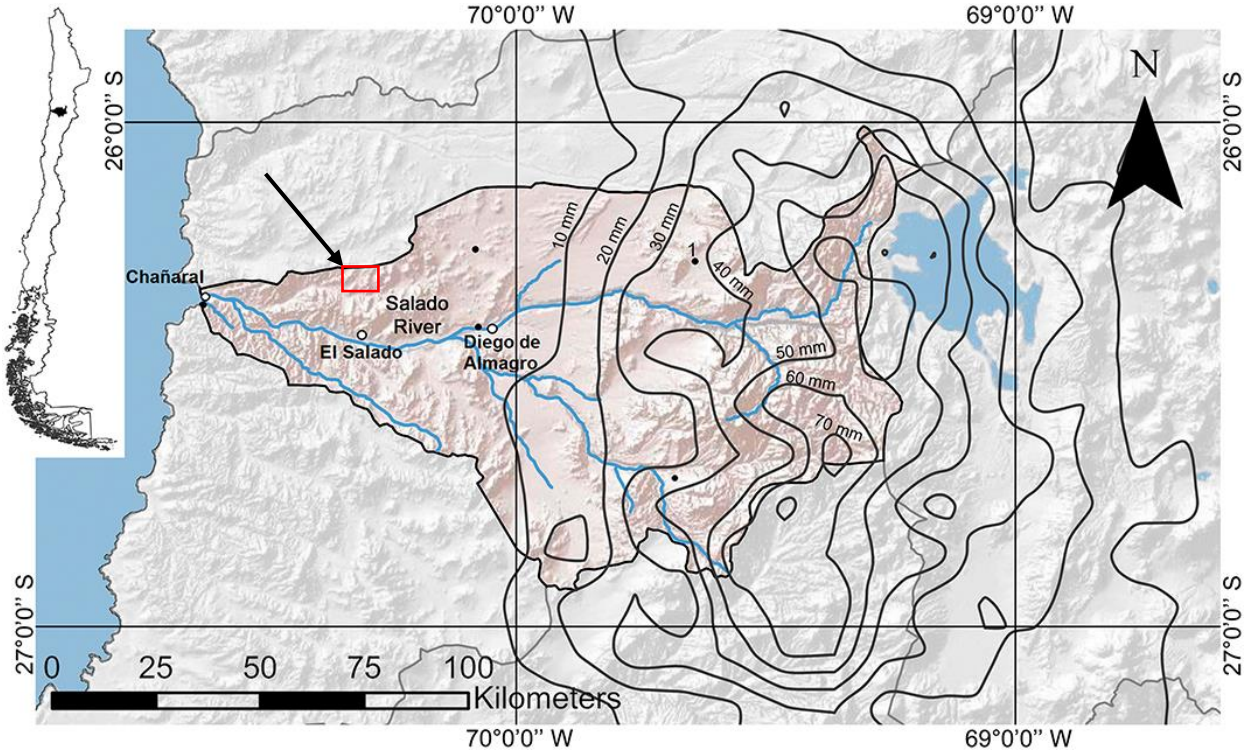

Figure 2. From: Wilcox et al. 2016. Map of the Salado river basin in the Atacama desert with satellite-based isohyets showing the spatial distribution of precipitation in mm, from Huffman et al. 2015).

3. Data Description

3.1. High Resolution Topography (HRT)

A survey was conducted with a drone that is useful in creating HRT data for answering the research questions of this research. The spatial extent for each study area separately is about 0.3 km². We assume that a point density of around 500/m² will be sufficient. Since we look at channels that have a width in the order of 0.5-3m we want to have a high georeferenced accuracy and a small footprint. The vegetation penetration as well as the ability to penetrate water to acquire the bathymetry do not apply, since the vegetation in the areas is negligible and there is no water present in the surrounding areas. For this research it is not useful to use coarse spatial resolution data which is available by e.g. Shuttle Radar Topography Mission data (SRTM). This SRTM data, with a spatial resolution of typically 90 to 30 m, does not capture the channel beds present in the study area and elevation changes caused by e.g. the dike intrusions. Therefore, the photogrammetric technique by structure from motion (James and Robson 2012) with an Unmanned Aerial Vehicle (UAV) is used to create a high resolution DEM. This method is relatively easy to carry out, light weight, cost efficient and useful for places in the study area that are hardly accessible by feet. We used a common UAV i.e. the Phantom DJI 3 professional. It has a 12 Megapixel camera and a lens with f/2.8 and a field of view of 94°. The 3 axis camera made photographs, while the drone was kept still at one place, to make photographs in four directions (N-E-S-W). The Inertial Measurement Unit (IMU) records and relays the smallest changes in tilt and movement and compensates for that automatically. This made it even possible to fly during strong winds. With the use of a remote controller connected to a tablet and the DJI GO app it was possible to localize and track the path of the drone while flying.

3.2. Georeferencing

Ground targets were placed for georeferencing the drone data to the UTM coordinate system. Also, these ground target points are used to investigate the internal accuracy of the DEMs. Therefore, A4 papers were placed on the surface that were visible from the sky and served as ground control points (GCP's). A hand-held GPS was placed exactly on the middle of the targets. The average coordinates were calculated over a time interval of 3 minutes to increase the accuracy of the ground target positions. Besides the GPS coordinates also the distance between the GCP's was measured with a laser beam. This laser beam calculated the horizontal, vertical and slope distance between the laser and a reflector placed exactly at the same height as the laser on top of the middle of another target. These distances are used as a double check to analyze the possible mismatched resolution and differences in altitude. The lengths measured with the laser beam between the targets are imported in the program Agisoft Photoscan Professional.

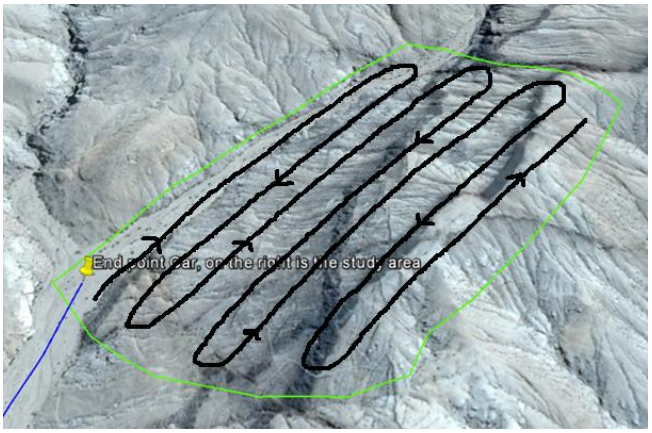

Figure 3. Example of optimal path for drone flight plan in area 2.

3.3. Drone Flight

Flights were started in the morning when there was less wind in the area, around 13:00 UTC. The best pattern for the drone that was used to fly is shown in figure 3. Flying a continuous path perpendicular to the hillslope, improves the photo alignment in Agisoft Photoscan due to the fact that the overlap between the pictures is increased and the drone is kept more stable when flying in steps horizontally. Besides, battery life is longer when the drone is displaced vertically less frequently. The drone pilot was standing halfway the hillslope to capture the lower half of the mountain slope and on top to capture the upper half. Also, to capture the total mountain ridge and the highest points, extra photos were taken at the borders to be sure to capture the total catchment contributing area(s). With the DJI GO phantom 3 app on the tablet the path of the drone was tracked while flying. At a height of around 20 m the drone was kept still every 10

meters horizontally to take pictures in four directions (North, East, South and West) by turning the drone and camera. The total path has been flown twice. The first time the camera position was oblique under an angle of around 30 degrees from the vertical. The second time only one picture every 10m horizontally was taken with a camera angle of zero degrees (vertical).

Table 1. Tasks and settings Agisoft Photoscan for DEM creation

	Task	Settings
1.	Create chunk and add photo's	Canon photos 1/2000 sec. f/2.8 3.61mm
2.	Align photos	Highest alignment, disabled
3.	Create dense cloud	Lowest, aggressive
4.	Add markers with coordinates	10 - 35
5.	Build mesh	Automatic
6.	Build texture	Automatic
7.	Create DEM	Automatic
8.	Add laser beam distances	Only slope distances (m)

3.4. Point Cloud Processing

The aim is to create a DEM that can be used in Matlab for analyzing topographic attributes such as slope, curvature and channel heads. To accomplish this the photos taken with the drone were processed and aligned with the program Agisoft Photoscan Professional. The program connects aerial photographs based on their x, y and z coordinates. For all 4 studied areas the same approach was used for the photo alignment i.e. by changing the settings that determines how rough or precise the program connects the photos. The amount of pixels per m² is based on the amount of photos, the quality of the photos and the overlap between the photos. A point cloud is the result of localizing and connecting all the used photos by recognizing similar pixel color -and geolocation information. In table 1, a summary is given of the steps and settings how the DEMs are created. The GCP's that were placed in the field on the surface, are used as markers. A marker on every image, on which there are targets visible, was added to assign the correct predetermined target number with its GPS coordinates. Next, the program is able to create an improved dense point cloud by aligning the photos again with the selected markers. Not all markers were used for photo alignment but also for error modeling which will be further explained in section 5.3. After creating the dense point cloud with the added markers you are able to check how the DEM changes when correcting with the GPS coordinates. The performance of the model can be validated by adding the distances measured with the laser beam that gives the error between calculated and measured distance.

3.5. DEM Uncertainty

Digital elevation models are created in the attempt to represent the real Earth surface by a gridded dataset. The DEM is an end product of a processing chain that involves data acquisition, interpolation and filtering operations, post-processing and georeferencing (Fisher and Tate, 2006). Assumptions and analytical uncertainties in each chain propagates in the final DEM and therefore also in DEM-derived products like river profiles. Schwanghart and Scherler (2017) found that especially artifacts in valley bottoms and overestimation of river elevations in steep topography in globally available DEMs cause a lot of uncertainty and a bad representation of the real world. Therefore, to characterize data uncertainties Schwanghart and Scherler (2017) created a new approach containing quantile carving and the CRS (constrained regularized smoothing) algorithm. This approach is able to reduce the elevation bias and errors in longitudinal river profiles. Moreover, this nonparametric approach is a free-form solution that uses as many parameters as there are elevation values. In other words, the river profile does not take a predetermined shape by using a model with fixed parameters. Common smoothening approaches use a running average and local regression in combination with flow enforcement. This new approach combines flow enforcement and smoothing, avoids drawbacks (increasing river profiles in downstream direction) and is more robust to outliers. The CRS algorithm is used to filter out noise that influences slope-drainage area relations.

3.6. Pebble Count

A Wolmann pebble count was carried out to test the spatial variability of the different grain sizes and lithologies of rock fragments in the four areas. In all four areas two or three channels were chosen to determine the size and lithology of randomly selected

grains. More channels were analyzed in areas in which the channel lengths were smaller to compare equal datasets. According to the pebble classification scheme the different sizes were assigned to a category, see table 2. With Rstudio the results were statistically tested with ANOVA to see if a significant difference exists between rock size, lithology and study area.

Table 2. Wolman Pebble count classification scheme

Size Class	Size Range (mm)
Bedrock	0
Sand	0 - 2
Very Fine Gravel	4 - 8
Fine Gravel	8 - 16
Medium Gravel	16 - 32
Coarse Gravel	16 - 32
Very Coarse Gravel	32 - 64
Small Cobble	64 - 90
Medium Cobble	90 - 128
Large Cobble	128 - 180
Very Large Cobble	180 - 256
Small Boulder	256 - 512
Medium Boulder	512 - 1024
Large Boulder	1024 - 2048
Very Large Boulder	2048 – 4096

4. Processing data

4.1. Topotoolbox

A useful set of Matlab functions for the analysis of geomorphology and hydrological processes in a non-Geographical Information System environment is TopoToolbox (Schwanghart and Kuhn 2010). According to Schwanghart and Scherler (2014) this novel technique is fast and memory efficient for the analysis of DEMs and the related calculation of flow directions and stream networks. TopoToolbox has improved the 3D visualization of matrices and therefore it is useful for the interpretation on how channels incise into the landscape by deriving the stream network from flow accumulation patterns.

4.2. Geonet

Another tool used for this research that is specialized in the extraction of channel heads from HRT data is Geonet 2.2 (Passalacqua, Tarolli et al. 2010). Other than previous methods this extraction tool combines nonlinear filtering of elevation data, a statistical analysis of curvature and geodesic minimization principles (Sangireddy, Stark et al. 2016). According to the authors especially the exclusion of the pit filling operation and avoiding the strict use of a flow accumulation threshold, are important improvements that have been used in classic channel network extraction work-flow applications. Therefore, a combination of both tools is used to do the stream network analysis.

4.3. Stream Network Analysis

The data processing for the stream network analysis contain the following steps;

1. *Preprocessing DEM from Agisoft*

With Agisoft photoscan the raw DEMs are created that further will be used for this research. Since the DEMs contain small errors when generating a stream network, this data needs to be preprocessed. In Topotoolbox the DEM can be imported and with the FLOWobj algorithm the flow direction can be derived. The flow direction can be determined after the DEM has been 'filled' or 'carved'. With the carve function you can, instead of finding the best path through the centerlines of flat sections with the filling option, find the path that runs towards the deepest part (the valley) through local depressions known as sinks. First the sinks are filled. Next, the difference with the filled level and the deepest point of the sink in the original DEM and the sill are identified. The sill is the point where the depression or flat terrain spills over into the even lower lying terrain. Eventually the total path network is created based on the minimum lengths between pixels on a grid with the Gray-weighted distance transform (GWDT) (Schwanghart, Groom et al. 2013).

2. *Determination of channel heads*

With Geonet is determined where in the catchment, channels start to incise. The Geonet method uses three steps in finding the best locations of the channel heads. These steps are i) nonlinear filtering of the digital elevation data, ii) the identification of likely channelized pixels through the statistical analysis of curvature and iii) the channel heads and channel network extraction based on geodesic minimization principles (Passalacqua, Belmont et al. 2015). These channel heads are further

used to calculate the total upstream area and if present also the area covered with dikes of this upstream part of the catchment.

3. *Combine channel heads with stream network*

It was not possible to import the smoothed DEM from Geonet to Topotoolbox. Only the channel heads could be extracted. Therefore, to do a further analysis with the calculated channel heads from Geonet, by using Topotoolbox in Matlab, we need to combine the stream network of both extraction methods. However, Geonet uses a slightly different approach to filter the DEM for channel network and channel head calculation compared to Topotoolbox. It appeared that the derived stream networks are slightly different and consequently some channel heads do not lie on the drainage network. The snap2stream tool from Topotoolbox is used to calculate the nearest point on the drainage network to the channel heads. These new locations on the drainage network are used as channel heads. By measuring the distances between the channel head from Geonet and the drainage network from Topotoolbox the further use of Topotoolbox is validated, see section 5.4.

4. *Smoothen the river profiles*

The carving method is used to calculate the channel network. However, instead of using the carved data, the raw unfiltered data (that lies on the location of carved channel network) is smoothed by the CRS algorithm and used for the calculation of the slope-drainage area relation. The CRS algorithm (Schwanghart and Scherler 2017) is used to smoothen channel profiles to get rid of small wiggles and errors that could influence the slope area plot a lot. Wiggles could be created by relatively large boulders and rock fragments lying in the channels. Positive slopes that create sink holes can now be filtered out. By changing the K-parameter in the algorithm you can dictate the degree of smoothing. For this research three values for this parameter were used to see the effect of this smoothing. The used values are; i) K=0 no smoothing, ii) K=500 for the exclusion of small wiggles and iii) K=10000 for a smoothing that roughly reflects the general channel profile.

5. *Find slope-area relationship*

The channel heads are used to find the transition from hillslope processes to alluvial bedrock channels. Namely, as indicated before, to test if the slope-drainage area power law scaling is affected by the supply of pebbles and boulders from the dikes, we need to know where the channel incision starts. When knowing the channel heads, the channel profiles, catchment sizes and the presence of dikes, it might be possible to analyze if this slope-drainage area power law and to investigate if differences in this relation are perceptible and can be related to the different study areas.

4.4. Dike Extraction From Orthophotos

With ArcGis two methods were used to extract the dikes from the orthophotos, exported from Agisoft, based on the RGB color information. The first method used for area 4 is the Supervised Image Classification with the following approach:

- First, you have to create small polygons in areas which you are certain of that have a basaltic lithology. The same is done for areas that certainly are granites. These polygons act as signatures and can be used to assign a code to every other pixel on the orthophotos.
- This is done with the Maximum Likelihood Classification tool. Every pixel has given a value, depending on the amount of signatures you create. For this research only two signatures are used.
- The Boundary clean and Aggregation tool were used to filter and resp. fasten the processing time of the map, but mainly to create larger cells with a single code and filter out little noise.
- The Group Region tool creates a map with all clusters of the same type. Now all cells are connected to neighboring cells if they have the same signature.
- The Set Null tool is used to filter out small cluster cells that represent small bushes and plants. Eventually all clusters of cells that are basalts get the same codename as well as all the granites ending up with a binary map. By setting the number of cells inside a cluster you can determine how large the objects are on your map you want to remove depending on the spatial resolution of you map.

This method only works if you have an orthophoto without a lot of dark pixels created by shades. Therefore, for area 2 an alternative method is used to extract the dikes from the picture, because of the negative influence of shades. This simplified method is just a manual version of the one described above:

- First, you have to draw a polygon very precise around all the dikes. Since the dikes are well distinguishable from the granites this method is assumed to work fine without a lot of errors, though it is more time consuming. Eventually you also create a map with 0's and 1's that stands for granites and basalts respectively. This map has further been used to determine the area of dikes in sub-catchments.

5. Results

5.1. Pebble Count

For every area, two or three channels in the same order of length, were investigated to get equal datasets. The results of the pebble count analysis for the individual channels are added together by study area, figure 4 a-d and figure 5. In total four different rocks were found in the areas. These rock types are 1) granite 2) andesite-basalt 3) fine diorite and 4) a more clustered type of granite also found as small dike intrusions, indicated as granite2. The amount of fine diorite was very minimal and local. Therefore, not representative for the whole area and not further taken into account. Clearly, the highest percentages for bedrock at the surface was found in area two and four in which dikes are present, see figure 5. Also it appears that in general the average size of the pebbles and boulders are higher in areas with dike intrusions. More rocks with a andesite-basaltic lithology were found in the two study areas in which dikes are present. To test if there is a significant difference in rock size and lithology between the four areas an ANOVA test is carried out. Before an ANOVA test can be done, the results have to be checked for normality. Transforming the data, by taking the logarithm of the pebble counts, the data appeared to be normally distributed (skewed to the left) and an ANOVA was executed. First an ANOVA test is performed for the whole dataset. The results show that there is a significant difference in rock size between the two areas without dikes and the two areas with dikes, since the p-values are <0.05. However, a Tukey test shows that between area 2 and 3, no significant difference exists in rock size (p-values of 0.21 i.e. >0.05).

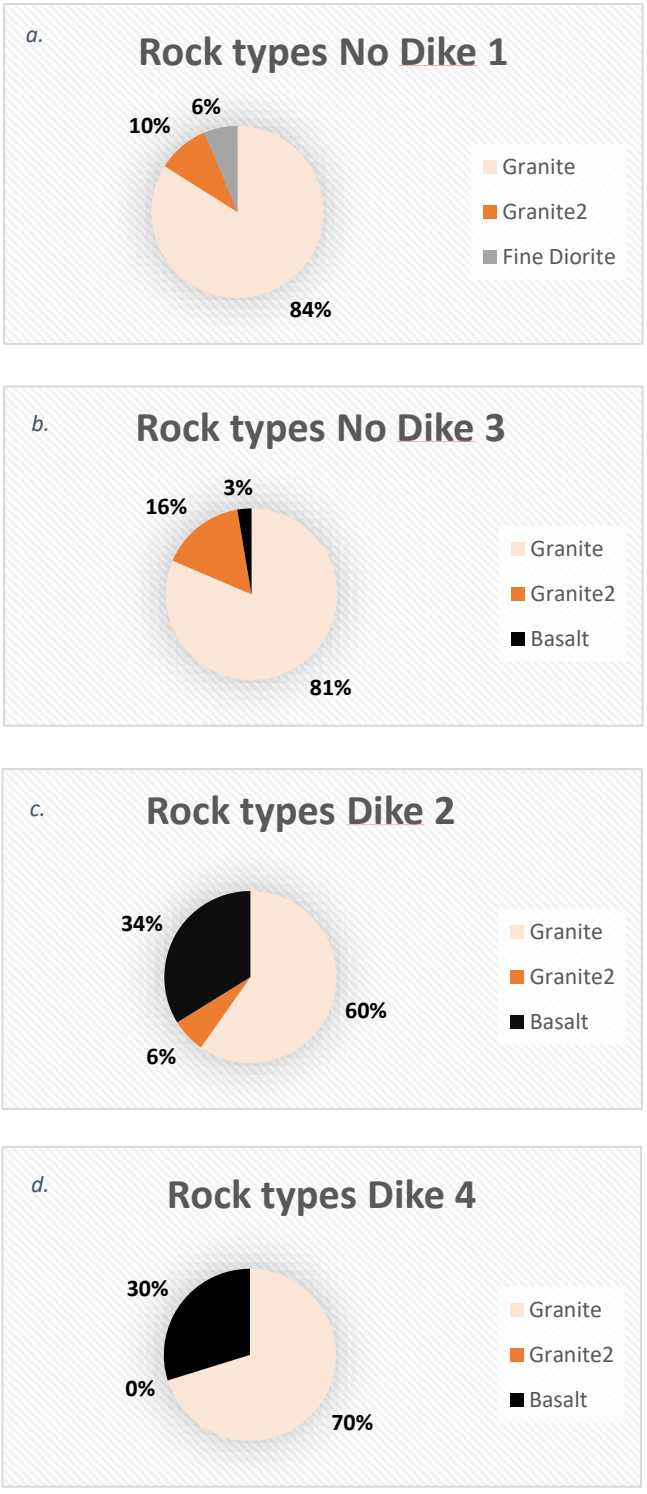

Figure 4. Circle diagram indicating the rock distribution in percentage for a. area 1, b. area 2, c. area 3 and d. area 4.

In area 4 the average rock size is significantly larger than in all the other areas, also between the two areas (2 and 4) with dikes.

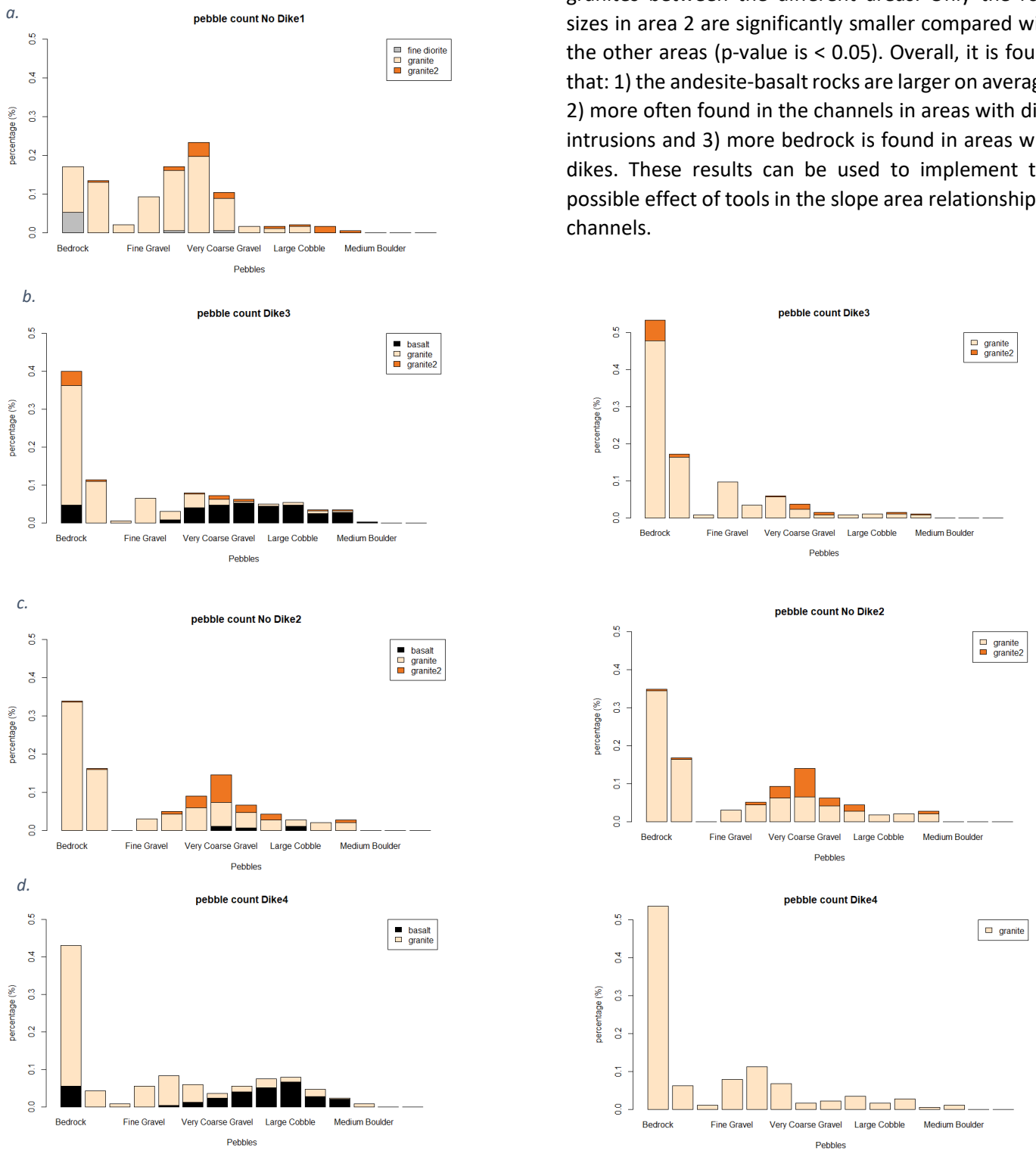

In addition, the results show that the granitic and the andesite-basaltic lithologies are significantly different from one another with the basalt having a larger rock size on average. The same test is performed but with excluding all the andesite-basalt from the data to see if there are differences in rock size only with respect to granites between the different areas. Only the rock sizes in area 2 are significantly smaller compared with the other areas (p-value is < 0.05). Overall, it is found that: 1) the andesite-basalt rocks are larger on average, 2) more often found in the channels in areas with dike intrusions and 3) more bedrock is found in areas with dikes. These results can be used to implement the possible effect of tools in the slope area relationship of channels.

Figure 5. Pebble count on the left figures including andesite-basalt and on the right figures the exclusion of andesite-basalt, a. area 1, b. area 2, c. area 3 and d. area 4.

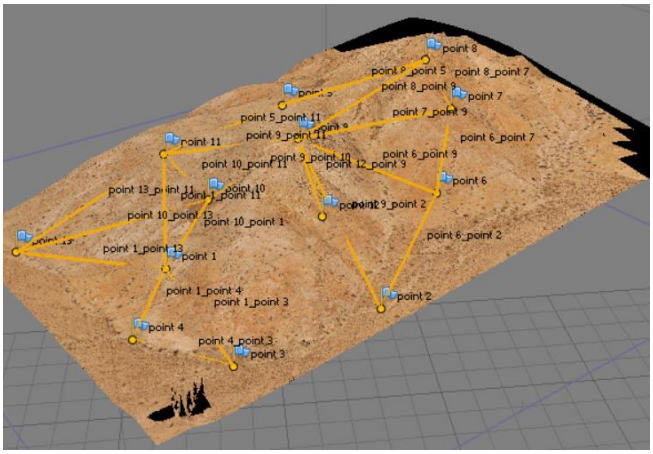

Figure 6. Build texture of area 1 in Agisoft Photoscan, yellow lines indicate measured distances between targets (blue).

Table 3. Errors given for the marker position and distance of measured laser beam.

Study Area	1	2	3	4
1. Cell size ver. (m)	0.13	0.14	0.26	0.16
2. Cell size hor. (m)	0.13	0.14	0.26	0.16
3. Rows (cells)	2871	4254	2956	2707
4. Columns (cells)	2822	3896	2918	2763
5. Total area (m^2)	$6.4e^4$	$1.5e^5$	$3.8e^5$	$8.9e^4$
6. Markers	13	33	14	12
7. Marker error (cells)	6.4	14.4	3.0	4.3
8. Scale bar error (m)	0.24	0.33	0.19	4.04
9. Average distance between markers (m)	57.38	57.78	99.31	146.74

5.2. Agisoft Photoscan – Laser Distance

In table 3 the error is given between the measured slope distance with the laser beam and the calculated distance from Agisoft based on the geolocations of the combined photos. Figure 6 is the meshed grids of area 1 in which the slope distances area drawn by yellow lines between the marker points (Appendix V for other areas). For Area 1, 2 and 3 the average error in meters is less than 0.33 m, but for area 4 this error is 4.3 meters. Unfortunately, only 3 markers in area 2 could be used to investigate the error between these points. Agisoft aligns the photos and determines where on the overall point cloud the marker will be. In table 3 also the errors (in pixels) are given for the individual markers. The error shows the averaged distance error between the location of that marker after the alignment of all the photos on which the marker is visible and the location of the marker on a specific photo.

By summing up all the errors of all the markers it shows that the average errors are 0.84, 2.01, 0.77 and 1.08 meters for area 1-4 resp. For this research it is not necessary that all the markers have exactly the right projection, but the main focus is on the right scaling distance. Overall, the small values of the average horizontal scale bar errors (m) indicate that the measured distance almost equals the distance between the points after Agisoft has aligned all the photos, calculated the location of the markers and the corresponding distances between them. Unfortunately the vertical distances could not be compared, the vertical distances calculated by the hand-held GPS was not trustworthy and consistent. The measured scale bar errors are less than 0.5 meter, but > 4 meter for area 4. Though, highest distances between the targets were measured in area 4 as well. Because the errors in distances between the markers are low, the DEMs are useful in further stream channels analysis. The results of the stream channel analysis with Topotoolbox and Geonet are given in the next sections.

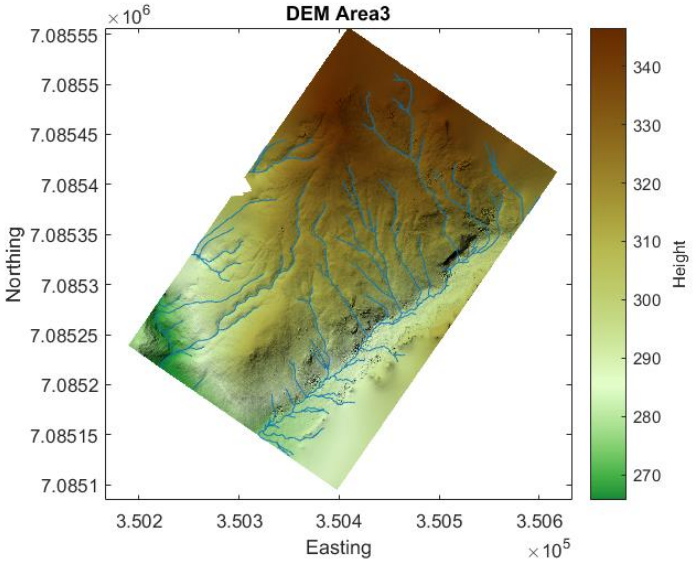

Figure 7. DEM with stream network from study area 1.

5.3. DEM resolution

The DEMs are created from the point clouds in Agisoft Photoscan and exported to Matlab, see figure 7. In table 3 the resolution is given for the four study areas. The pixel sizes are 0.13 by 0.13, 0.14 by 0.14, 0.26 by 0.26 and 0.16 by 0.16 m. for area 1-4 resp. The pixel sizes are not the same among the study areas due to a difference in amount of points calculated by Agisoft Photoscan. The pixel size of area 3 is almost twice as

high as compared to the other study areas. Therefore, the possible effect that a different pixel size could have on slope-area relationships is further investigated in section 5.5. To test if the sub-catchment areas are different among the four study areas, an ANOVA is carried out. The mean sub-catchment areas are $1.5e^3$, $5.1e^3$, $3.8e^3$ and $3.3e^3$ m² for study area 1-4 resp. There is not a statistically significant difference between the areas as determined by an ANOVA $F(3, 26) = 2.862$, $p = 0.0561$. However, a post hoc Tukey test showed that the sub-catchment areas in study area 1 are significantly smaller from the sub-catchment areas in study area 2 at p=0.038, see also the boxplot in figure 8.

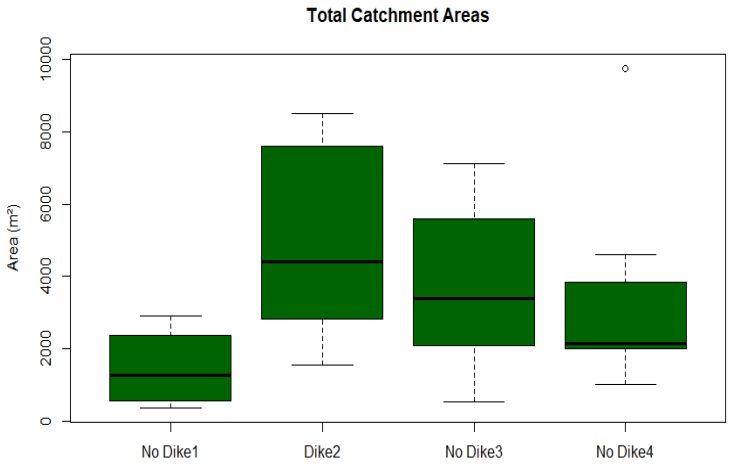

Figure 8. Boxplot of total sub-catchment areas in the four study areas.

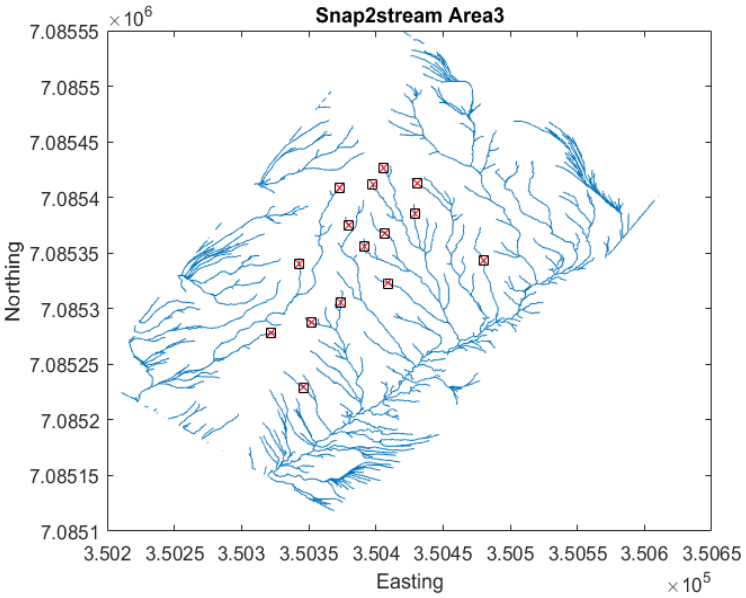

Figure 9. Snap the channel head from Geonet to flow network of Topotoolbox.

5.4. Flow Accumulation and Drainage Network

In this chapter, the results from the DEM creation in Agisoft and processing of the data in Topotoolbox and Geonet are described. The created DEMs (figure 7, Appendix VIa)) have been exported to Matlab and processed by Geonet to come up with the locations of the channel heads. A selection of channel heads is made to only have the ones higher up in the landscape and not the ones that start too close to the valley. The flow accumulation threshold in Geonet was set to 3000 pixels. This threshold is used to find channel heads above a contributing drainage area of 3000 times the squared cell size. Since the cell sizes differ, this threshold is not the same for every area. For area 1 the flow accumulation threshold value is equal to 50 m², while in area 3, with the highest cell sizes, this threshold is already 200 m². In study area 3, the cell area is four times greater than in the other areas. Therefore, the threshold value for the flow accumulation, to search for channel heads, was set to a lower value. Since the program gave errors for the channel head calculation with the use of flow accumulation thresholds lower than 1000, this value of 1000 was used for area 3. Channel heads starting close to the valley are expected to have small channel lengths that results in little data points and makes the analysis of the slope-drainage area relationship difficult. Besides, the attempt is made to select channels with the same channel lengths to facilitate the comparison between the four areas. These channel heads were exported to Topotoolbox to analyze the channel profiles from valley to channel head. In Topotoolbox the DEMs are carved to get rid of pits and sinks to create a connected flow accumulation. The threshold value of the flow accumulation was initially set to a relatively low value (e.g. 500 pixels) to create a dense drainage network with a lot of small tributaries. Just like setting the flow accumulation threshold in Geonet a higher value of 3000 or even 4000 was sufficient to create a less dense channel network that still captures all the calculated channel heads. Although the pixel size determines the threshold value and consequently the density of the drainage network, this does not affect the channel lengths that are investigated. Since, only the trunk channel from channel head (from Geonet) till outlet is analyzed, without taking tributaries into account. This threshold

value is only used, and adjusted manually among the areas, to be sure that the calculated channel heads match the stream network created by Topotoolbox. With the snap2stream tool the channel head locations are connected to the nearest stream channel, see figure 9. The result is that every calculated channel head by Geonet fits almost perfectly on the drainage network from Topotoolbox. The mean Euclidian distance between the calculated channel head by Geonet and the channel network are 0.13±0.08, 0.18±0.15, 0.23±0.09 and 0.56±1.0 m. for area 1-4 resp. The high standard deviation in area 4 is created by a single outlier of more than 4 m. Also, it appeared that the Euclidian distance is not higher in area 3. Apparently, the higher pixel size in area 3 does not result in a worse fit of the channel heads to the stream network. The combined mean Euclidian distance between channel head and stream network of the four areas combined is 0.26±0.53 m. This result shows that the way in which Topotoolbox and Geonet derive their flow accumulation and flow network do not differ much. Therefore, it is assumed that the channel heads can be useful in combination with the drainage network derived with Topotoolbox. Using this drainage network facilitates further use of tools in Topotoolbox in finding out how the channels erode the landscape for the different areas.

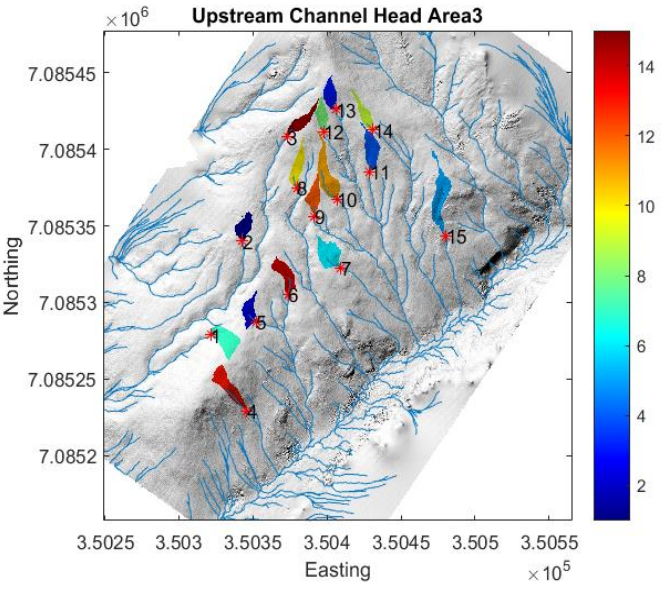

Figure 10. Upstream channel head areas in study area 3.

5.5. Upstream Channel Head Area

The channel heads as calculated by Geonet are used to calculate the area that flows into the channel at the moment of channel incision, see figure 10. The upstream areas from the individual channel heads are calculated in m² for the four areas. The boxplot (figure 11) shows that the upstream areas in all four study areas are almost equal. There is not a statistically significant difference between the areas as determined by an ANOVA $F(3, 59) = 1.96$, $p = 013$. Also with a Tukey test no significant difference has been found between the four study areas, $p > 0.05$. The mean upstream channel head areas are 195, 157, 180 and 111 m² for study area 1-4 resp. These values are all above the used threshold value of 50 – 70 m² (i.e. the threshold range for area 1-4 resp.).

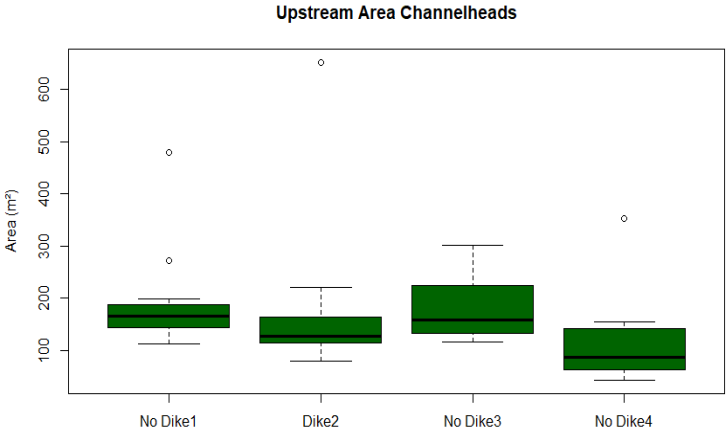

Figure 11. Boxplot of upstream channel head area for the four study areas.

To test if the upstream areas are influenced by the amount of dikes in the area, the relation between the dike area and the upstream channel head area is analysed, see figure 12. For the study areas 2 and 4 with dikes the relation between dike area and upstream area is investigated by a linear regression. The $R^2 = 0.3659$ and it seems that for larger upstream channel head areas covered by dikes, the total upstream channel head area is also larger. Interestingly, higher upstream channel head areas are found in study area 2 and 4 for areas with higher andesite-basalt coverage. However, as mentioned earlier (figure 11), this effect shrinks into insignificance compared to areas with no dikes (1 and 3).

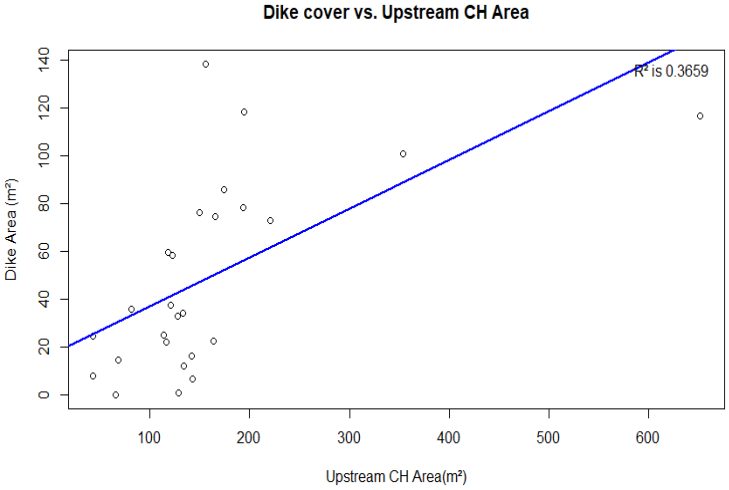

Figure 12. Relation between Dike Area and Upstream channel head area.

5.6. Test of Power-Law Scaling

The power-law scaling is tested with the original DEM by using a couple of different approaches. For all approaches the individual sub-catchments are analyzed as well as a combination of all sub-catchment per study area. In the first approach, the power-law scaling is tested by using all the data points in the catchments of the DEM. Second, this scaling is tested with only the mean of all the points. Third, for only the points that lie in the channel. Fourth, only the largest stream channel, i.e. the trunk, is used. Only a single (the longest) channel in the sub-catchment is used without any tributary. Besides, for this fourth approach the CRS algorithm is used to smoothen the channels by three steps; no smoothing, mild smoothing and rough smoothing to investigate the effect of possible errors in the channel profiles. At last, the scaling is tested after the threshold for channel head incision is shifted and starts earlier.

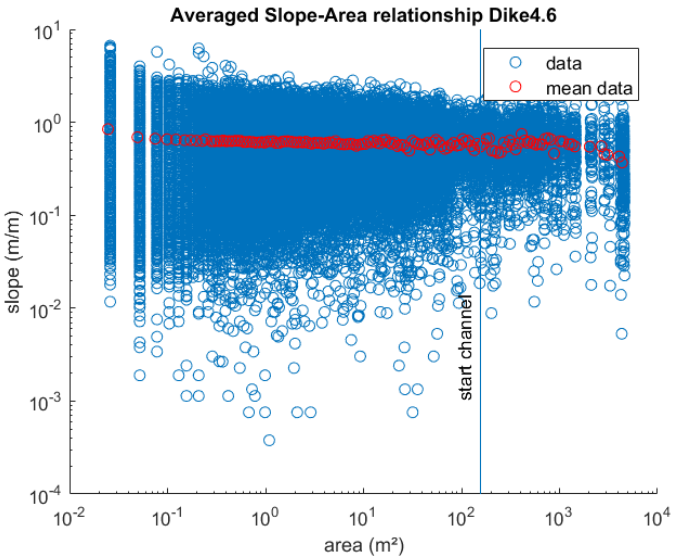

Figure 13. Example of the relation between slope and upstream area for channel 6 in study area 4. Vertical line indicates start of channel head.

5.6.1. All Data Points

Every pixel in the DEM has got a certain value of its slope and the area that flows into that single pixel. This relationship between slope and area is analyzed by using all these points in a scatterplot, figure 13. The DEM for each study area is divided into 7 or 8 sub-catchments for which this relationship is analyzed.

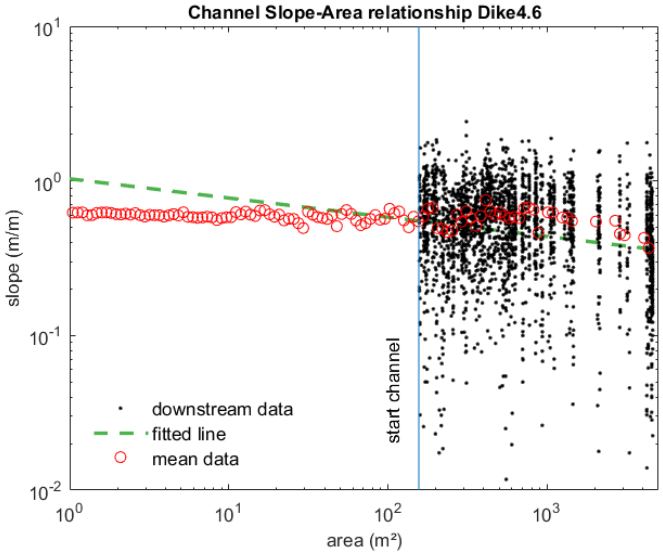

Figure 14. Regression fit through all points at the moment the channel starts to incise.

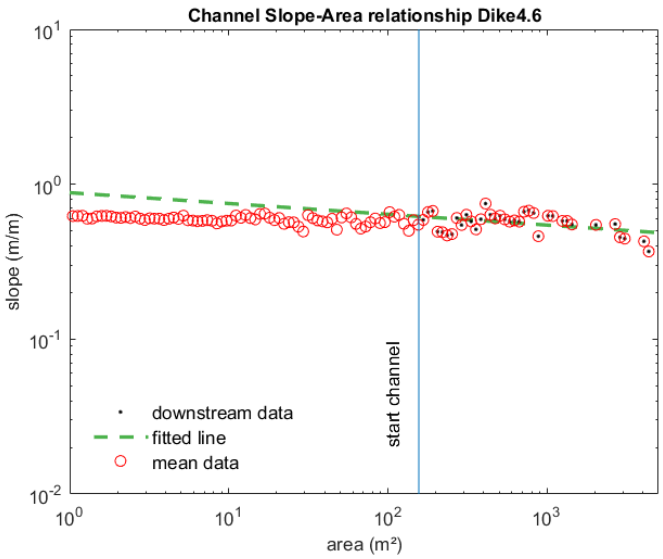

Figure 15. Regression fit through the mean of all points at the moment the channel starts to incise.

Since there are sometimes more channel heads starting in a sub-catchment, the mean upstream area of these channel heads is used. This mean upstream area is used to indicate in the slope-area plots where the channel incision starts, see figure 14. All the points that are on the right of this line are used in the regression analyses. The reason to do this is because all the points that are larger than the threshold line are supposed to be part of the channel network. All the points left from this line are belonging to the hillslope i.e. hillslope processes instead of alluvial processes. At last also a regression is fitted through the mean of all points, see figure 15. This mean, already indicated by red dots in figure 13 and 14, is calculated by taking the average of all points over a range of equally distributed bins of the whole dataset. In this case a bin contains 200 data points. Every point has a slope value and an upstream drainage area flowing into that single point. Based on these upstream areas, the whole dataset is sorted from smallest to largest. Eventually, the average slope and drainage area is taken over these 200 data points in every bin and repeated for every bin. These slope-area plots of all data points and the means are made for every sub-catchment of the four areas, see Appendix VIII.

5.6.2. Only Channel Points

By plotting only the points in the slope-area graphs that lie in the channel network, noise or possible errors in the data that influence the power law relationship are excluded. The transition is shown from a dense

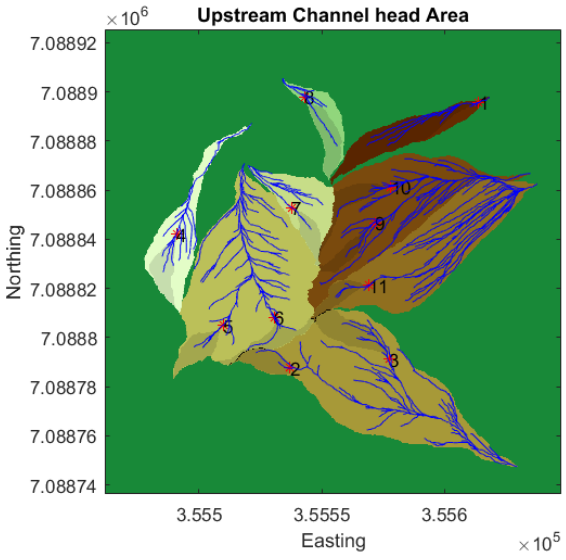

Figure 16. Original drainage pattern with many tributaries.

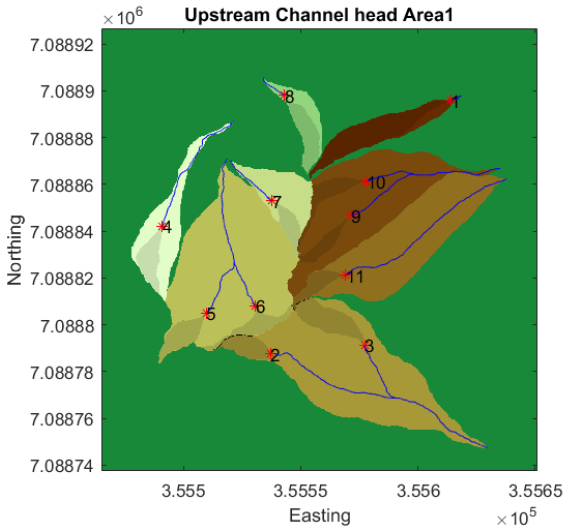

Figure 17. Different sub-catchments study area 1, small tributaries are excluded. Numbered stars indicating calculated channel heads.

drainage network towards a more simplistic pattern of channels by the exclusion of small tributaries, see figures 16 and 17. The channels are shown by the blue lines starting in the valley bottom till the numbered channel heads. The different sub-catchments are indicated by the different colors, as well as the upstream drainage area above the numbered channel heads. Since the pixel sizes of the DEMs are not the same, the data has been filtered to take the average slope and drainage area over a length of 5 m. The average slope is taken over a distance of 5 meter along the channel profile and plotted against the upstream draining area flowing into that point, see figure 18. This is repeated for all the individual channels of the four areas. Besides the individual channels, also all data points in the channels are combined per study area.

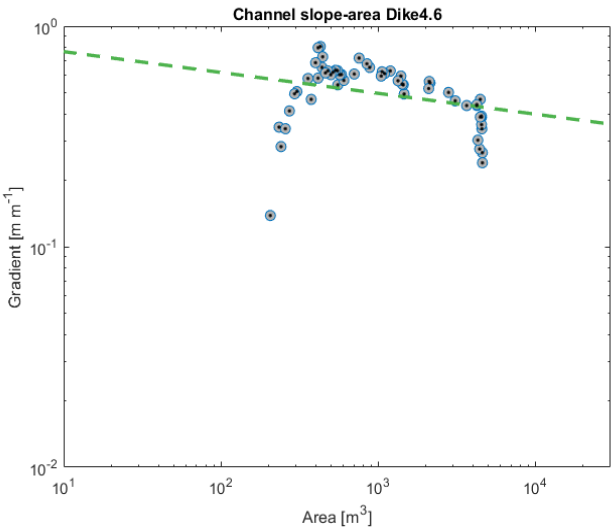

Figure 18. Example of slope area plot of channel 6 in study area 4 with binned data points over a length of 5 m.

Though, instead of taking the binned data, figure 17 can also be more simplified by only investigating a single channel from one channel head (e.g. point 6 in figure 17) till outlet. This is done to neglect tributaries and use a true channel head instead of a mean of channel heads. This single channel, i.e. trunk channel, is illustrated in figure 19 by using all data points that lie in channel 6 in area 4. For the trunk channels the slope-drainage area relation is analyzed by using different smoothing parameter values and repeated for the other study areas as well, see next section.

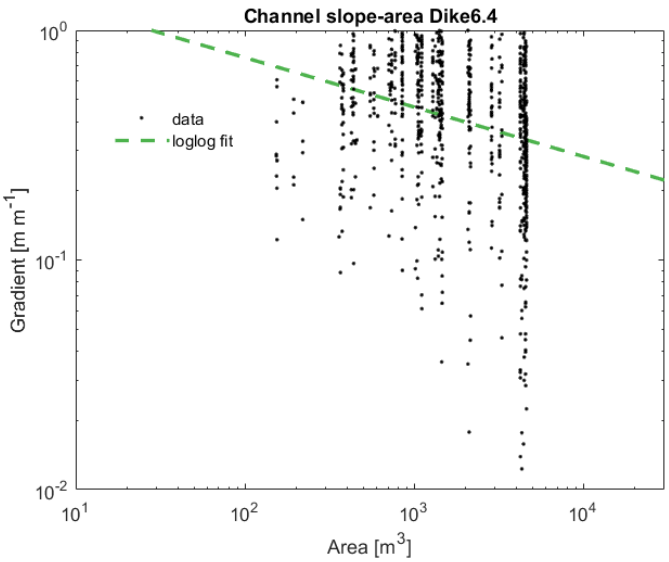

Figure 19. Example of channel 6 in study area 4 with data points from channel head till outlet.

5.6.3. Smoothed Channels

With the CRS algorithm the channel profiles can be adjusted by changing the degree of smoothing. For this research it is investigated if the power-law scaling

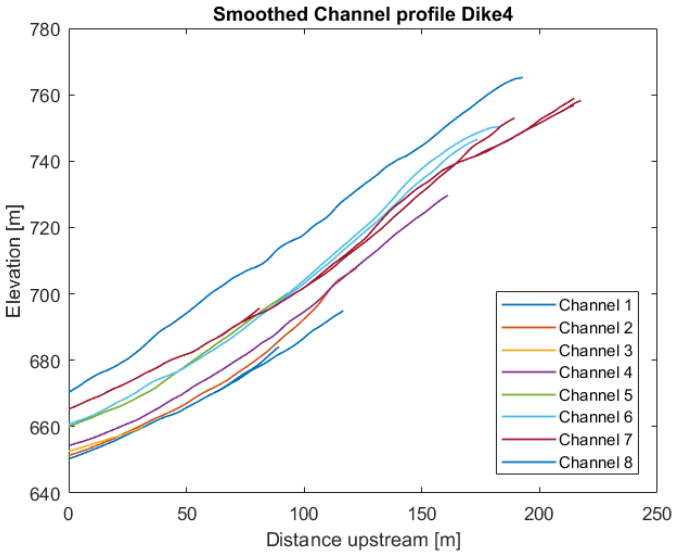

Figure 21. Smoothed channel profiles of study area 4 – with dikes.

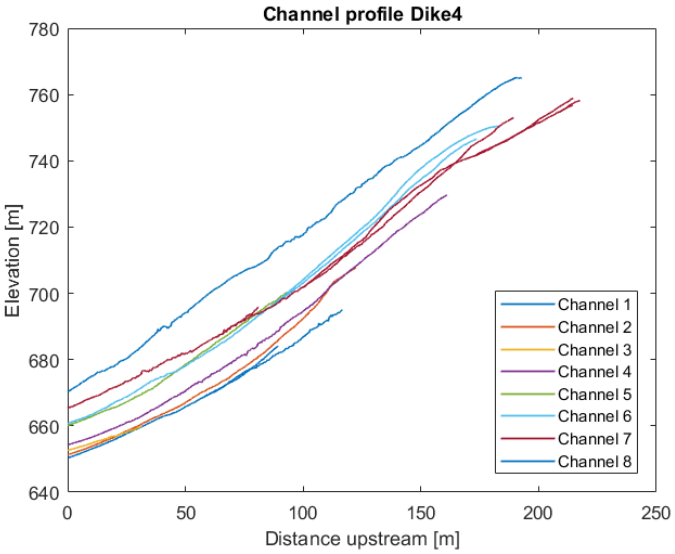

Figure 20. Raw channel profiles.

regression improves after smoothing the channel profiles. If the channel profiles are extracted from the DEM without any smoothing degree, the combined channel plot per area look like presented in figure 20 and Appendix VIIa. The small scale wiggles in the profiles can have an effect on the scatter of the points in the slope-area graphs.

After smoothing all the channels with K=500, the channels don't have the small scale wiggles anymore, see figure 21 and Appendix VIIb. Though, still a lot of larger wiggles are present that could still affect the data drastically. To get rid of these larger bumps and wiggles the channels are smoothed by a degree of K=10000, see figure 22 and Appendix VIIc.

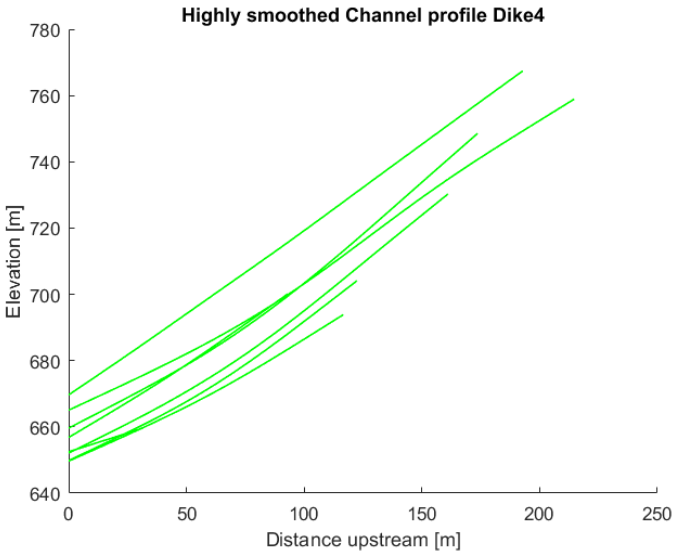

Figure 22. Highly smoothed channel profiles of area 4 – with dikes.

Figure 19 showed the non filtered slope-drainage area plot of trunk channel 6 in study area 4. This data is much more scattered compared to the smoothed data of the same channel in figure 23 and 24, by K=500 and K=10000 resp. The regression for individual channels becomes better with a higher value of K in the CRS-algorithm. Though, in some cases the rough filtering removes kinks in the river profiles of more than 10 m, see Appendix X. The gaps in the data, indicated by the red arrow in figure 23 are due to the exclusion of tributaries. Due to this exclusion, sudden jumps in consecutive data points are the result. In other words, the upstream drainage area entering the channel suddenly increases a lot.

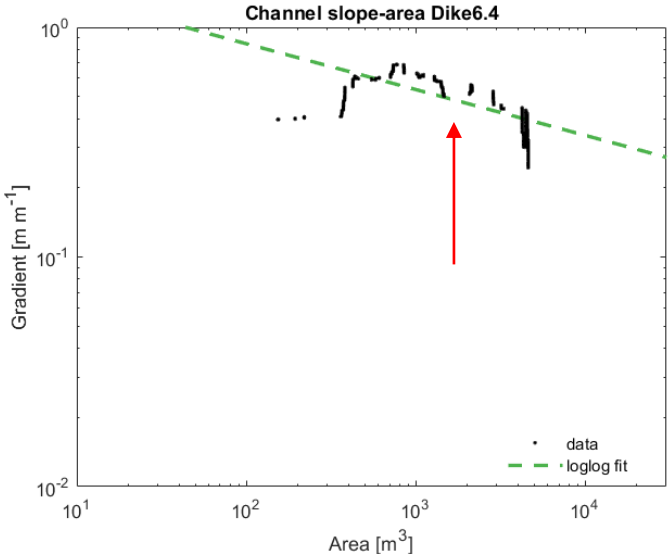

Figure 23. Channel-slope area regression through filtered data of channel 5 in area 2 with dikes, with K=500.

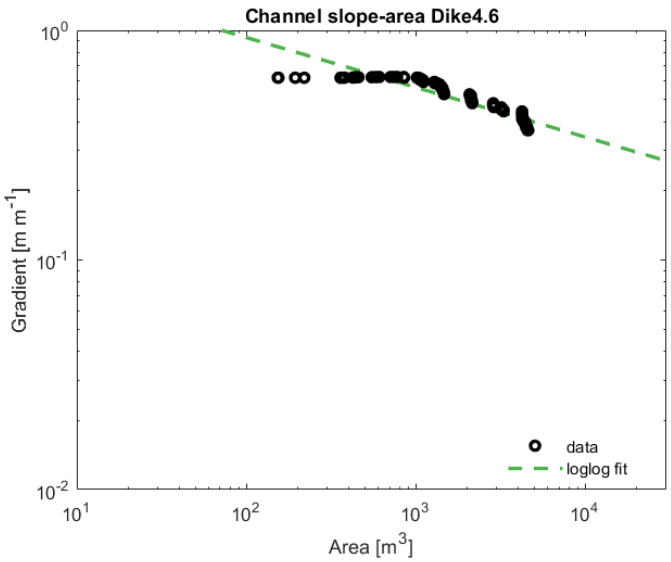

Figure 24. Example of slope area plot of highly smoothed channel 6 in study area 4 including all points.

In the example of study area 4 in figure 25 all channel data points are merged and an overall regression is fitted through the points. The regression fit through all these points becomes worse due to the large differences in slope-area relationships among the individual channels in the same study area. However, for individual channels the relationship becomes better, see R^2 values in Appendix III.

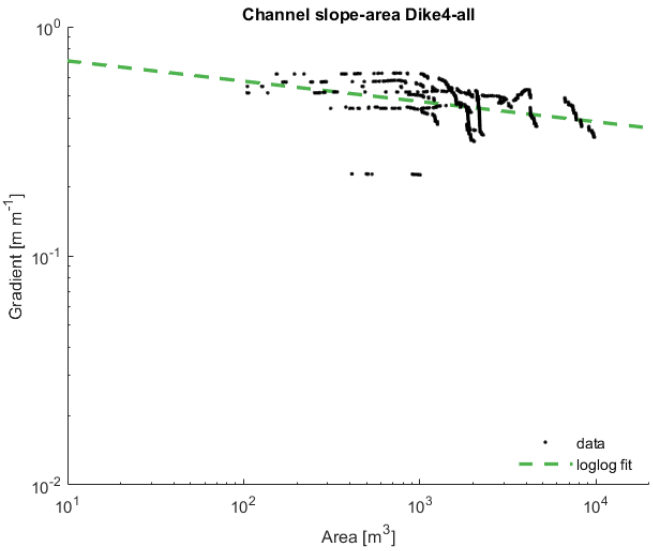

Figure 25. Highly smoothed channel data points combined for study area 4 – with dikes.

Overall, using all data points in the catchment does not result in a good power law relationship between slope and drainage area. Using only the binned mean results in a higher correlation, but filters out lots of data points. The regression improves by using only data points that lie inside the channel. Using binned data every 5 m improves the regression a little, but again also filters out large parts of the channel. Using all data and the CRS algorithm for the removal of outliers, by using a relatively low value of K, improves the regression. Though, the use of high K-values (K=10000), results in channel profiles far from reality. Therefore, further analyses in the next sections about the concavity and k_{sn} values are done with all data points and the use of smaller K values in the CRS algorihm (K=500), to stay close to the original measured field data and limit the effect of outliers.

5.6.4. Decreasing Upstream Area

In the field, point locations are taken with a hand-held GPS. These points are located at the beginning and the end of the stream channels in which the size of pebbles and boulders is measured. Although the

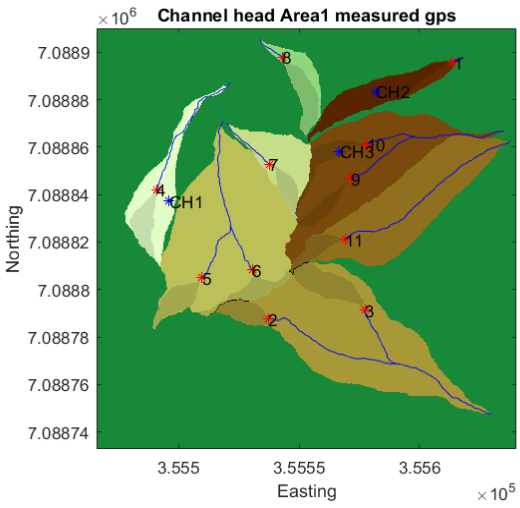

Figure 26. Calculated and measured GPS channel heads for the four study areas.

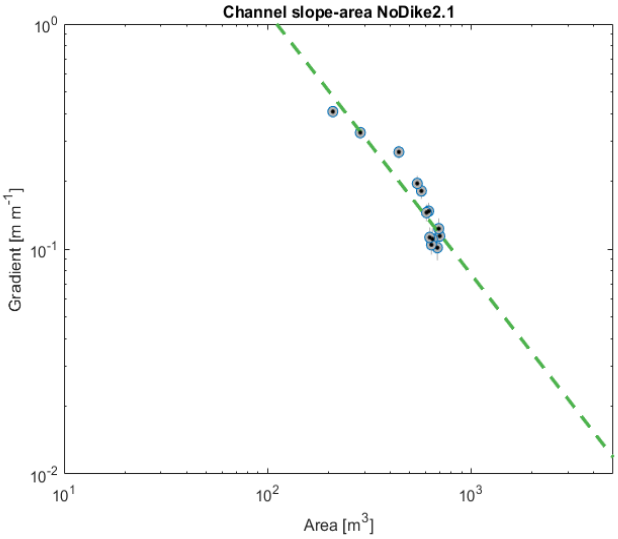

Figure 27. Channel head start calculated by Geonet.

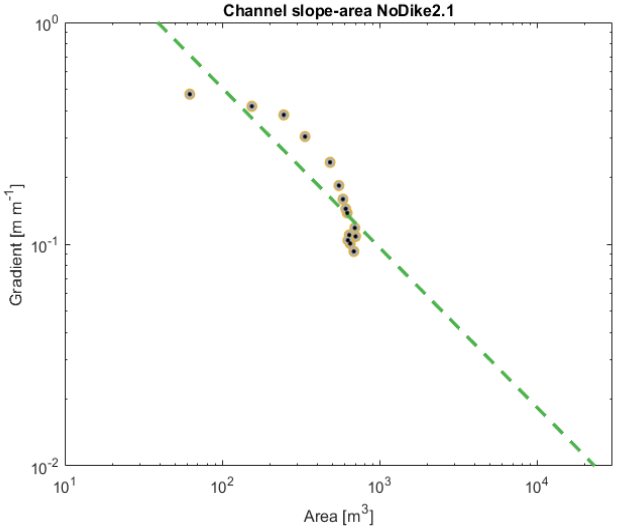

Figure 28. Example of slope area plot when upstream area is decreased and channels start earlier incising.

accuracy of the hand-held GPS is not very good, it gives insight in the difference between the locations that in the field were appointed as being the channel head start and what Geonet calculates. In figure 26 the channel heads measured with the hand-held GPS are almost in all the four study areas higher up in the landscape as compared to the locations determined by Geonet, see Appendix VIc. Not all points however are inside the investigated channels and cannot be well compared with the channel heads from Geonet. Besides, the GPS measurement are too little, therefore the channel heads from Geonet will be used in the further analysis. However, to investigate if the slope-area relationship changes, the threshold value for rivers to be visible in Topotoolbox is decreased. The rivers now start incising higher up in the landscape with smaller upstream areas. In figure 27 and 28, the difference is given for a single channel in area 1. For this specific example the smaller upstream area does not result in a better regression fit. This is repeated for all the other rivers from all study areas and the regressions became worse.

5.7. Dike Distribution

In the study areas with dikes the amount and location of the andesite-basalt layers in the landscape differ among the sub-catchments. To investigate what the dike distribution is over the different catchments and what influence this could have on the channel profiles, the area of dikes is measured at the height where it comes to the surface. First of all, the orthophotos are created in Agisoft. Next, the orthophotos are exported to Arcmap to filter out the dikes based on their RGB color information, see figure 29 and 30. These

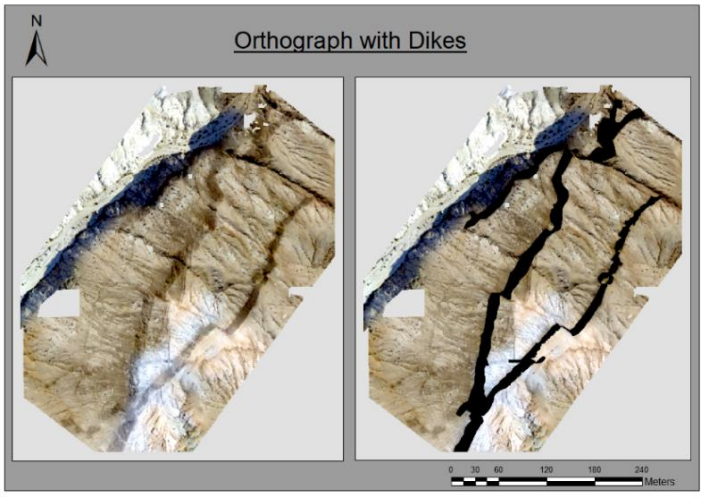

Figure 29. Dike cover in study area 2.

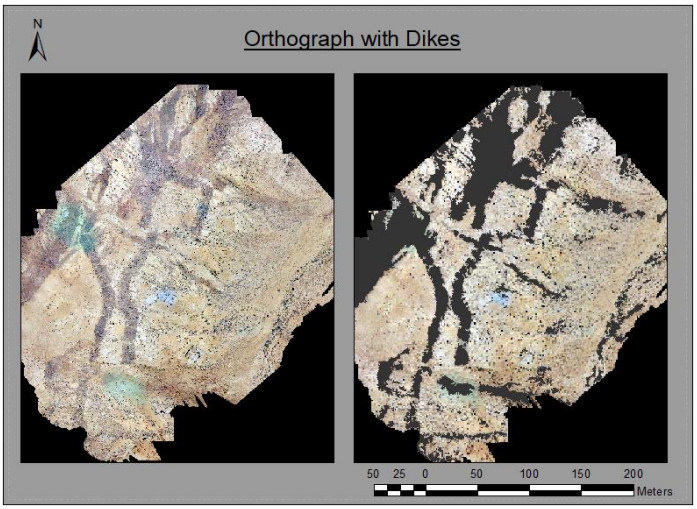

Figure 30. Dike cover in study area 4.

orthophotos are of high quality which made it possible to detect the dikes very precise by zooming in. The upstream area threshold for the channel network is decreased to get a very dense drainage network. This dense drainage network is minimalized by the trunk channel, to end up with a channel that starts almost at the top and ends at the valley bottom. This trunk channel is used to investigate the hillslope profile, to see where channels start to incise, how the channels react when crossing a dike with a different lithology and how the channel evolves after the dike has been crossed. Therefore, for each sub-catchment per study area a comparison is made between the dike distribution in the catchment and the channel profile. For the example in figure 31a the dike distribution is shown of sub-catchment 4 in study area 2. The arrow on the right in figure 31b indicates the channel head start. For the same example in the red rectangular box in figure 32 the channel crosses the dike layers. The channel head starts above the dike layer and crosses the first larger dike layer at around 750 m (AMSL) and the second layer at around 735 m (AMSL). Above the dike, the channel is steep. But at the moment when the channel crosses the first dike layer, the elevation decreases and eventually decreases even more when passing the second dike layer, indicated by the blue bar in figure 31b. For study area 4 the dike distribution, the channel profile and the steepness index are only given for channel 7, but this analysis is repeated for all sub-catchments of both study area 2 and 4 to analyze how the dike influences the landscape processes. The channel steepness index will be further discussed in section 5.9.

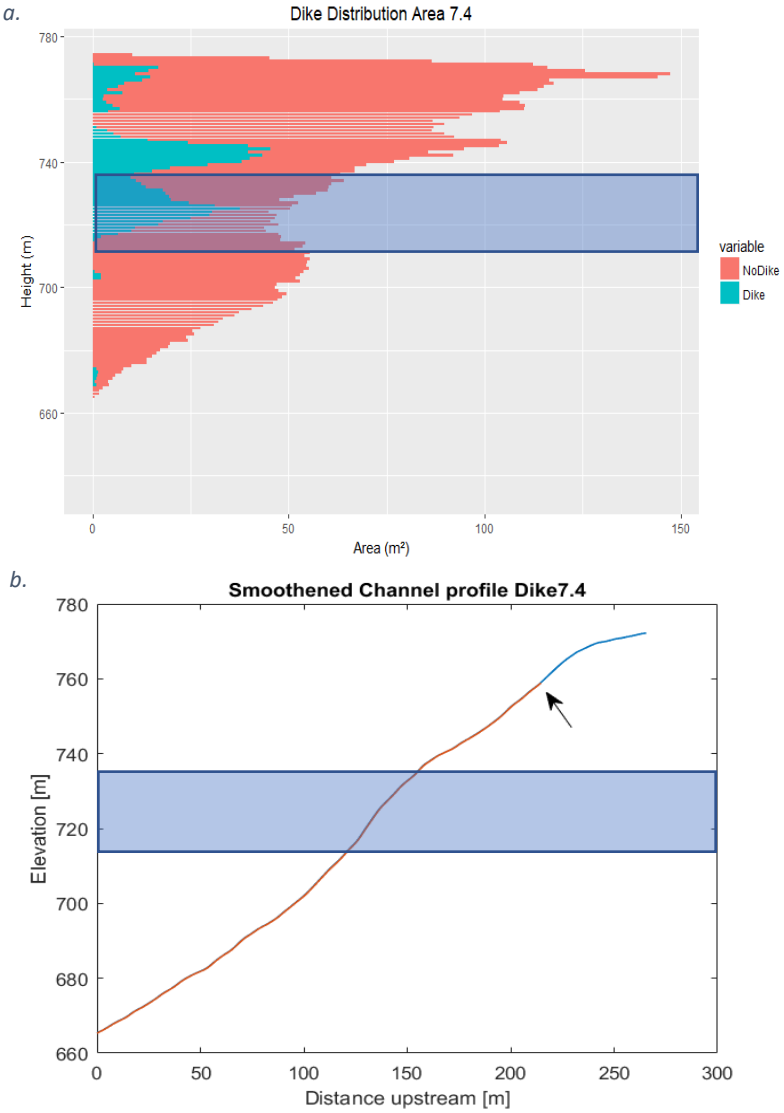

Figure 31. Example of channel profile and the locations where dikes occur for study area 4. Blue bar indicates area of dike incision. a) Dike area distribution with dikes (blue) and granite (red), b): channel slope.

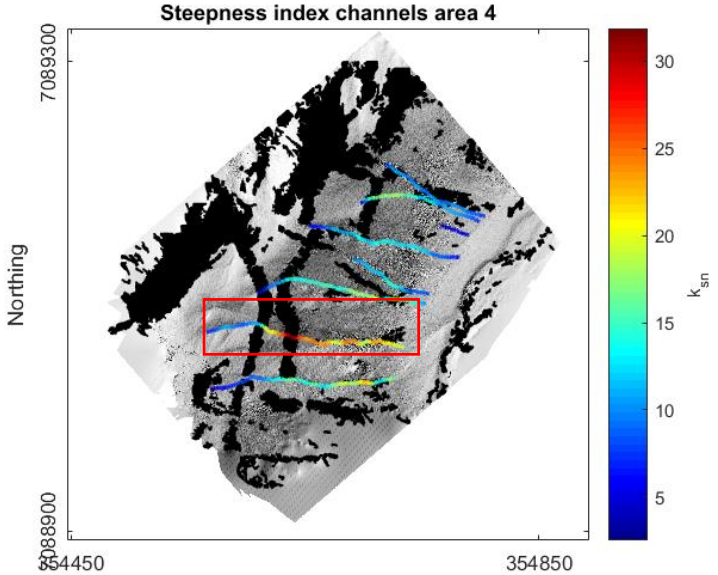

Figure 32. k_{sn} value along trunk channel profiles in area 4. Red box indicate example channel 7.4 crossing dike intrusions.

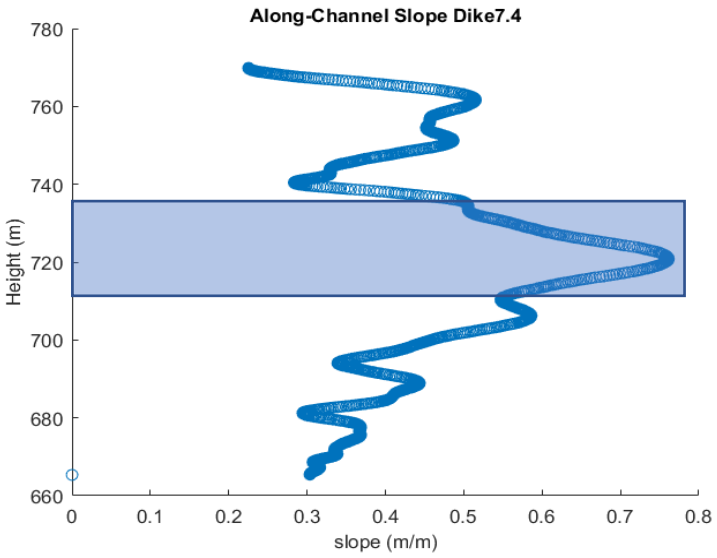

Figure 33. Example of channel slope along the channel profile and the locations where dikes occur for channel 7 in study area 4. Blue bar indicates the area of dike incision.

5.8. Slope profile

The channel gradient or slope is investigated for the individual trunk channels with a smoothing parameter of K = 500. The slopes are investigated to see at what locations along the channel profile the slopes are steep for individual channels and if there is a linkage with the specific lithologies. In a broader perspective, to see if there are differences between slopes among the study areas due to the presence of dike intrusions. At the locations where channels are crossing the dikes the slope increases as can be seen in the example figure 33. For every point along the channel profile the slope values are analyzed. The slope data from all areas combined is normally distributed with a little skewness to the right by inspecting the histogram and qqplot, Appendix XI. To test in which area(s) the slopes are the highest an ANOVA is carried out. A boxplot shows that the mean slope of all channels combined per area is higher in study area 2 and 4, i.e. with dikes, see figure 34. There was a statistically significant difference between the areas as determined by an ANOVA F(3, 19137) = 2670, p < 2e-16). A post hoc Tukey test showed that all areas differ significantly at p<0.05; with the highest slopes found in area 4. The mean slope for areas S1-S4 are; 0.26±0.26 , 0.4±0.13, 0.24±0.02 and 0.45±0.19 [m/m] respectively, see figure 34. The skewness to the right is due to the relatively high slopes found in area 2. As can be seen already in example figure 33, highest slopes can be found at locations with dikes, see also Appendix XII. Therefore, the parts of the channels that cross the andesite-basalt lithologies are extracted from the total channel length to investigate the slope values, figure 35. There was a statistically significant difference between the areas as determined by an ANOVA F(5, 19943) = 2292, p < 2e-16). A post hoc Tukey test showed that the slopes through dikes in area 2 and 4 differ significantly from the mean slope in all areas at p<0.05. However, both slope dike data (D2all and D4all) from area 2 and 4 are not significantly different from each other, p=0.99. The mean slope for areas D2all and D4all are; 0.67±0.41 and 0.66±0.4 [m/m] respectively, see figure 34. These mean values are significantly higher than the mean slope of all data for each individual area.

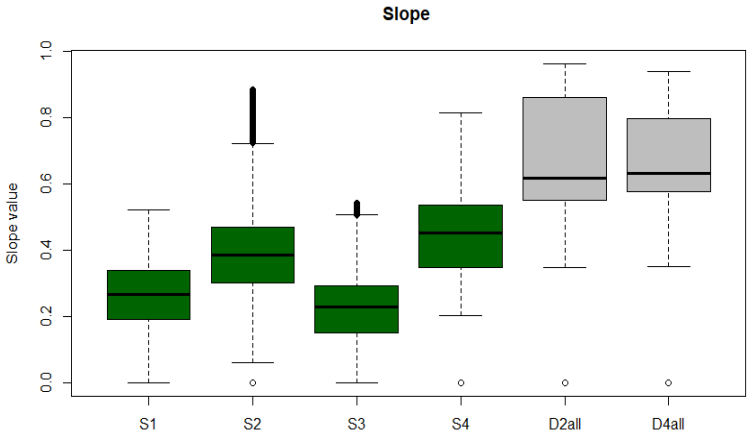

Figure 34. Boxplot of Slope data for study area 1-4, D2all and D4all are only slope data from channels crossing dike intrusions.

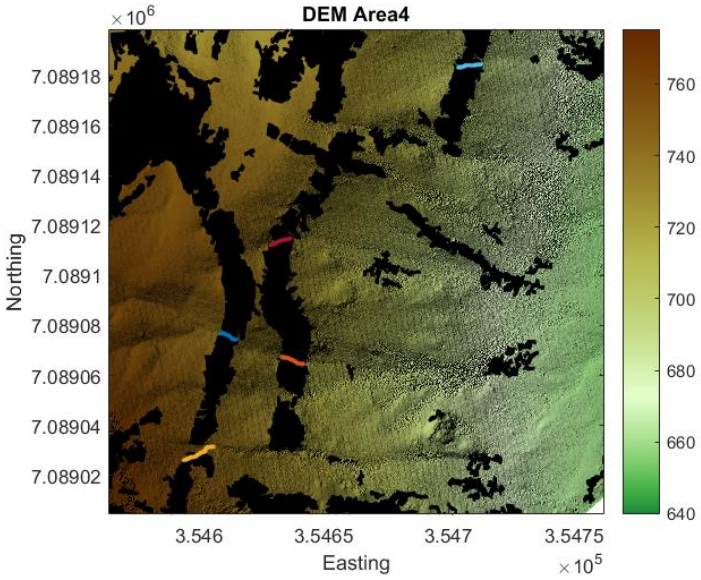

Figure 35. Channel segments in area 4 crossing dike layers used for Slope values analysis.

5.9. Channel Steepness Index

The channel steepness index (k_{sn} value) is calculated for the trunk channels in the four study areas, see figure 32 and Appendix XIV. The channel steepness index gives insight in the shape of the channel profiles and how channels incise. First of all, the k_{sn} value is determined for every point along the channel. After a log transformation of the original data the data appears to be normally distributed by a visual inspection of the histogram and qqplot (Appendix XIII). The mean k_{sn} value is significantly different between the four areas, see figure 36. The mean k_{sn} values are 5.07±5.07, 13.51±8.44, 7.208±2.14 and 13.38±8.31 for area 1 to 4 resp. A Tukey test shows that the areas with dikes have a significantly higher k_{sn} value than the areas without dikes, p-values are both < 0.05 (p=0.000).

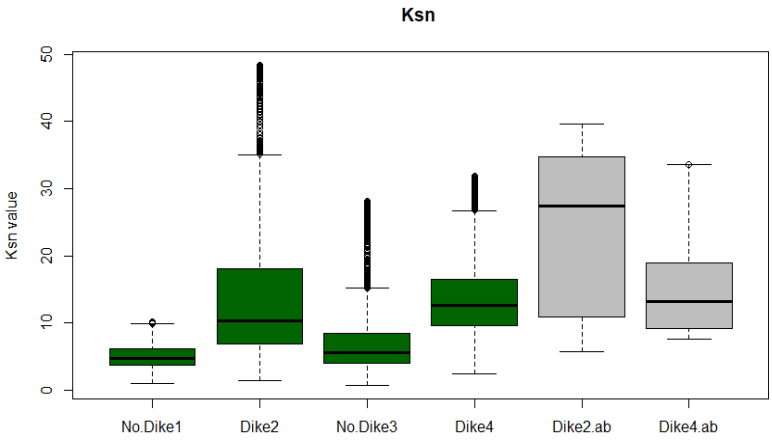

Figure 36. Boxplot of k_{sn} values for areas 1-4 and for only segments with andesite-basalt (ab) in area 2 and 4, i.e. Dike2.ab and Dike4.ab.

However, both areas with dikes as well as areas without dikes are also significantly different from each other (p=0.000), i.e. p < 0.05. Also, both k_{sn} values of channel parts only crossing the dikes (Dike2.ab and Dike4.ab) are also significantly different from the other groups. With a mean and standard deviation of 23.7±18.62 and 16.39±11.32 resp. the highest k_{sn} values are found in area 2. Though the k_{sn} values of channels crossing dikes are statistically significantly higher, the standard deviation is rather high. Besides inspecting the average k_{sn} values of all points together for the individual channels, also the k_{sn} values are given from the regression analysis, see appendix (). From these regression analysis it is clear that the R^2 is very different for each individual channel. The use of the CRS algorithm has improved the regression a lot compared to the R^2 of the original data. The huge scatter of the data points is filtered out which results in a higher R^2 value for all channels. Although the R^2 of the regressions are not very high, it still gives information about the general value of the channel steepness index per study area. For area 1 and 4 the value of the k_{sn} value is mostly positive and for area 2 and 3 this value is mostly negative. On a logarithmic scale this implies that in area 1 and 4 the k_{sn} values are more positive than in area 2 and 3. The mean k_{sn} value of the trunk channels are; 2.5, 0.1, 0.05 and 3 for area 1-4 resp.

5.10. Concavity Index

The concavity index is given by the slope of the linear regression analysis through the slope-drainage area points. In Appendix IV the results of the concavity index are given for each trunk channel that has been analyzed in the four study areas. It is assumed that the use of a K value of 500 in the CRS algorithm gives realistic channel profiles by the exclusion of outliers. Therefore, the slope-drainage area graphs and the resultant values from the regression analysis from these channels are used to interpret the concavity index. The values are compared to the unfiltered data points of the same trunk channels. As mentioned before, the correlations between slope and drainage area are not very high, but it gives information about the general value of the concavity index per study area. Namely, in area 1 and 4 in most cases the concavity index has a negative value, indicating a more concave channel profile. On the other hand, more positive concavity indices are found in area 2 and 3, indicating a more convex channel profile.

6. Discussion

This research investigates the role of tools with different lithologies in channel incision processes. High resolution digital elevation models are used to clarify the cover and tools effect. The expected power law scaling between the drainage area and slope, that rivers should obey in a topographic steady state landscape according to the stream power model, is analyzed. If the stream power model mimics Flint's power-law it is expected to see an effect of tools in the power-law slope-drainage area scaling relation due to the difference in rock properties (e.g. rock strength), amounts and sizes of the different lithologies. A set of

sub-questions has been analyzed to get an answer to this main hypothesis.

1. What are the grain sizes and lithologies of the tools in the areas with abundant dikes and no dikes?

Rock presence and properties in the four study areas are analyzed to answer this first sub-question. The most found rock types are granite and andesite-basalt. Obviously, as expected more andesite-basalt is present in the channels in areas with dikes. However, in area 3 also andesite-basalt was found in low quantities, while dike intrusions were absent. A possible explanation for

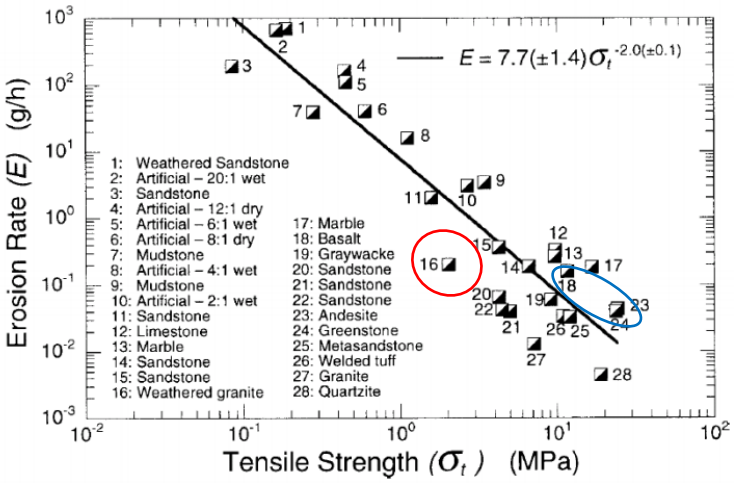

Figure 37. From: Sklar & Dietrich 2011, power scaling relation between rock tensile strength and erosion rate for different rock types. Red: weathered granite, Blue: andesite-basalt.

this finding could be that these rocks are from outside the study area. These tools might came from higher altitudes and ended up in the channels due to rock movement and rolling boulders that were able to pass the catchment boundaries. More bedrock is found in areas with dikes. Interestingly, the mean rock sizes of andesite-basalt are higher compared to granite. The finding of higher rock sizes, more bedrock and the steeper channel slopes on average, give the impression that the larger tools from the dikes wash away the bedrock cover when large boulders are moving downstream. According to Sklar and Dietrich (2001) is the rock tensile strength (k_e) a measure of erodibility and influences channel incision, according to the stream power incision law (equation 6). The difference in erosion rate between granite and weathered granite is quite large just as the difference between andesite and basalt. In figure 11 the rock tensile strength is plotted for a range of lithologies. The rock tensile strength is lower for weathered granite (red) than andesite-basalt (blue) and also the erosion rate of weathered granite appears to be higher. The results of the channel profiles and the location of the dikes give the impression that most knickpoints occur at the locations where channels cross these andesitic-basalt formations. Moglen en Bras (1995) already found that spatial heterogeneity in erosivity influences landscape-scale relationships between drainage area and slope. Studies by Selby (1980, 1982, 1987) and Moon (1984) concluded that adjustment of hillslope gradients to rock strength is widespread based on correlations between rock mass strength and the gradients of bedrock slopes. They stated that this general relation between erosive potential and slope would result in more erosion resistant rocks having steeper slopes than more erodible rocks to maintain the same erosion rate across a lithological variable landscape. The different lithologies not only provide tools in the channels, channels in their turn also incise through these different lithologies. The dikes create knickpoints due to the different rock properties compared to the host rock that influences the power-law scaling. It was found that slopes are steeper at locations where dikes occur. The harder, compacter and more resistant andesite-basalt dike intrusions have steeper slopes, likely to balance the uplift forces, since it is more difficult to erode. The steeper channel slopes found in areas with dikes, might be a possible explanation for the lower channel bed cover. The heavier boulders remain on the channel bed, while smaller grains are washed away.

2. Does the size of the dikes influence the provision of tools and consequently the relationship between slope and drainage area?

Investigation of the channel profiles showed that most of the channel profiles are straight and convex. It was expected to find more concave channel profiles in a landscape with only one lithology (granite) that is assumed to be in topographic steady state. The relation between the slope and the drainage area is not very high and not consistent according to the R^2's and from a visual inspection of the slope-area plots for individual and combined channels of the four study areas. Although the relation is not very high, most power law scaling relations of the investigated channels per study area have the same general trend.

For area 1 and 4 the concavity index is in most cases negative, indicating a concave channel profile. While, in area 2 and 3 most often a positive concavity index was found, indicating a convex channel profile. However, after inspecting the slope-drainage area graphs of area 2 and 3, it appears that in most cases the power law relation goes from concave to convex or from straight to concave to suddenly convex. Especially near the channel outlet the channel slopes in area 2 and 3 increase. A possible explanation for the steep slopes near the outlet could be the effect of valley processes. Area 1 and 4 have in common that these areas are at higher elevations compared to area 2 and 3. In the past e.g. water from higher elevations flowing into the valley, perpendicular to the mountain ridges, could have shaped the steep valley sides. Moreover, the fact that area 1 and 4 are at higher elevations, could also cause small difference in amount of precipitation, temperature and the influence of wind. These factors might have a significant effect on the channel profiles over a timescale of millions of years. The relatively low R^2s indicate that most investigated channels do not show the expected negative power-law scaling between slope and area. Not only the current state of the landscape, but also multiple other factors (climate, knickpoints, lithology, spatial variation in rock uplift) could all contribute to a failure of this scaling. From the channel profile data combined with the dike distribution data it appears that the slopes where dikes occur are significantly steeper. Since concave channel profiles are not clear and present in all study areas it is hard to compare the areas based on the slope-area relationship and investigate the role of tools. One of the possible explanations could be that the study areas are not close to topographic steady state. In that case it is not a coincidence that the overall power law scaling is bad. However, other explanations are possible as well and will be further discussed.

3. If a difference in erosional efficiency caused by the presence of dikes exist, how is this effect reflected in the start of channel incision i.e. the upstream areas?

To answer this question the start of the channel heads are compared, the total upstream areas and the presence of dike intrusions. The results of the channel head analysis indicate that there is not a difference in channel head start between the areas. Also the presence of dikes is not related to the upstream channel head, if we assume that the calculated channel heads have been calculated correctly by Geonet. For areas that experience the same rate of uplift but differ in rock type it was expected to find differences in channel head start. The reason to find these differences is because of the erodibility of rocks. Rocks that are harder to erode have steeper slopes (Duval 2004). It was expected to find larger upstream channel head areas, in areas with dikes, to create the force by waterflow for the erosion of harder bedrock. However, another possibility could have been the opposite; the harder, compacter and more resistant rock provides less infiltration, more runoff and could therefore even be more efficient in causing flow and need smaller upstream areas. In other words; the steeper slopes already provide the extra energy needed for the erosional capacity and therefore have smaller upstream areas and channels starting earlier to incise. Fresh granites are more erosion resistant compared to andesite-basalts of the same age, see figure 37. However, in the study areas, the granites are old, heavily weathered and found in channels as small disintegrated pieces, while the larger andesite-basalt boulders appeared to be less weathered. However, no clear prove can be given that relates the difference in erosional efficiency (due to different lithologies) to the start of channel incision. A striking part of testing if the stream power incision law mimics Flint's power-law scaling relationship, regardless of whether this scaling is applicable for these areas, is the determination of the channel heads. The exact moment at which channels start to incise is hard to calculate, because it depends on a couple of factors: the quality of the DEM (e.g. pixel size), the preprocessing of the DEM, the algorithm used for determining the flow direction and the flow accumulation. For this research the Geonet toolbox is used to calculate the channel heads. Other methods of channel heads have not been tested, but could have been better. The pixel size in area 3 is almost twice as high compared to the other study areas. The higher pixel size might influence the detection of small channels and their channel heads. The channels in their way are just like the determination of the channel heads dependent on the factors described above. The moment at which the channels start to incise is important for the validation of the stream power law. When channel heads start earlier in reality than calculated you miss data points

that could influence the slope-area relation. On the other hand, if channel heads start later in reality than calculated, data points are taken into account that do not belong to alluvial processes but to hillslope processes. Obviously, this also influences the calculation of the upstream channel head drainage areas. Considering the quality of the DEM, small wiggles in the river profiles can already have a quite large effect on the slope area plots due to the large scattering. Since area 3 has a higher pixel size it could be that the upstream channel head area is underestimated. However, also area 1 without dikes has equal upstream channel head areas compared to the areas with dikes. Therefore, it is likely that the calculated channel heads and resultant upstream areas in area 3 are trustworthy results as well. A small value is used for the channel profile filtering parameter K to reduce these small scale wiggles, but it is hard to say where this limit is. The CRS algorithm filters out these small scale errors, but maybe also natural knickpoints when a high value for this filtering is used. Another characteristic that might influence the validation of Flint's law is the catchment size. The catchment sizes in these study areas are relatively small compared to the analyzed catchments in previous studies. In a study by Montgomery (2001) the alluvial part in slope area plots was found to start at larger upstream areas. In their study different drainage area-slope relations were found corresponding with different portions of the landscape and geomorphological processes. E.g. drainage areas in the order of 10^2 and 10^3 m^2 correspond to hillslope slope-dependent transport processes, the region from 10^3 to 10^4 m^2 corresponds to hillslope-channel transition and the region from 10^4 to 10^5 to the alluvial segment. All these segments are likely to have different process laws and therefore different values of the parameters in the stream power incision law. Equation 8 can only be applied above a critical drainage area in the order of 10^5 - $5*10^6$ m^2 , because the power scaling relation between slope and drainage area on the hillslope is different than the power scaling relation for alluvial processes (Montgomery and Foufoula-Georgiou 1993, Lague and Davy 2003, Snyder, Whipple et al. 2003, Stock and Dietrich 2003, Ramsey, Hovius et al. 2006). The investigated catchments are in the order of 10^2 - 10^4 m^2. The analyzed catchments might be too small to find a possible effect of tools in alluvial bedrock channels. Colluvial processes like debris flows and landslides are likely to dominate the fluvial processes in these relatively small catchments.

What is the effect of tools on the erosion efficiency in an arid climate and can this effect be derived from the slope-drainage area power-law scaling?

Overall, it appeared to be hard to find clear relations in the slope-drainage area power law scaling and the start of channel heads that could be explained by the effect of tools. As mentioned before this could be due to the areas that are investigated, but if we look more in-depth at the channel profiles other reasons are possible as well. In this study the average normalized channel steepness (k_{sn}) was measured for a couple of channels in every study area. The results showed a significant difference between areas without and with dike intrusions, with the latter having higher k_{sn} values and slope values on average. Also, for segments of the channels that cross the dikes the slope and k_{sn} values were even higher than the average of all four areas. Since it was found that the upstream channel head areas are not significantly different between the four study areas, a higher k_{sn} value indicates that these channels have a steeper slope for equal draining areas. Higher k_{sn} values confirm the findings of Selby and Moon that the erosivity of andesitic-basalt is lower than weathered granite, the cause of the steeper slopes. The slopes were especially steeper in areas where dikes occur at the surface. The question is however, if the steeper k_{sn} values and slope values are only found at the locations where the channel crosses these dikes, or that these dikes also influence the erosion and resultant channel slopes at non-andesitic-basaltic lithologies downhill by the supply of tools. In other words, one of the factors that influence how channels incise is the lithology, but the lithology also influence other lithologies downstream by the supply of tools into the stream network. Therefore it is recommended to take the height into account at which different lithologies occur when investigating the slope-area relationship. Dikes found near the top would probably have more effect on channel incision than dikes only present at the foot slope part of the catchment. A better way would be to compare k_{sn} values of different segments of the profile. It is recommended to compare k_{sn} values of the same lithologies before and after a channel crosses a

different rock type. Under the assumption of steady state, steeper slopes indicate a lower erosion efficiency. Therefore, a comparison of the slope and k_{sn} values of channel parts incising through granite only, could explain if the dikes also influence the rate of erosion of the host rock (granite) by the supply of tools. Finally, the effect that the climate has on erosion processes has not been taken into account. In a simulation experiment the effect of climate and climate change on hillslope evolution was investigated by Ahnert (1988). Results showed that both the time between climate events and the duration of rainfall events have a decisive influence on hillslope development. An important factor that is hard to trace back is climate, but could be an important factor influencing the power law slope-drainage area scaling in these study areas. It is known that the study areas are close to one of the driest locations on earth (Atacama Desert) and the annual precipitation is low. Channels might have been created by single high intensive precipitation events that wash away the weathered surface layer. These rain events might not have the ability to create a well-developed drainage network which is a boundary condition for Flint's power law scaling. Already suggested by Bookhagen and Burbank (2016) should one compare the scaling of channel geometry directly with discharge characteristics (mean annual discharge and variability) rather than drainage area. If past climate conditions were different and channels are relatively young in their development, than channels still show the profile of the hillslope. If present climate did not much change over time than other factors might have affected channel incision processes that explain why no concave river profiles are found.

The findings of the remarkable combination of small channels and dike intrusions in an arid climate were the motivation for this research. The attempt of investigating the effect of tools on erosion processes with the use of the power-law scaling relation appears to be hard, since both areas with and without dikes show river profiles with sudden slope changes. Though, climate cycles are complex and the landscape response to it even more, Rinaldo, Dietrich et al. (1995) stated the following: "In landscapes with active uplift and the associated increase in erosion, the topography evolves due to the current climate and relict features are reflecting only previously experienced even wetter conditions. Moreover, paleomagnetic data indicates no significant latitudinal movement of the Atacama desert since the late Jurassic (150Ma) and suggests that it is the oldest extant desert on earth, (Hartley et al., 2005). The presence of channels that have not deeply incised and carry characteristics of hillslopes support the idea that these channels could be young relicts of high uncommon precipitation events from the past.

7. Conclusion

The combination of the climate, the different lithologies, the rate of uplift, the location close to sea and the additional effect of strong oceanic winds are factors that influence how the landscape has evolved over time. The use of the power-law slope-drainage area scaling appeared not to be useful to find differences in erosion efficiency caused by tools with an andesite-basalt lithology intruding the granite. The possible cover or tools effect that could be visible in the power law scaling relation between drainage area and channel slope was hard to see, since channel profiles have fluctuating slopes and do not have the expected concave channel profile. Due to the scatter of the data (small scale wiggles and knickpoints), the small catchment sizes and mostly straight channel slopes did not result in a clear negative drainage area-slope relationship. The use of a filter algorithm to smoothen the channel profiles improved the drainage area-slope relationship and resulted in straight slopes most often. Due to the variability of the channel profiles inside the individual study areas it remains difficult to detect a change in concavity index (θ) or the channel steepness index (k_s). However, the average normalized channel steepness index of the channels in areas with dikes are higher than in areas without dikes. Also the ksn values are higher in channel segments with an andesite-basaltic lithology. Besides the ksn values, also slope values are significantly higher in channel segments crossing the dike intrusions. The findings of gullies and rills created by intensive precipitation events close to the study area, the straight hillslopes, the variability in start of channel heads and small drainage areas support the idea that the channels found in the study area are young and carry the profile of hillslope.

It can be concluded that the andesite-basalt is less weathered than the granite and therefore resulted in steeper slopes in areas with dikes. It is likely that due to debris flow and landslides preferential stream paths enhance hillslope erosion by the supply of the harder dike material. The significantly larger rocks that were found in the channels in areas with dikes could contribute to this.

8. Acknowledgements

First of all many thanks to Dirk Scherler who gave me the opportunity to let me collect field work data in Chile and supervised me during this MSc thesis. I learned a lot in collecting, preprocessing, scripting and analyzing digital elevation data in Matlab for which I am thankful and which definitely will be useful knowledge for my later career. Besides that it was a joy to travel together with, this research would not have been a success without the help and experience from Renee van Dongen who arranged a lot of logistics in advance and was great help during the fieldwork. Thanks to Jeroen Schoorl whom I always could rely on here in Wageningen when necessary. Special thanks to Jose Gutierrez from the Conaf organization for his work to recollect field data that was lost due to robbery. I thank Luca Mao and his pHD students for borrowing his drone and learn me how to control it to collect the aerial photographs I needed.

9. References

Ahnert, F. (1988). "Modelling landform change." Modelling Geomorphological Systems. John Wiley and Sons New York. 1988. p 375-400, 18 fig, 31 ref.

Bagnold, R. (1973). The nature of saltation and of'bed-load'transport in water. Proceedings of the Royal Society of London A: Mathematical, Physical and Engineering Sciences, The Royal Society.

Bagnold, R. (1977). "Bed load transport by natural rivers." Water Resources Research **13**(2): 303-312.

Barrett, B. S., D. A. Campos, J. V. Veloso and R. Rondanelli (2016). "Extreme temperature and precipitation events in March 2015 in central and northern Chile." Journal of Geophysical Research: Atmospheres **121**(9): 4563-4580.

Bell, C. (1987). "The origin of the Upper Palaeozoic Chañaral melange of N Chile." Journal of the Geological Society **144**(4): 599-610.

Berg, K. and A. Baumann (1985). "Plutonic and metasedimentary rocks from the Coastal Range of northern Chile: RbSr and UPb isotopic systematics." Earth and Planetary Science Letters **75**(2-3): 101-115.

Flint, J. (1974). "Stream gradient as a function of order, magnitude, and discharge." Water Resources Research **10**(5): 969-973.

Gilbert, G. (1877). "Chapter V Land Sculpture." Report on the Geology of the Henry Mountains. Department of the Interior, US Geographical and Geological Survey of the Rocky Mountain Region, Washington: Government Printing Office: 93-144.

Hancock, G. S., R. S. Anderson and K. X. Whipple (1998). "Beyond power: Bedrock river incision process and form." Rivers over rock: Fluvial processes in bedrock channels: 35-60.

Howard, A. D. (1998). "Long profile development of bedrock channels: Interaction of weathering, mass wasting, bed erosion, and sediment transport." Rivers over rock: Fluvial processes in bedrock channels: 297-319.

Howard, A. D., W. E. Dietrich and M. A. Seidl (1994). "Modeling fluvial erosion on regional to continental scales." Journal of Geophysical Research: Solid Earth **99**(B7): 13971-13986.

Howard, A. D. and G. Kerby (1983). "Channel changes in badlands." Geological Society of America Bulletin **94**(6): 739-752.

James, M. and S. Robson (2012). "Straightforward reconstruction of 3D surfaces and topography with a camera: Accuracy and geoscience application." Journal of Geophysical Research: Earth Surface **117**(F3).

Johnson, J. P. and K. X. Whipple (2007). "Feedbacks between erosion and sediment transport in experimental bedrock channels." Earth Surface Processes and Landforms **32**(7): 1048-1062.

Johnson, J. P., K. X. Whipple, L. S. Sklar and T. C. Hanks (2009). "Transport slopes, sediment cover, and bedrock channel incision in the Henry Mountains, Utah." Journal of Geophysical Research: Earth Surface **114**(F2).

Kirby, E. and K. X. Whipple (2012). "Expression of active tectonics in erosional landscapes." Journal of Structural Geology **44**: 54-75.

Lague, D. and P. Davy (2003). "Constraints on the long-term colluvial erosion law by analyzing slope-area relationships at various tectonic uplift rates in the Siwaliks Hills (Nepal)." Journal of Geophysical Research: Solid Earth **108**(B2).

Lavé, J. and J. Avouac (2001). "Fluvial incision and tectonic uplift across the Himalayas of central Nepal." Journal of Geophysical Research: Solid Earth **106**(B11): 26561-26591.

Magilligan, F., P. S. Goldstein, G. Fisher, B. Bostick and R. Manners (2008). "Late Quaternary hydroclimatology of a hyper-arid Andean watershed: Climate change, floods, and hydrologic responses to the El Niño-Southern Oscillation in the Atacama Desert." Geomorphology **101**(1): 14-32.

Meteoblue (2017). 2006.

Moglen, G. E. and R. L. Bras (1995). "The effect of spatial heterogeneities on geomorphic expression in a model of basin evolution." Water Resources Research **31**(10): 2613-2623.

Montgomery, D. R. (2001). "Slope distributions, threshold hillslopes, and steady-state topography." American Journal of Science **301**(4-5): 432-454.

Montgomery, D. R., T. B. Abbe, J. M. Buffington, N. P. Peterson, K. M. Schmidt and J. D. Stock (1996). "Distribution of bedrock and alluvial channels in forested mountain drainage basins." Nature **381**(6583): 587.

Montgomery, D. R. and E. Foufoula-Georgiou (1993). "Channel network source representation using digital elevation models." Water Resources Research **29**(12): 3925-3934.

Passalacqua, P., P. Belmont, D. M. Staley, J. D. Simley, J. R. Arrowsmith, C. A. Bode, C. Crosby, S. B. DeLong, N. F. Glenn and S. A. Kelly (2015). "Analyzing high resolution topography for advancing the understanding of mass and energy transfer through landscapes: A review." Earth-Science Reviews **148**: 174-193.

Passalacqua, P., P. Tarolli and E. Foufoula-Georgiou (2010). "Testing space-scale methodologies for automatic geomorphic feature extraction from lidar in a complex mountainous landscape." Water Resources Research **46**(11).

Ramsey, L., N. Hovius, D. Lague and C. S. Liu (2006). "Topographic characteristics of the submarine Taiwan orogen." Journal of Geophysical Research: Earth Surface **111**(F2).

Rinaldo, A., W. E. Dietrich, R. Rigon, G. K. Vogel and I. Rodrlguez-Lturbe (1995). "Geomorphological signatures of varying climate." Nature **374**(6523): 632.

Sangireddy, H., C. P. Stark, A. Kladzyk and P. Passalacqua (2016). "GeoNet: An open source software for the automatic and objective extraction of channel heads, channel network, and channel morphology from high resolution topography data." Environmental Modelling & Software **83**: 58-73.

Schwanghart, W., G. Groom, N. J. Kuhn and G. Heckrath (2013). "Flow network derivation from a high

resolution DEM in a low relief, agrarian landscape." Earth Surface Processes and Landforms **38**(13): 1576-1586.

Schwanghart, W. and N. J. Kuhn (2010). "TopoToolbox: A set of Matlab functions for topographic analysis." Environmental Modelling & Software **25**(6): 770-781.

Schwanghart, W. and D. Scherler (2014). "TopoToolbox 2-MATLAB-based software for topographic analysis and modeling in Earth surface sciences." Earth Surface Dynamics **2**(1): 1.

Schwanghart, W. and D. Scherler (2017). "Bumps in river profiles: the good, the bad, and the ugly." Earth Surf. Dynam. Discuss. **2017**: 1-30.

Sepúlveda, S. A., S. Rebolledo, J. McPhee, M. Lara, M. Cartes, E. Rubio, D. Silva, N. Correia and J. P. Vásquez (2014). "Catastrophic, rainfall-induced debris flows in Andean villages of Tarapacá, Atacama Desert, northern Chile." Landslides **11**(3): 481-491.

Sklar, L. and W. E. Dietrich (1998). River longitudinal profiles and bedrock incision models: Stream power and the influence of sediment supply, Wiley Online Library.

Sklar, L. S. and W. E. Dietrich (2001). "Sediment and rock strength controls on river incision into bedrock." Geology **29**(12): 1087-1090.

Sklar, L. S. and W. E. Dietrich (2004). "A mechanistic model for river incision into bedrock by saltating bed load." Water Resources Research **40**(6).

Snyder, N. P., K. X. Whipple, G. E. Tucker and D. J. Merritts (2003). "Importance of a stochastic distribution of floods and erosion thresholds in the bedrock river incision problem." Journal of Geophysical Research: Solid Earth **108**(B2).

Stock, J. and W. E. Dietrich (2003). "Valley incision by debris flows: Evidence of a topographic signature." Water Resources Research **39**(4).

Turowski, J. M., D. Lague and N. Hovius (2007). "Cover effect in bedrock abrasion: A new derivation and its implications for the modeling of bedrock channel morphology." Journal of Geophysical Research: Earth Surface **112**(F4).

Whipple, K., R. DiBiase and B. Crosby (2013). Bedrock rivers. Treatise on geomorphology, Elsevier Inc.

Whipple, K. X. and G. E. Tucker (1999). "Dynamics of the stream-power river incision model: Implications for height limits of mountain ranges, landscape response timescales, and research needs." Journal of Geophysical Research: Solid Earth **104**(B8): 17661-17674.

Whipple, K. X. and G. E. Tucker (2002). "Implications of sediment-flux-dependent river incision models for landscape evolution." Journal of Geophysical Research: Solid Earth **107**(B2).

Wilcox, A. C., C. Escauriaza, R. Agredano, E. Mignot, V. Zuazo, S. Otárola, L. Castro, J. Gironás, R. Cienfuegos and L. Mao (2016). "An integrated analysis of the March 2015 Atacama floods." Geophysical Research Letters **43**(15): 8035-8043.

Willett, S. D. and M. T. Brandon (2002). "On steady states in mountain belts." Geology **30**(2): 175-178.

Wobus, C., K. X. Whipple, E. Kirby, N. Snyder, J. Johnson, K. Spyropolou, B. Crosby and D. Sheehan (2006). "Tectonics from topography: Procedures, promise, and pitfalls." Geological Society of America Special Papers **398**: 55-74.

Wohl, E. E. (2000). Mountain rivers, Amer Geophysical Union.

Wolman, M. G. (1954). "A method of sampling coarse river-bed material." EOS, Transactions American Geophysical Union **35**(6): 951-956.

Zhou, J. and K. Lau (1998). "Does a monsoon climate exist over South America?" Journal of climate **11**(5): 1020-1040.

10. Appendices

Appendix I – Study area with fault lines

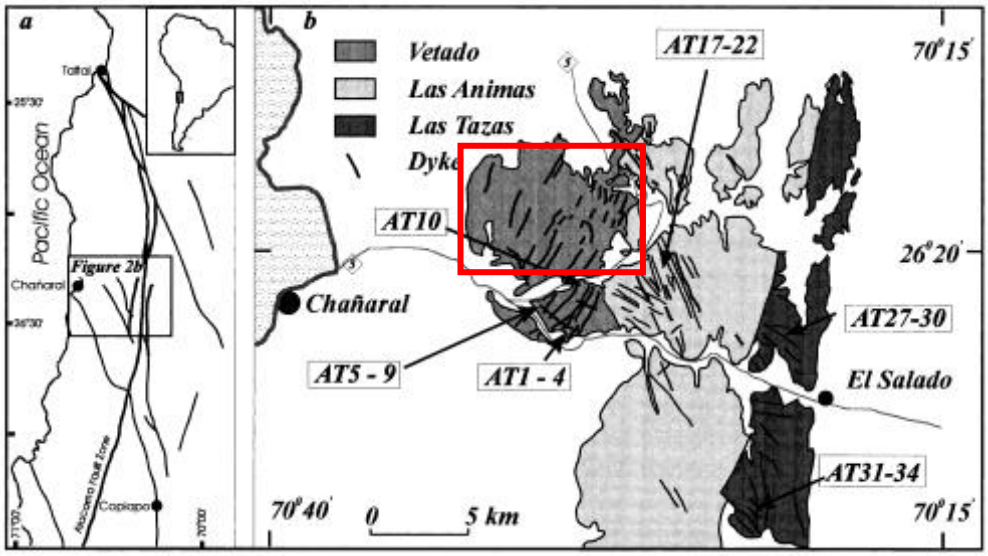

Appendix II – Wind rose and wind speed

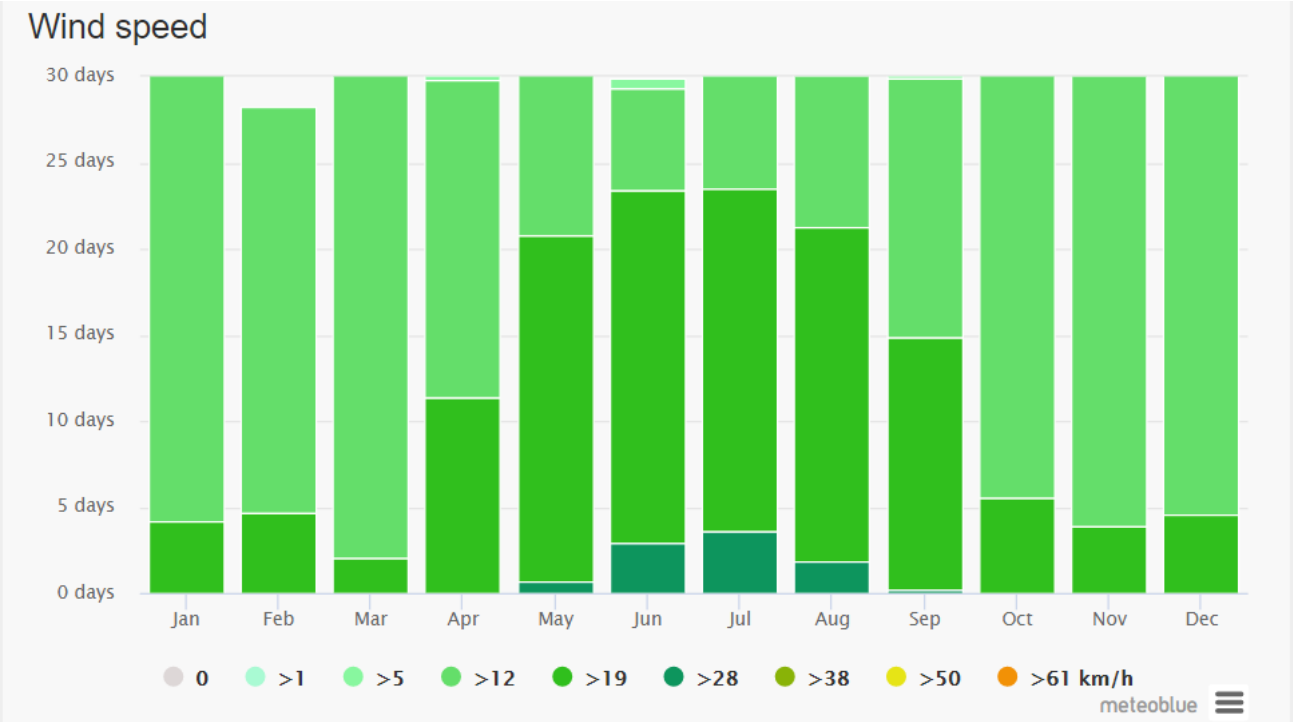

Appendix III – R^2 relations slope-drainage area

Area.Channel	R^2-all points	R^2-mean	R^2-channel	R^2-channel-5m	R^2-channel crs k=500	R^2 channel crs K =10000
1.1	0.2449	0.7668	0.2397	0.3641	0.4355	0.4136
1.2	0.4916	0.8383	0.4912	0.8964	0.9057	0.5207
1.3	0.1549	0.3842	0.0743	0.3864	0.3808	0.6062
1.4	0.2282	0.3004	0.3479	0.5935	0.6127	0.7914
1.5	0.0339	0.1467	0.0503	0.1807	0.197	0.6255
1.6	0.0392	0.0868	0.0244	0.0205	0.0172	0.4916
1.7	0.0473	0.0773	0.0464	0.2052	0.2296	0.8079
1.8	0.0801	0.1009	0.0758	1	1	0.5152
total 1	**0.0556**	**0.218**		**0.1038**		**0.0743**
2.1	0.0402	0.008	0.0535	0.0114	0.2129	0.723
2.2	0.0014	0.0041	0.0386	0.0721	0.0678	0.1151
2.3	0.0014	0.1501	0.0885	0.1979	0.2212	0.4987
2.4	4.40E-05	0.0057	0.0088	0.0063	0.0188	0.2379
2.5	0.1474	0.0017	0.0306	0.0191	0.1056	0.0012
2.6	0.0838	0.2429	0.1509	0.459	0.6361	0.9225
2.7	0.0044	0.0399	0.0203	0.0483	0.0309	0.6094
total 2	**6.55E-04**	**0.0045**		**0.1131**		**0.1181**
3.1	0.0063	0.0045	0.0578	0.0638	0.1435	0.8896
3.2	1.08E-09	0.0706	0.1015	0.2767	0.3509	0.4323
3.3	0.093	0.2384	0.0174	0.0672	0.6316	0.8038
3.4	0.0056	0.093	0.1077	0.3079	0.3795	0.9434
3.5	0.0722	0.356	5.78E-05	0.0449	0.008	0.646
3.6	0.1686	0.8461	0.0535	0.3224	0.1593	0.7208
3.7	1.43E-04	0.0413	0.0359	0.708	0.8799	0.9543
total 3	**0.0808**	**0.1799**		**0.0211**		**0.0364**
4.1	0.028	0.0013	0.1838	0.4851	0.7235	0.8353
4.2	0.0141	0.3147	0.0418	0.2092	0.269	0.3514
4.3	0.0145	0.0985	0.023	0.0365	0.8365	0.7854
4.4	0.0571	0.5265	0.0082	0.273	0.3354	0.5577
4.5	0.0201	0.1495	0.0619	0.591	0.5308	0.9239
4.6	8.17E-05	0.003	0.0325	0.1092	0.374	0.7888
4.7	0.004	0.0165	0.0173	0.019	0.0345	0.1622
4.8			0.0029	0.0018	3.01E-06	0.4816
total 4	**0.0053**	**0.0212**		**0.2229**		**0.1731**

All R^2 are calculated between the slope and the drainage area for 1) All points of the whole catchment 2) The mean of all points 3) Only the points that lie in the channel network 4) Only the points that lie in the channel network, but binned over a distance of 5 meter 5) Only the points that lie in the smoothed channel network with K=500 and 6) Only the points that lie in the smoothed channel network with K=10000.

Appendix IV – R^2 relations slope-drainage area

Area.Channel	df	R^2-no filter	Ksn	Θ	df	R^2-K500	Ksn	Θ
1.1	76	0.2397	4.2918	-1.9851	76	0.3507	0.6169	-0.4444
1.2	410	0.4912	2.6611	-1.2919	410	0.8661	2.396	-1.1755
1.3	154	0.0743	1.3347	-0.8249	154	0.3067	0.6002	-0.4873
1.4	484	0.3479	0.5574	-0.4293	484	0.8381	0.5186	-0.4024
1.5	726	0.0503	-1.3123	0.2132	727	0.2008	-1.1396	0.1695
1.6	543	0.0244	0.3709	-0.3442	543	0.0647	0.1747	-0.2561
1.7	493	0.0464	-0.0948	-0.15	493	0.301	-0.0073	-0.1688
1.8	33	0.0758	11.5179	-4.4657	33	0.5122	0.0587	-0.2524
2.1	1101	0.0535	-0.9034	0.1361	1206	0.2129	-0.8998	0.1412
2.2	1061	0.0386	-0.6693	0.0905	1067	0.0678	-0.5297	0.0592
2.3	1028	0.0885	-0.9016	0.1452	1029	0.2212	-0.9184	0.1592
2.4	1418	0.0088	-0.6967	0.046	1444	0.0188	-0.5835	0.0254
2.5	1262	0.0306	-0.684	0.0768	1263	0.1056	-0.666	0.0816
2.6	624	0.1509	-1.9365	0.4852	629	0.6361	-2.3572	0.638
2.7	716	0.0203	-0.6503	0.022	736	0.0309	-0.6876	0.0457
3.1	865	0.0578	-1.1618	0.1086	905	0.1435	-1.369	0.1833
3.2	142	0.1015	-0.0453	-0.1791	143	0.3509	-0.1806	-0.1246
3.3	352	0.0174	-0.7651	0.0213	363	0.6316	-1.2051	0.1833
3.4	453	0.1077	-1.8616	0.3334	504	0.3795	-2.1765	0.4438
3.5	574	5.78E-05	-0.7553	0.0211	615	0.008	-0.6997	0.0136
3.6	465	0.0535	-1.1094	0.152	477	0.1593	-0.8897	0.0972
3.7	163	0.0359	-1.8665	0.5437	166	0.8799	-2.5035	0.7828
4.1	553	0.1838	1.6736	-0.6804	618	0.7235	0.9939	-0.4527
4.2	648	0.0418	0.6411	-0.3289	661	0.269	0.897	-0.3889
4.3	156	0.023	-0.1511	-0.1922	167	0.8365	0.0437	-0.2372
4.4	793	0.0082	0.3163	-0.2425	865	0.3354	0.4989	-0.2775
4.5	455	0.0619	1.8989	-0.7616	494	0.5308	1.5169	-0.6015
4.6	912	0.0325	0.312	-0.2155	935	0.374	0.3276	-0.1996
4.7	1032	0.0173	-0.2981	-0.0333	1142	0.0345	-0.1254	-0.0688
4.8	965	0.0029	-0.2919	-0.0279	1040	3.01E-06	-0.3159	0.002

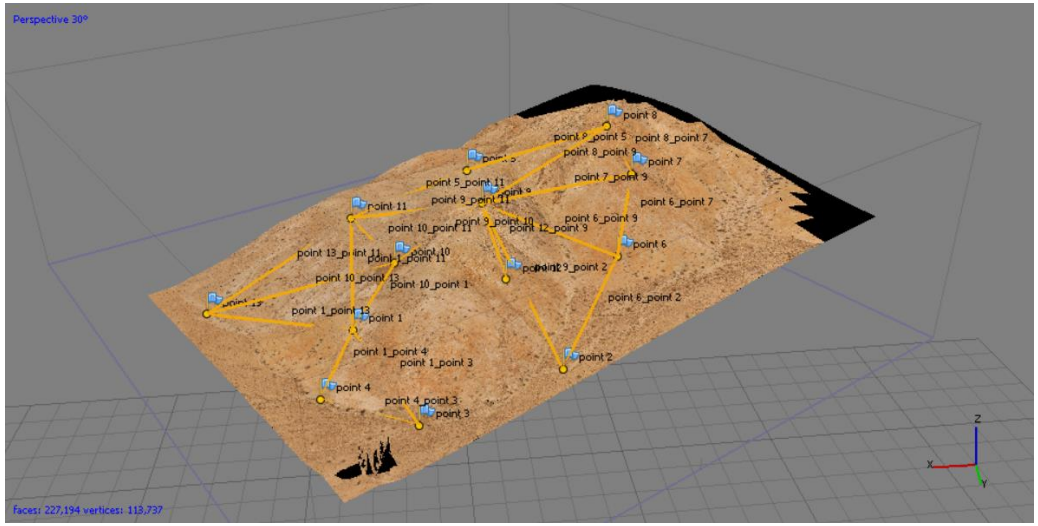
Perspective 30°
Faces: 227,194 vertices: 113,737

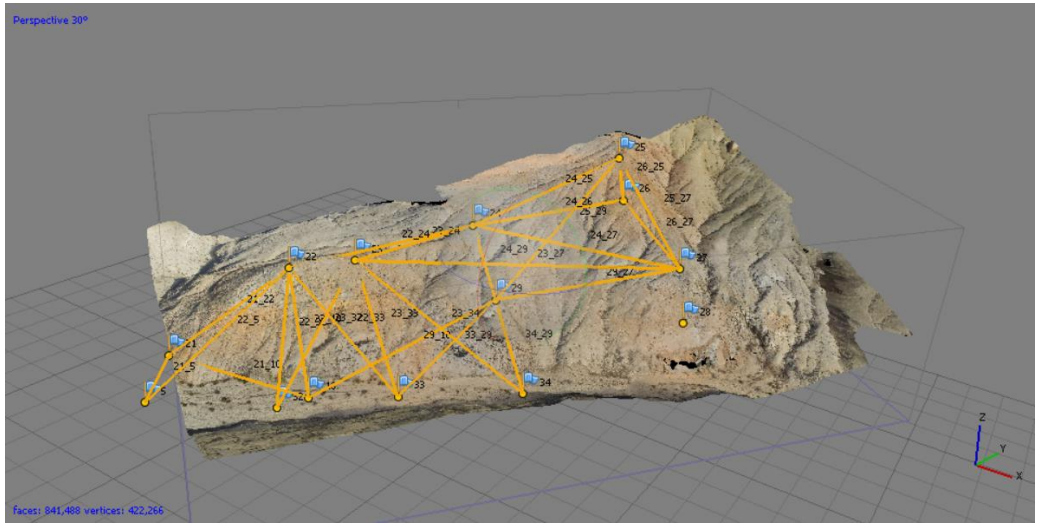
Perspective 30°
Faces: 841,488 vertices: 422,266

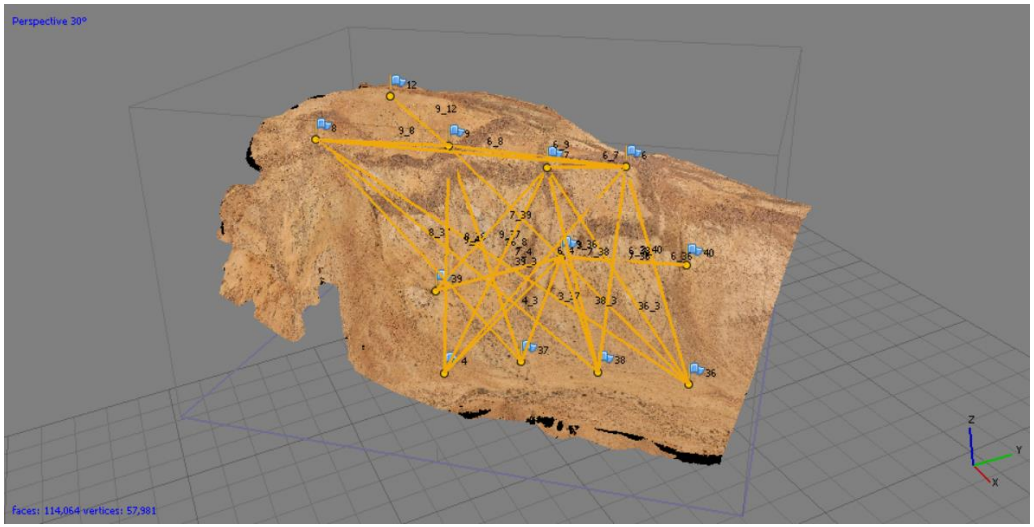
Perspective 30°
Faces: 114,064 vertices: 57,981

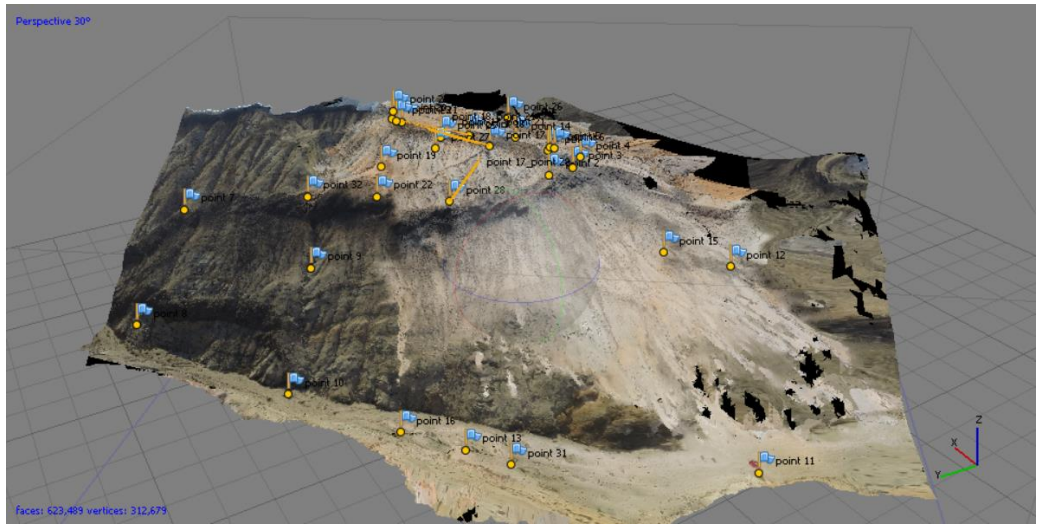
Perspective 30°
Faces: 623,489 vertices: 312,679

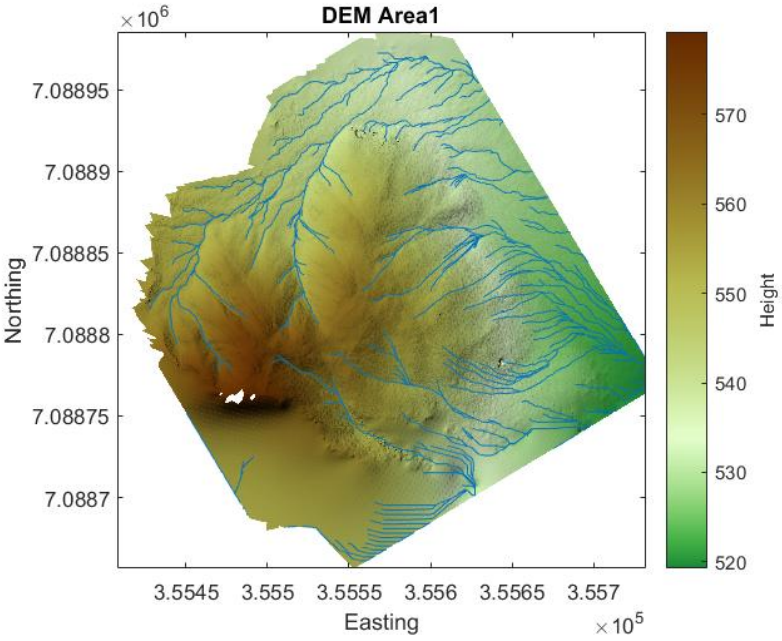
DEM Area1
×10^6
7.08895
7.0889
7.08885
7.0888
7.08875
7.0887
Northing
3.5545
3.555
3.5555
3.556
3.5565
3.557
×10^5
Easting
570
560
550
540
530
520
Height

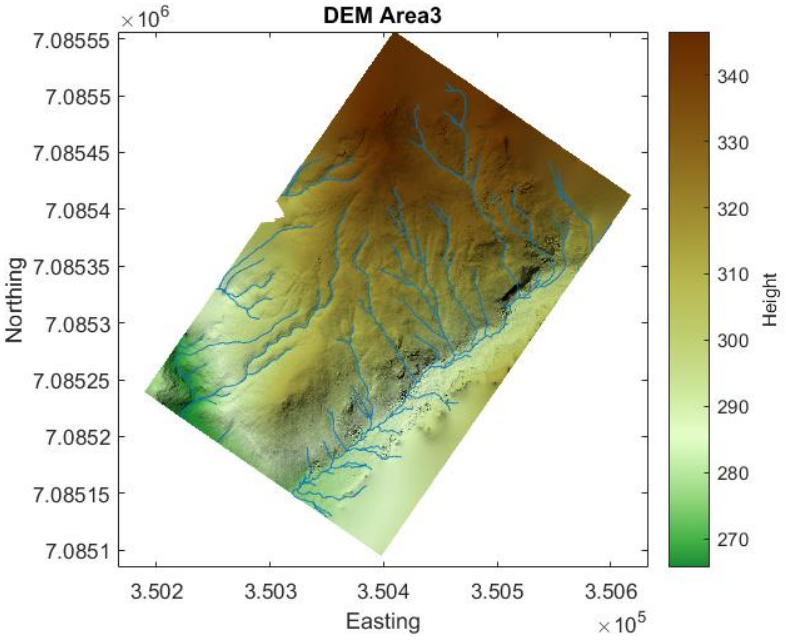
DEM Area3
×10^6
7.08555
7.0855
7.08545
7.0854
7.08535
7.0853
7.08525
7.0852
7.08515
7.0851
Northing
3.502
3.503
3.504
3.505
3.506
×10^5
Easting
340
330
320
310
300
290
280
270
Height

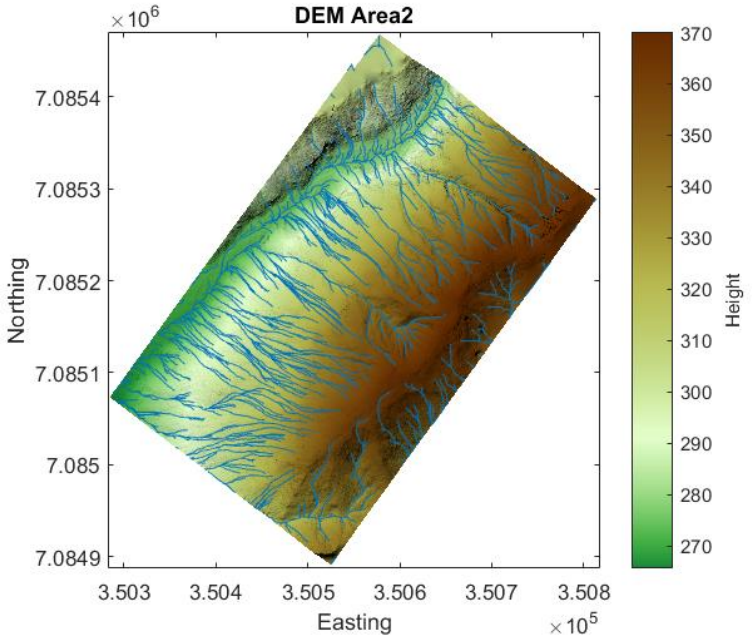
DEM Area2
×10^6
7.0854
7.0853
7.0852
7.0851
7.085
7.0849
Northing
3.503
3.504
3.505
3.506
3.507
3.508
×10^5
Easting
370
360
350
340
330
320
310
300
290
280
270
Height

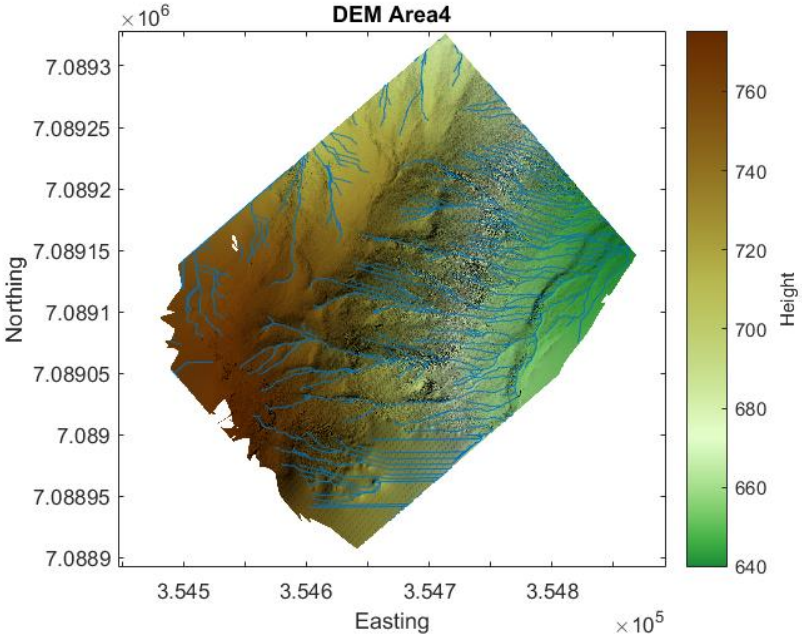
DEM Area4
×10^6
7.0893
7.08925
7.0892
7.08915
7.0891
7.08905
7.089
7.08895
7.0889
Northing
3.545
3.546
3.547
3.548
×10^5
Easting
760
740
720
700
680
660
640
Height

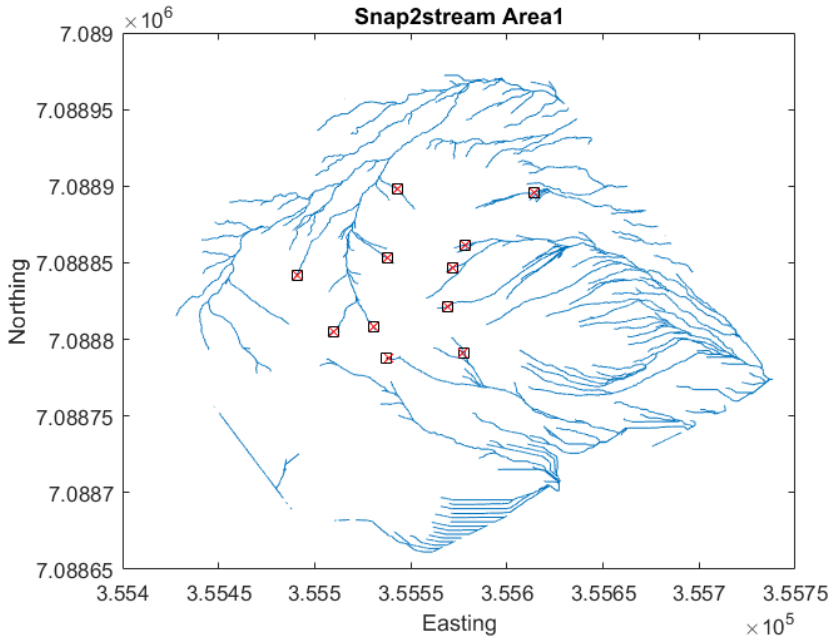
Snap2stream Area1
×10^6
7.089
7.08895
7.0889
7.08885
7.0888
7.08875
7.0887
7.08865
Northing
3.554
3.5545
3.555
3.5555
3.556
3.5565
3.557
3.5575
Easting
×10^5

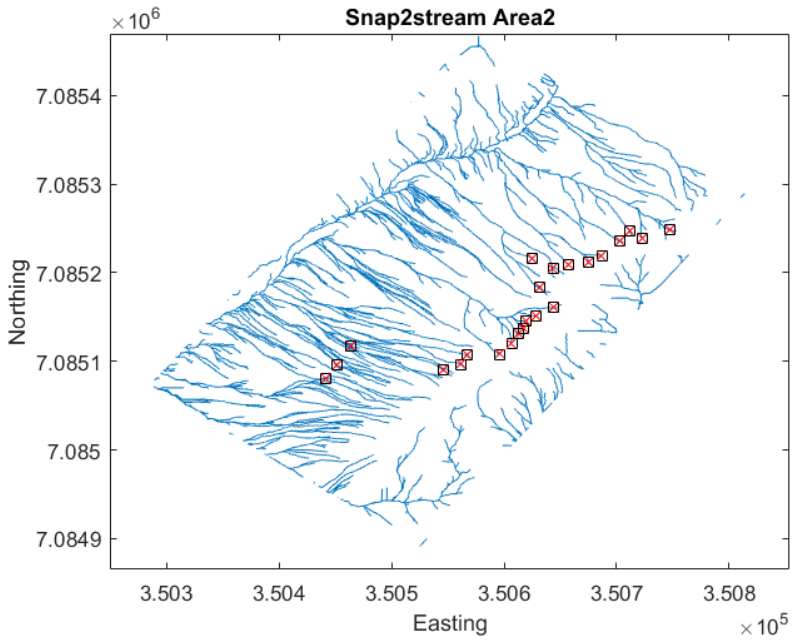
Snap2stream Area2
×10^6
7.0854
7.0853
7.0852
7.0851
7.085
7.0849
Northing
3.503
3.504
3.505
3.506
3.507
3.508
Easting
×10^5

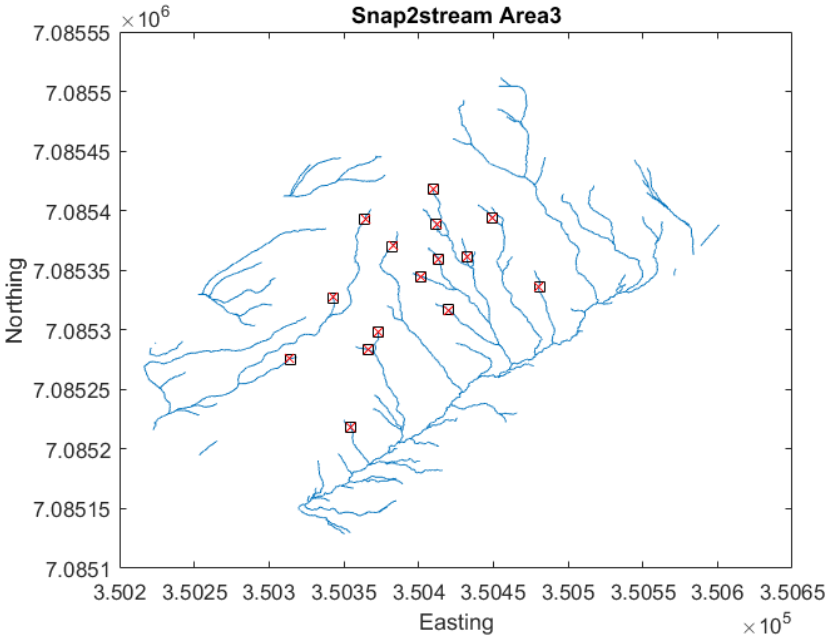
Snap2stream Area3
×10^6
7.08555
7.0855
7.08545
7.0854
7.08535
7.0853
7.08525
7.0852
7.08515
7.0851
Northing
3.502
3.5025
3.503
3.5035
3.504
3.5045
3.505
3.5055
3.506
3.5065
Easting
×10^5

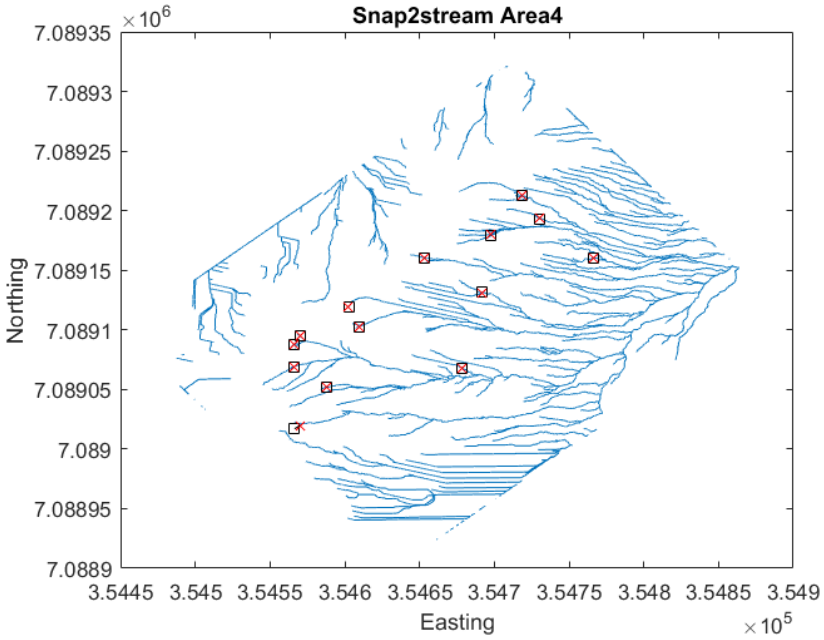
Snap2stream Area4
×10^6
7.08935
7.0893
7.08925
7.0892
7.08915
7.0891
7.08905
7.089
7.08895
7.0889
Northing
3.5445
3.545
3.5455
3.546
3.5465
3.547
3.5475
3.548
3.5485
3.549
Easting
×10^5

a.

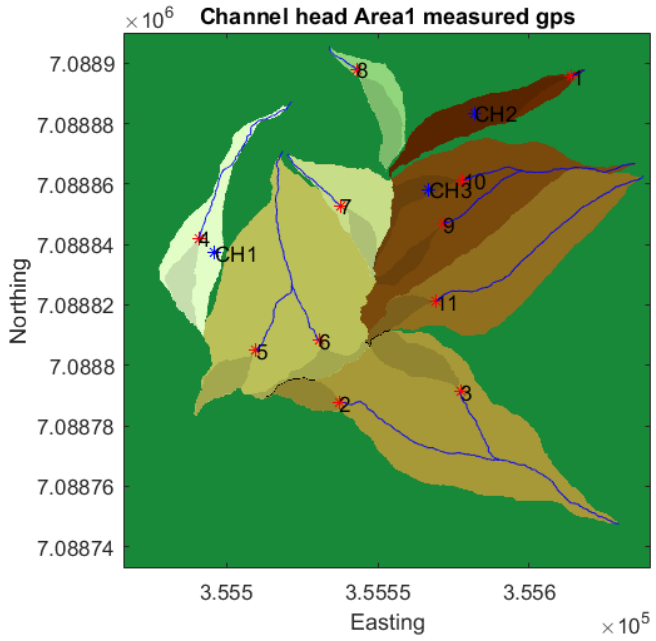
Channel head Area1 measured gps
×10^6
7.0889
7.08888
7.08886
7.08884
7.08882
7.0888
7.08878
7.08876
7.08874
Northing
3.555
3.5555
3.556
Easting
×10^5
CH1
CH2
CH3

b.

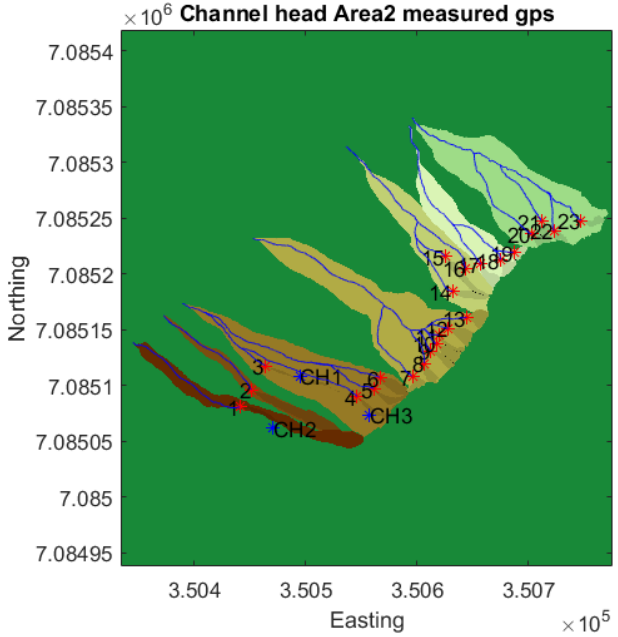
Channel head Area2 measured gps
×10^6
7.0854
7.08535
7.0853
7.08525
7.0852
7.08515
7.0851
7.08505
7.085
7.08495
Northing
3.504
3.505
3.506
3.507
Easting
×10^5
CH1
CH2
CH3

c.

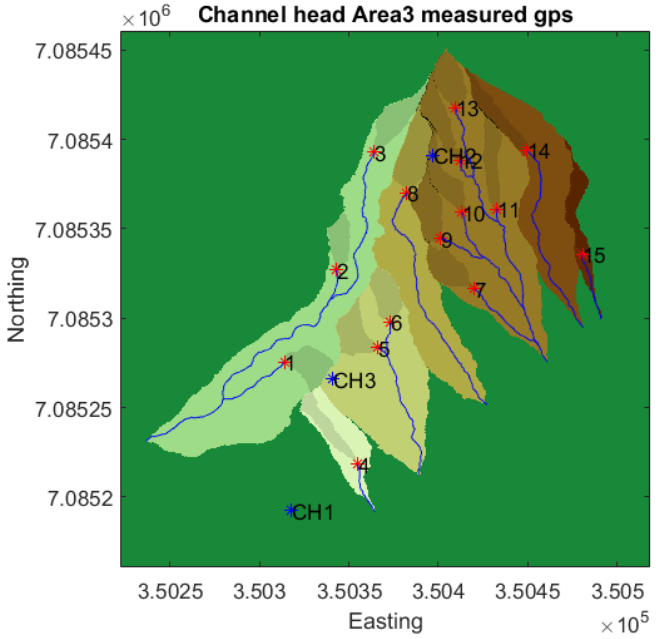
Channel head Area3 measured gps
×10^6
7.08545
7.0854
7.08535
7.0853
7.08525
7.0852
Northing
3.5025
3.503
3.5035
3.504
3.5045
3.505
Easting
×10^5
CH1
CH2
CH3

d.

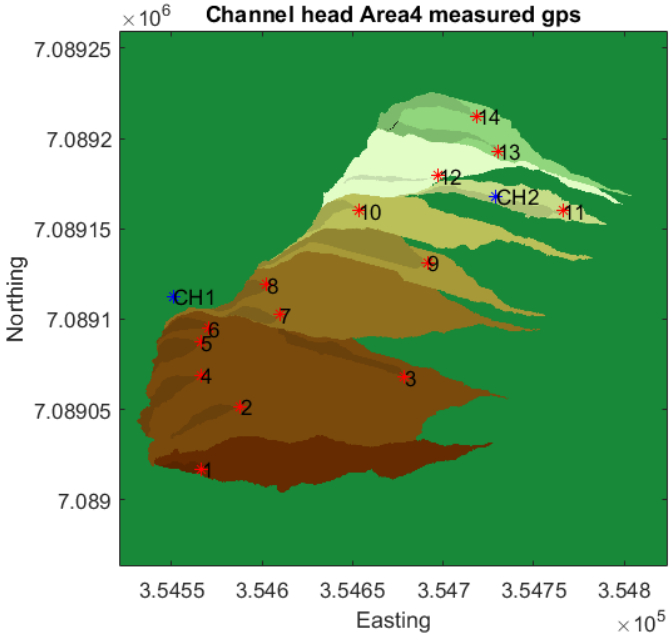
Channel head Area4 measured gps
×10^6
7.08925
7.0892
7.08915
7.0891
7.08905
7.089
Northing
3.5455
3.546
3.5465
3.547
3.5475
3.548
Easting
×10^5
CH1
CH2

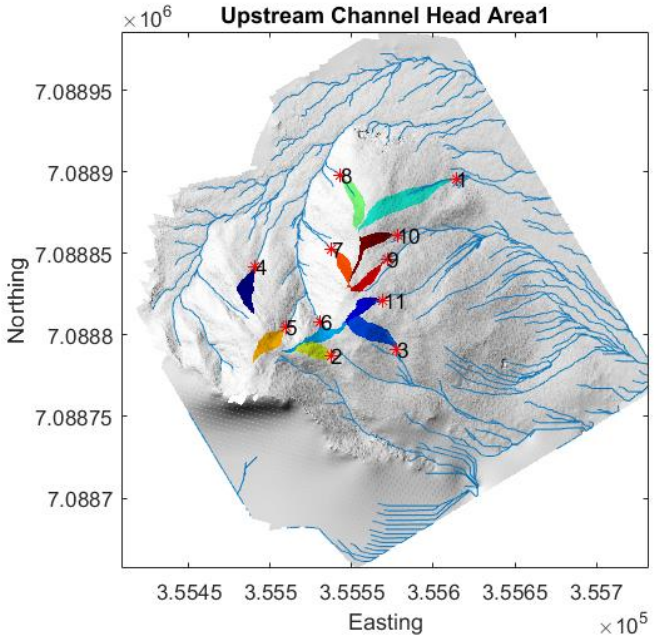
Upstream Channel Head Area1
×10^6
7.08895
7.0889
7.08885
7.0888
7.08875
7.0887
Northing
3.5545
3.555
3.5555
3.556
3.5565
3.557
×10^5
Easting

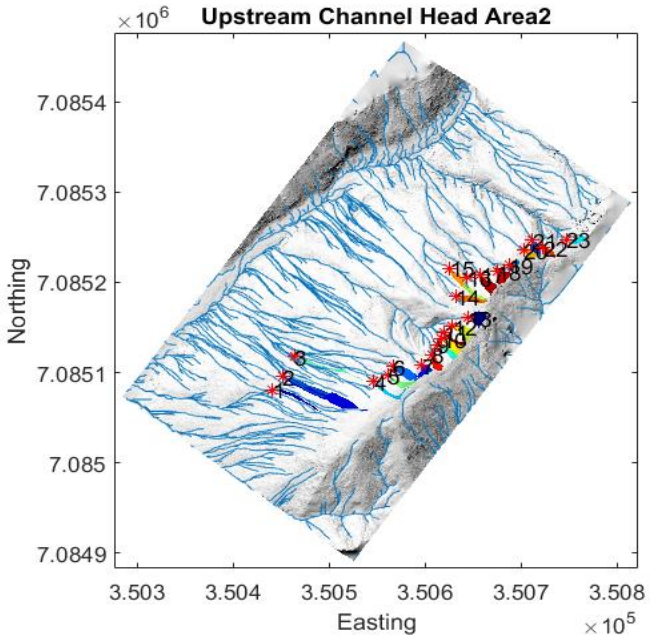
Upstream Channel Head Area2
×10^6
7.0854
7.0853
7.0852
7.0851
7.085
7.0849
Northing
3.503
3.504
3.505
3.506
3.507
3.508
×10^5
Easting

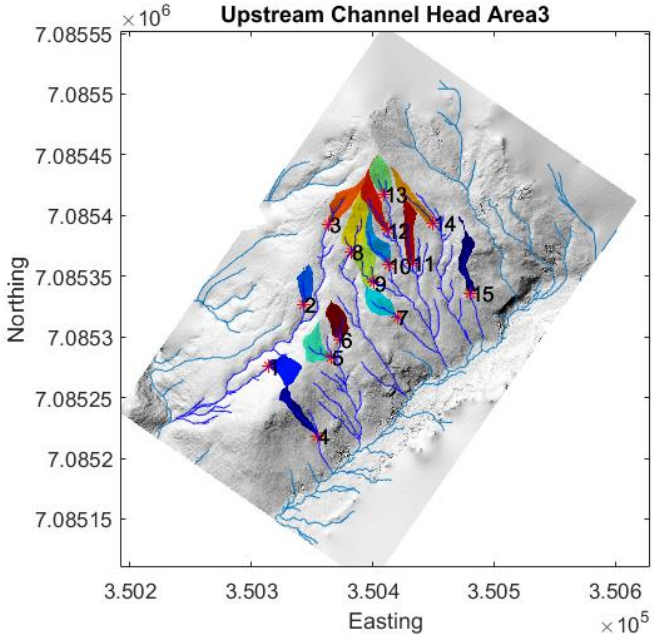
Upstream Channel Head Area3
×10^6
7.08555
7.0855
7.08545
7.0854
7.08535
7.0853
7.08525
7.0852
7.08515
Northing
3.502
3.503
3.504
3.505
3.506
×10^5
Easting

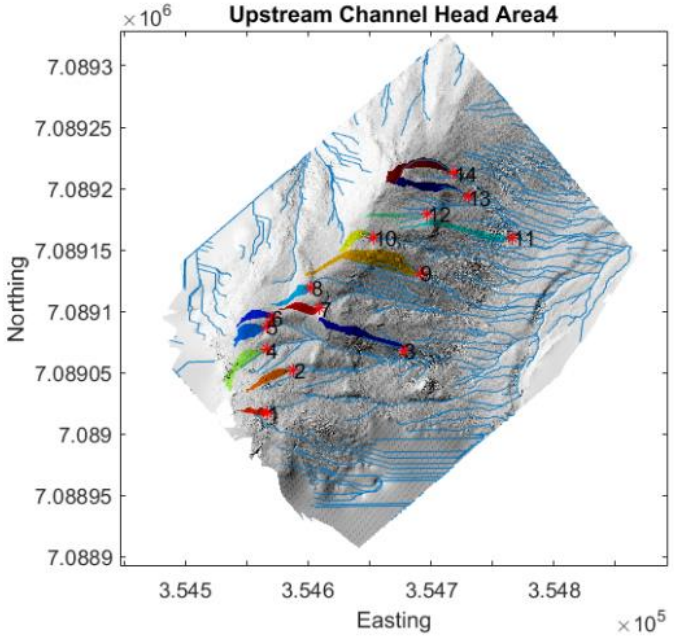
Upstream Channel Head Area4
×10^6
7.0893
7.08925
7.0892
7.08915
7.0891
7.08905
7.089
7.08895
7.0889
Northing
3.545
3.546
3.547
3.548
×10^5
Easting

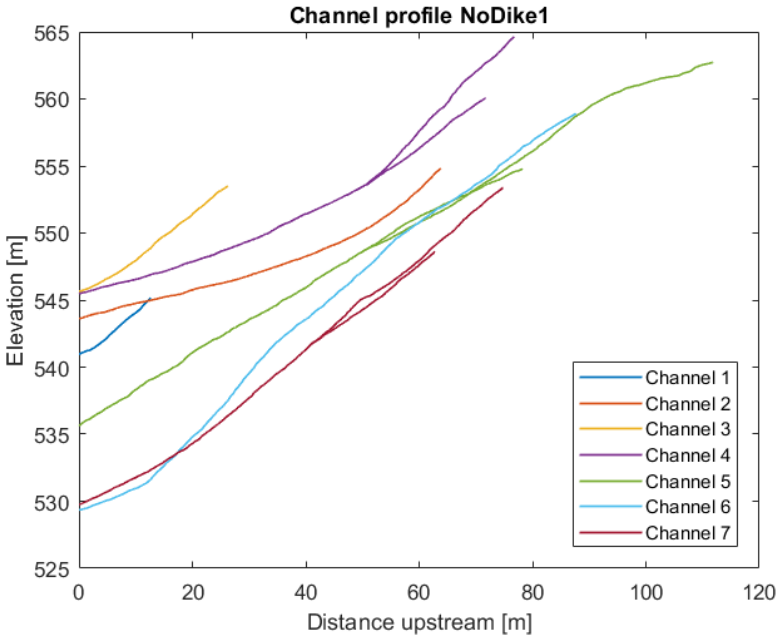
Channel profile NoDike1
Elevation [m]
Distance upstream [m]
Channel 1
Channel 2
Channel 3
Channel 4
Channel 5
Channel 6
Channel 7

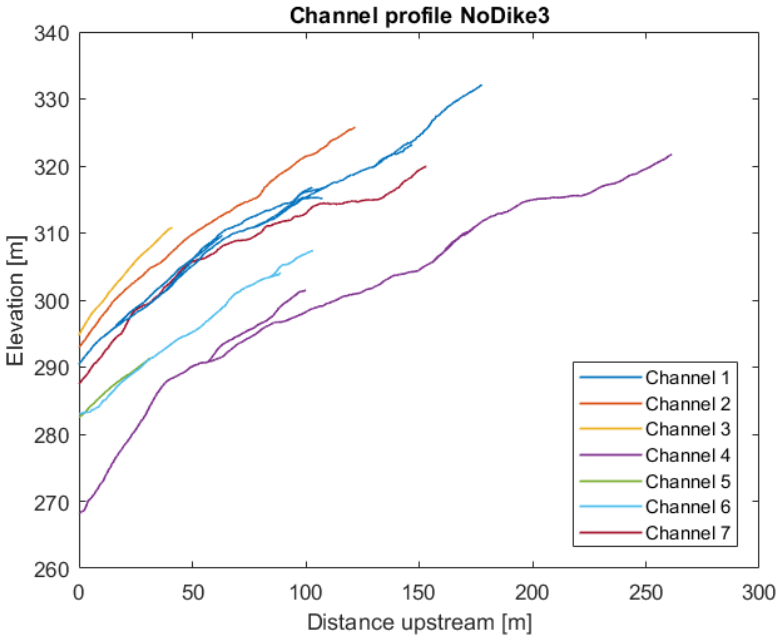
Channel profile NoDike3
Elevation [m]
Distance upstream [m]
Channel 1
Channel 2
Channel 3
Channel 4
Channel 5
Channel 6
Channel 7

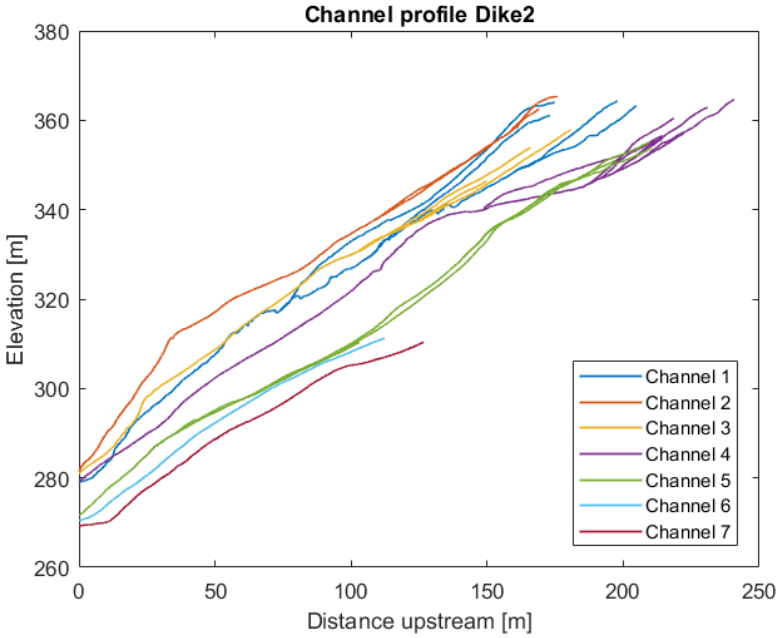
Channel profile Dike2
Elevation [m]
Distance upstream [m]
Channel 1
Channel 2
Channel 3
Channel 4
Channel 5
Channel 6
Channel 7

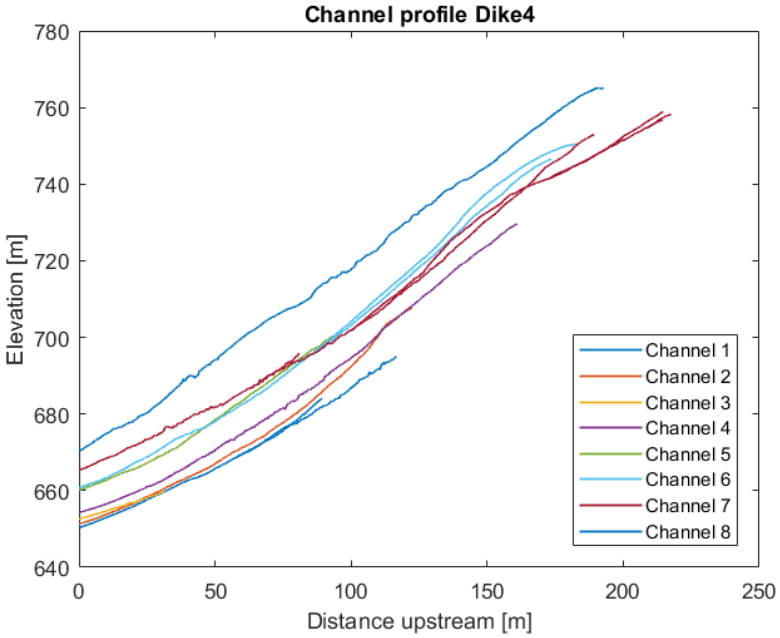
Channel profile Dike4
Elevation [m]
Distance upstream [m]
Channel 1
Channel 2
Channel 3
Channel 4
Channel 5
Channel 6
Channel 7
Channel 8

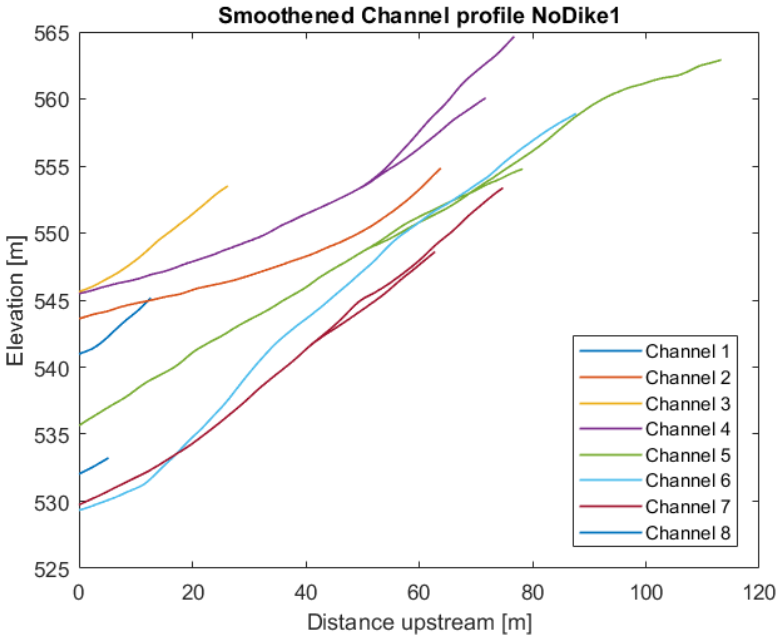
Smoothened Channel profile NoDike1
Elevation [m]
Distance upstream [m]
Channel 1
Channel 2
Channel 3
Channel 4
Channel 5
Channel 6
Channel 7
Channel 8

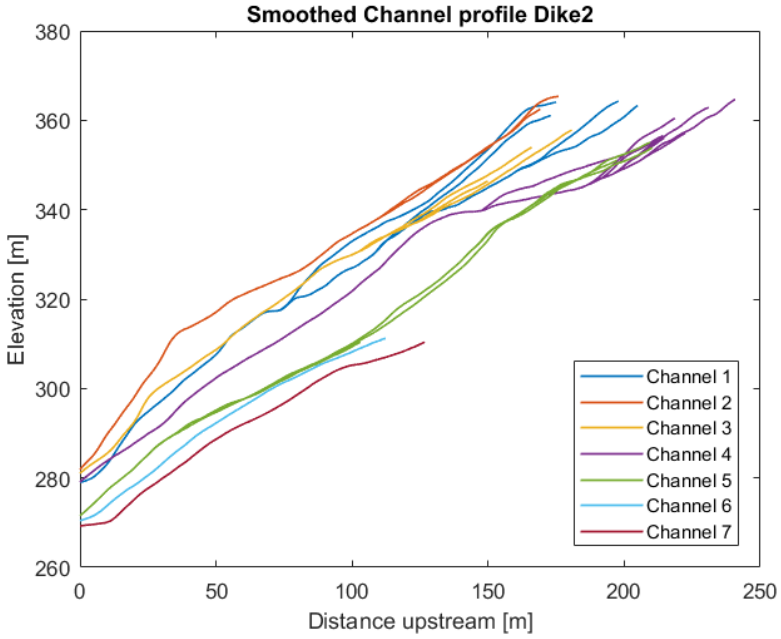
Smoothed Channel profile Dike2
Elevation [m]
Distance upstream [m]
Channel 1
Channel 2
Channel 3
Channel 4
Channel 5
Channel 6
Channel 7

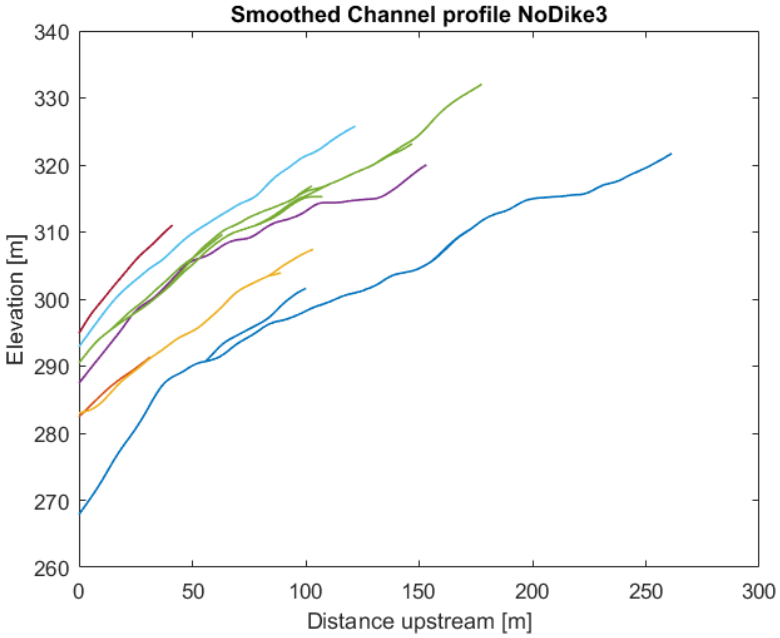
Smoothed Channel profile NoDike3
Elevation [m]
Distance upstream [m]

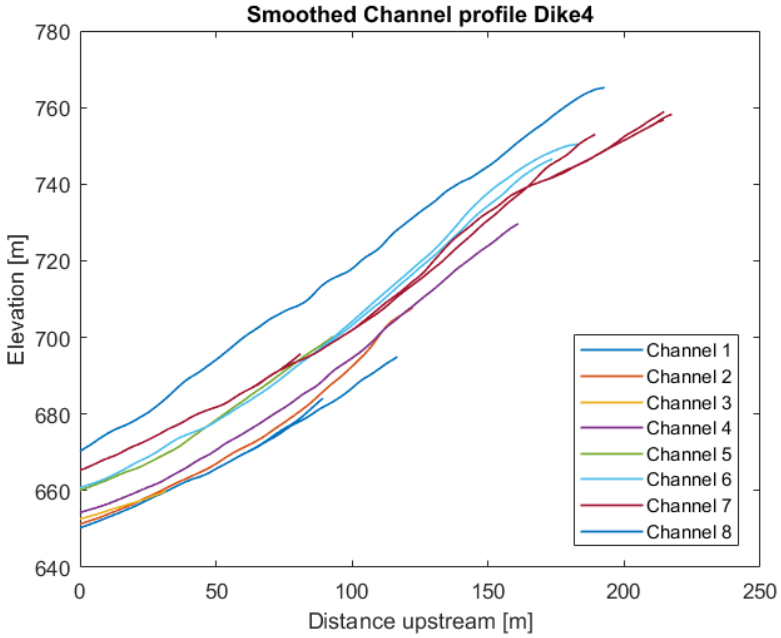
Smoothed Channel profile Dike4
Elevation [m]
Distance upstream [m]
Channel 1
Channel 2
Channel 3
Channel 4
Channel 5
Channel 6
Channel 7
Channel 8

a.

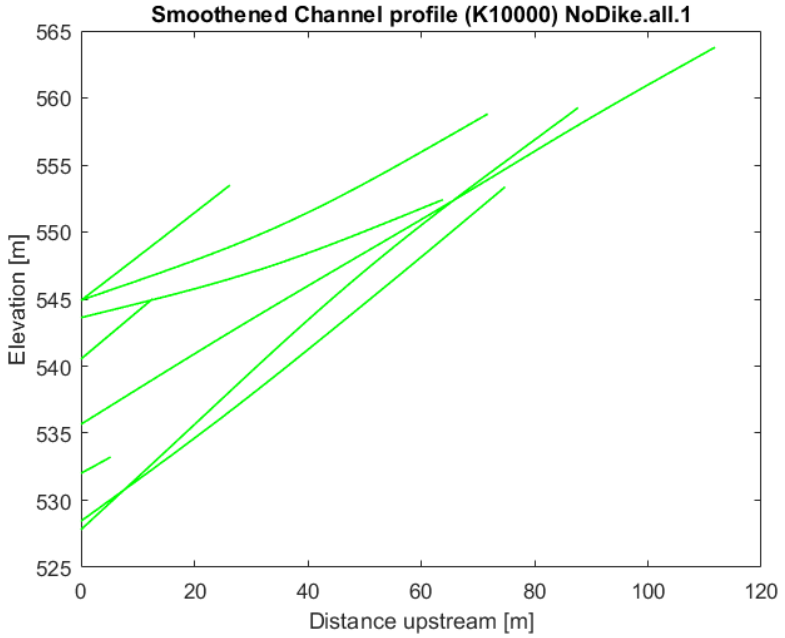
Smoothened Channel profile (K10000) NoDike.all.1
Elevation [m]
Distance upstream [m]
565
560
555
550
545
540
535
530
525
0
20
40
60
80
100
120

b.

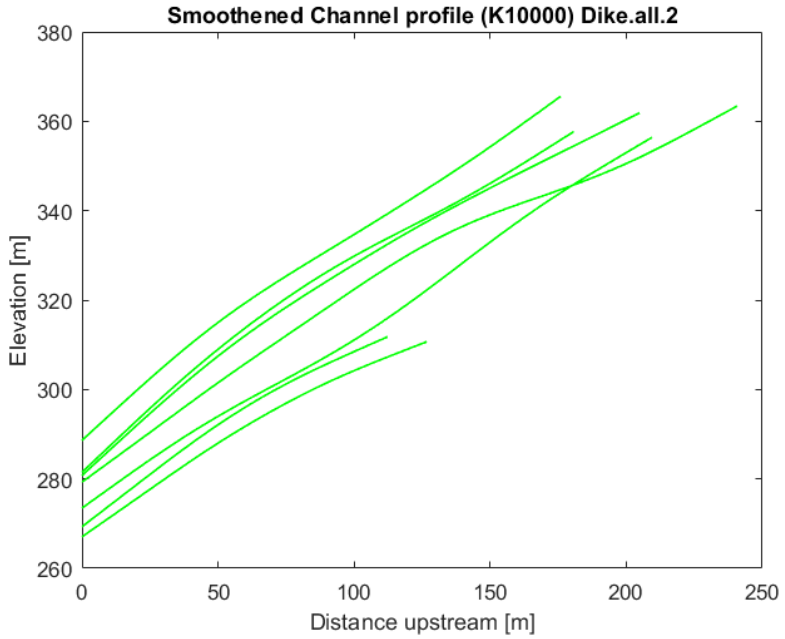
Smoothened Channel profile (K10000) Dike.all.2
Elevation [m]
Distance upstream [m]
380
360
340
320
300
280
260
0
50
100
150
200
250

c.

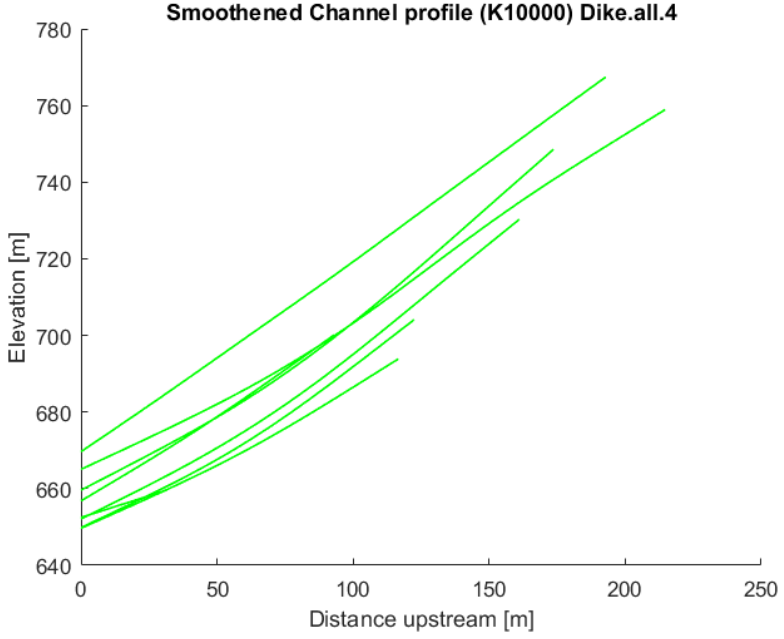
Smoothened Channel profile (K10000) Dike.all.4
Elevation [m]
Distance upstream [m]
780
760
740
720
700
680
660
640
0
50
100
150
200
250

d.

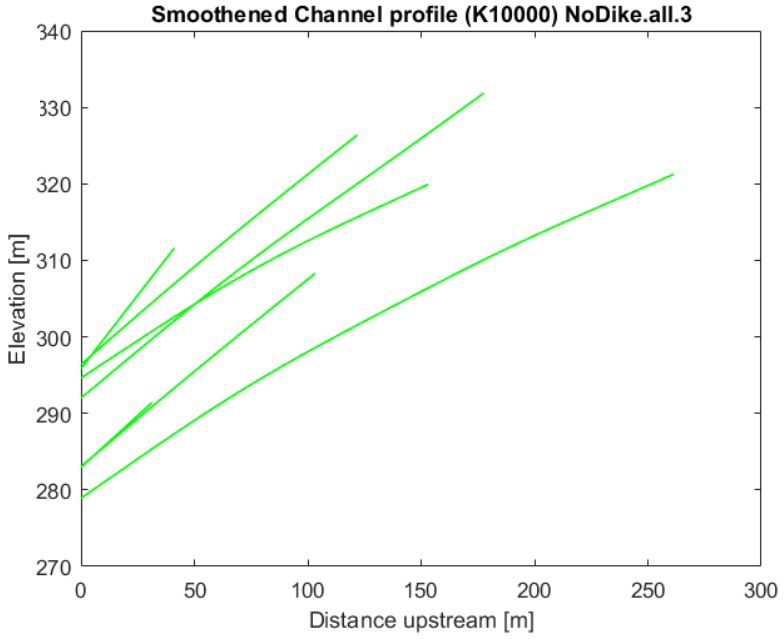
Smoothened Channel profile (K10000) NoDike.all.3
Elevation [m]
Distance upstream [m]
340
330
320
310
300
290
280
270
0
50
100
150
200
250
300

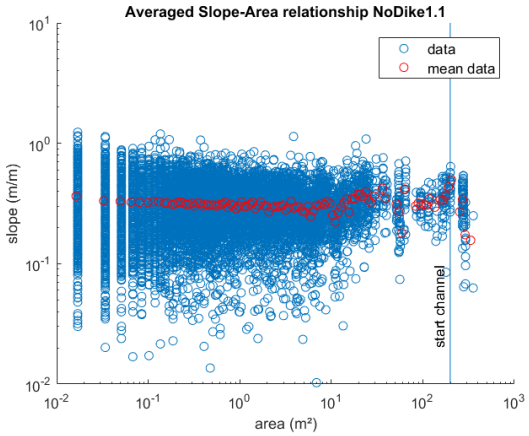

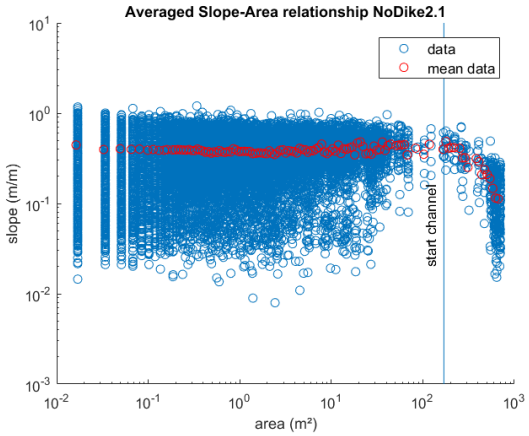

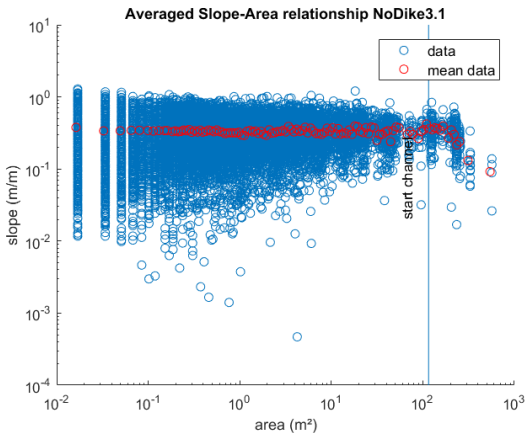

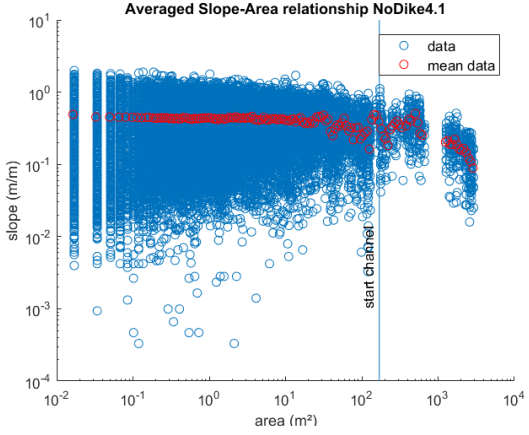

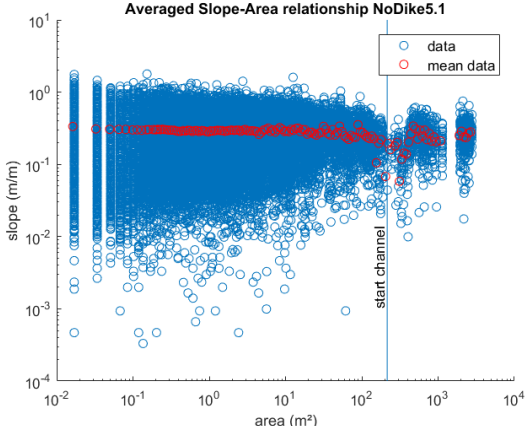

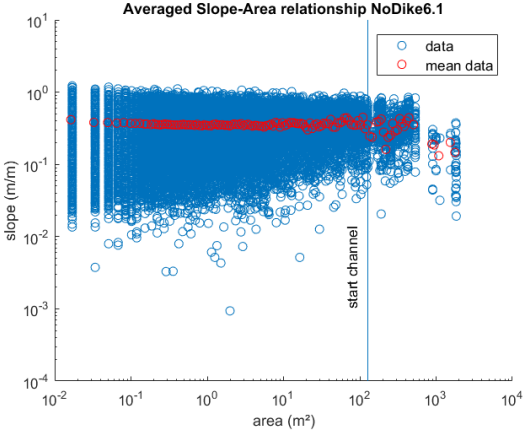

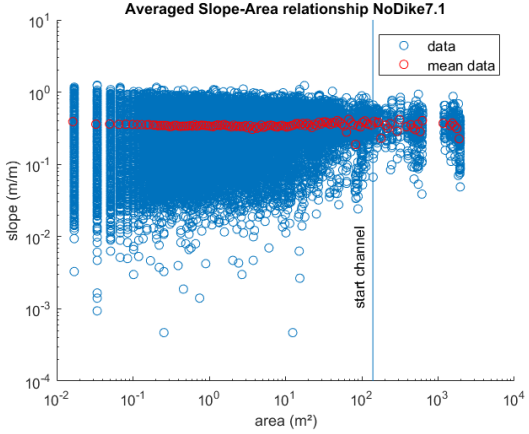

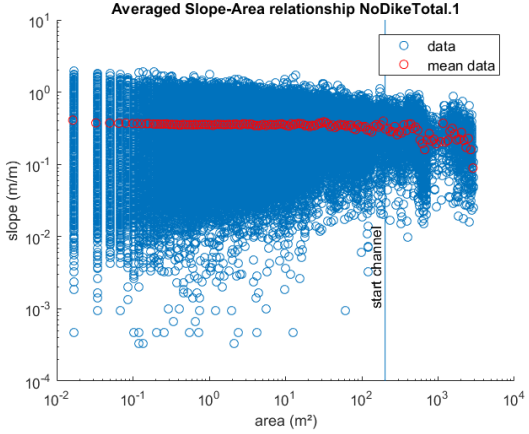

Slope-drainage area relationship with all points for the catchments in study area 1 with no dikes.

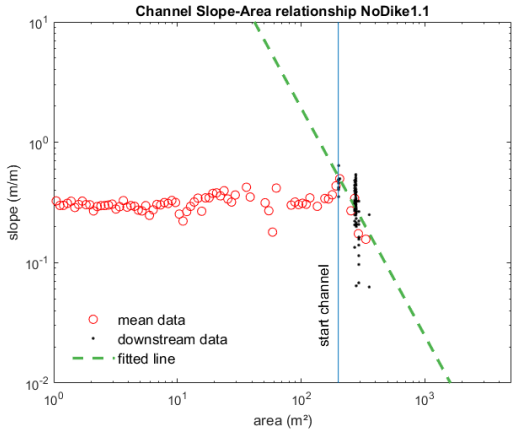

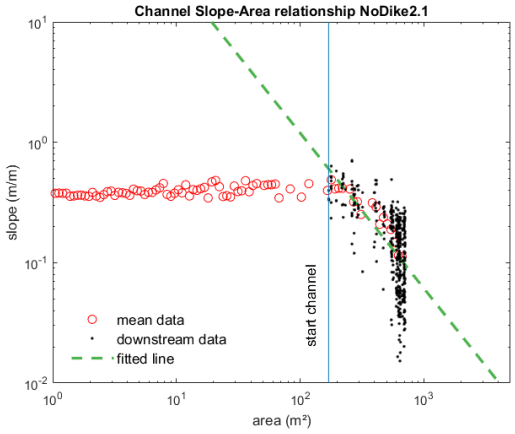

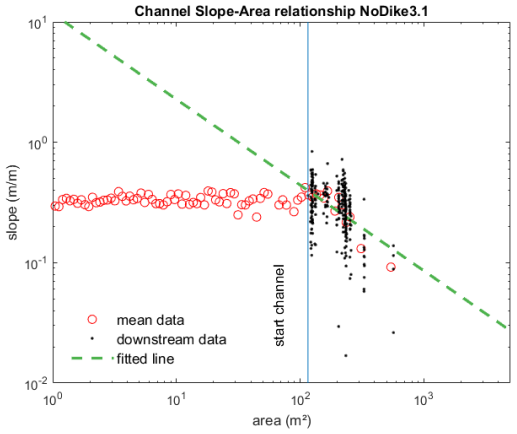

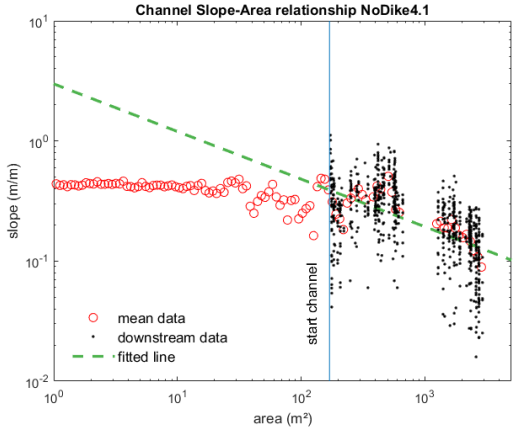

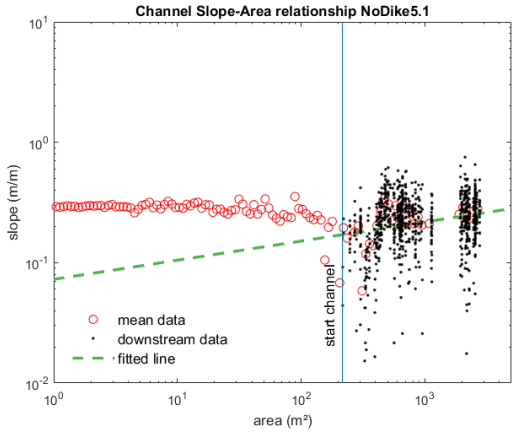

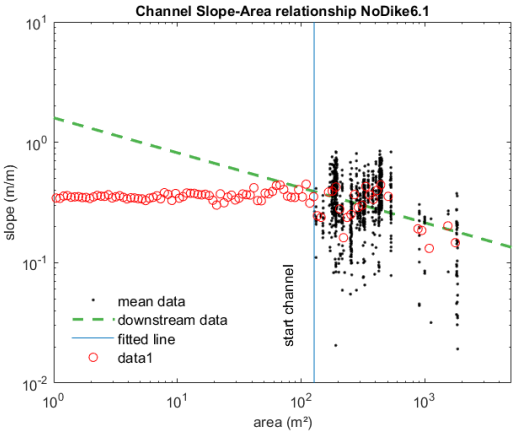

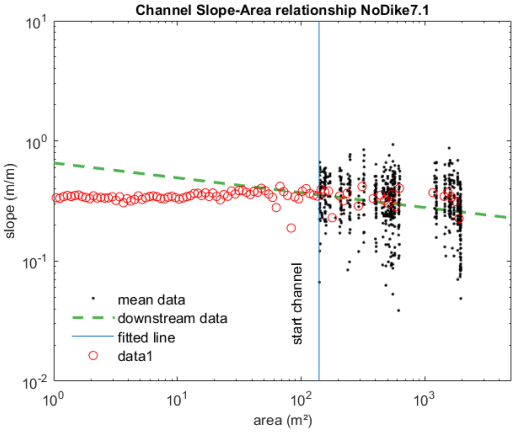

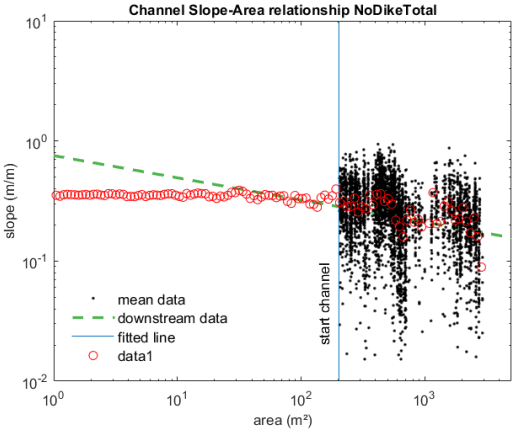

Slope-drainage area relationship with all points for the catchments in study area 1 with no dikes when channels start to incise.

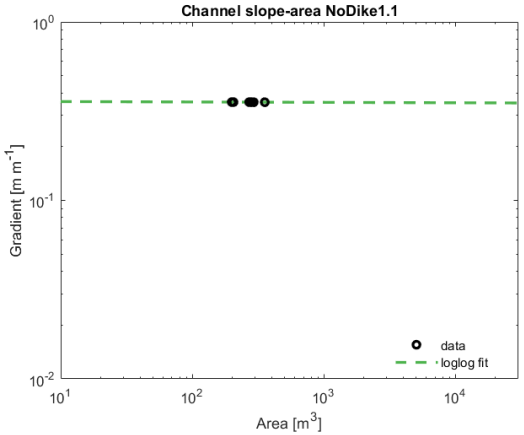

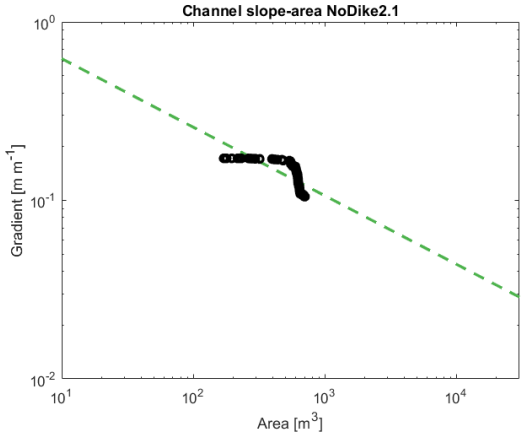

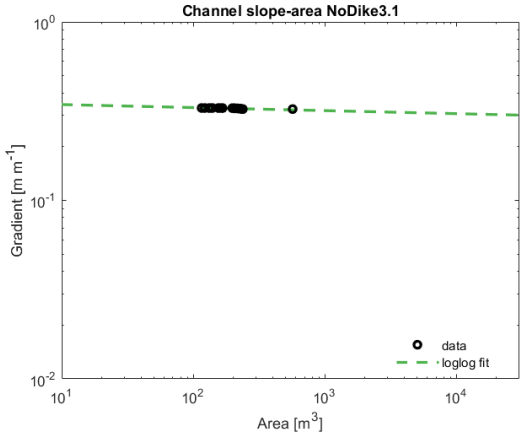

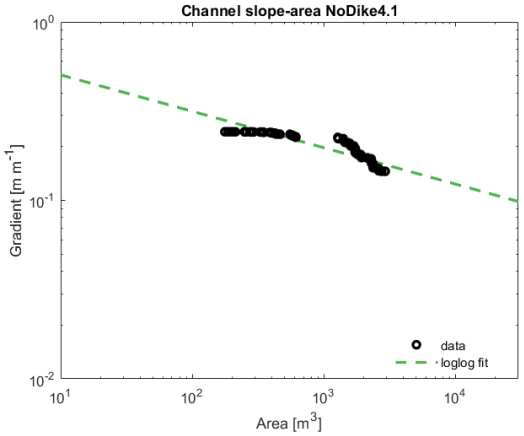

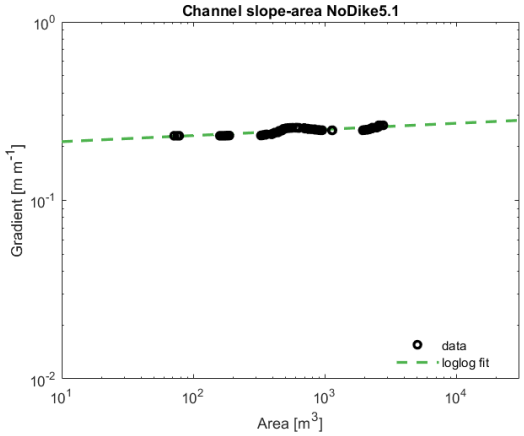

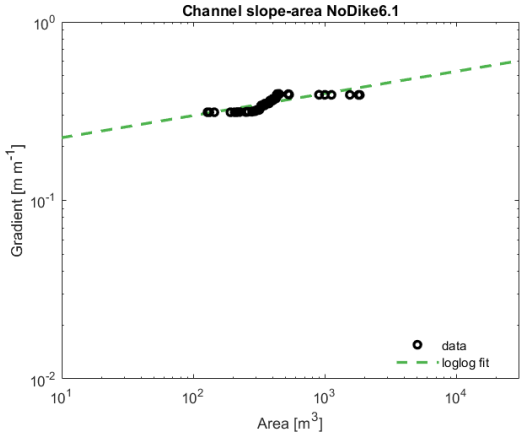

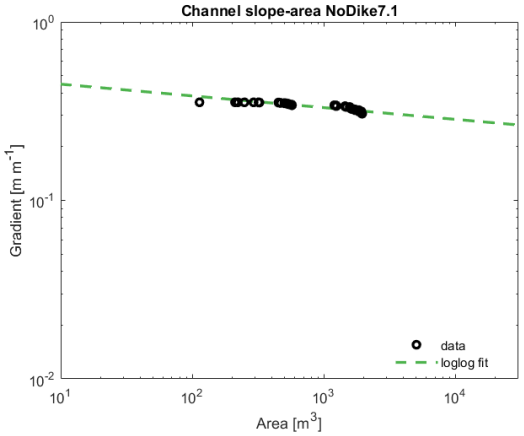

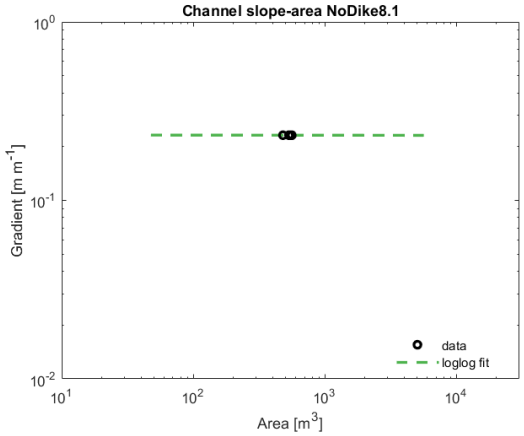

Slope-drainage area relationship with all smoothed data points by K = 10000 with the CRS algorithm for the trunk channels in study area 1 without dikes.

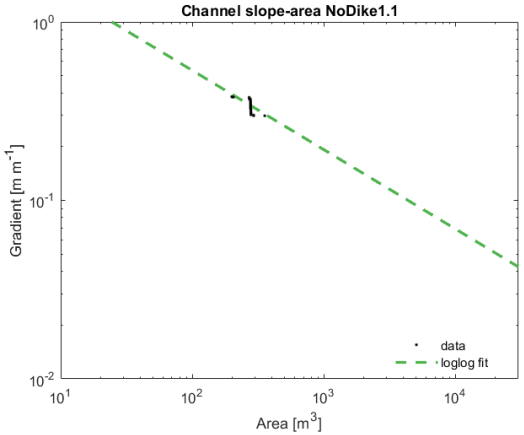

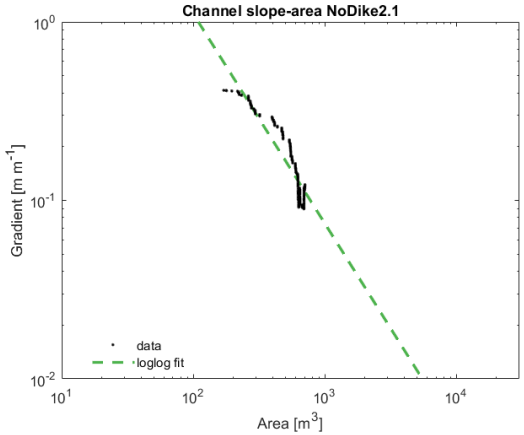

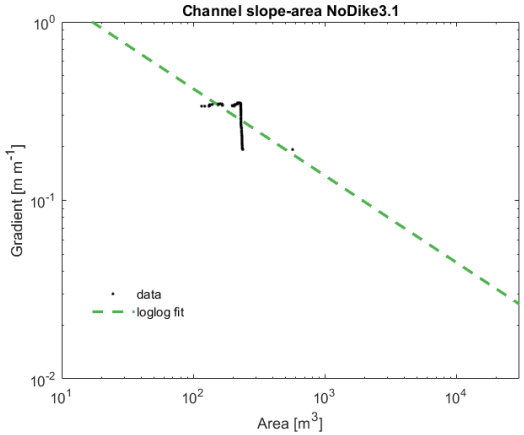

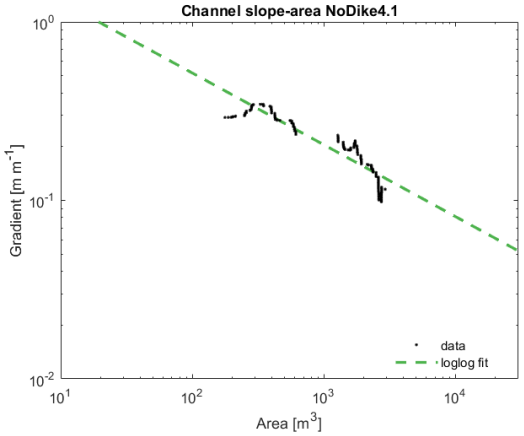

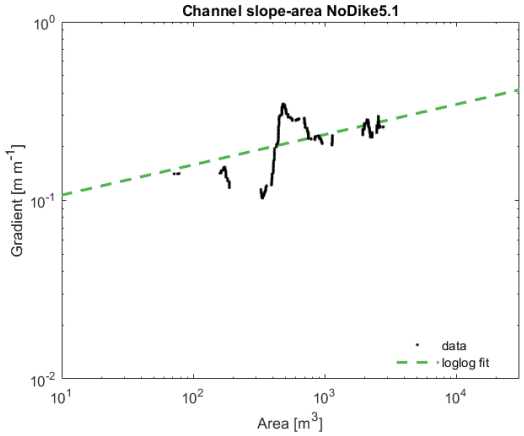

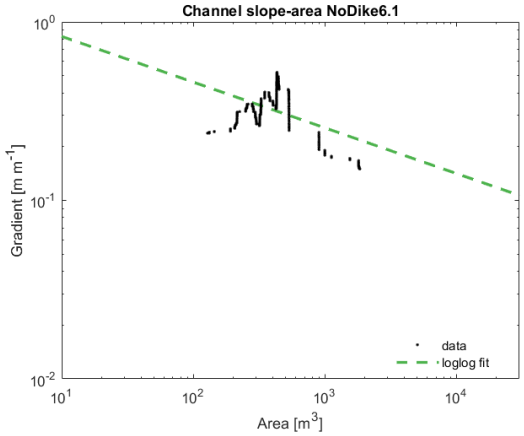

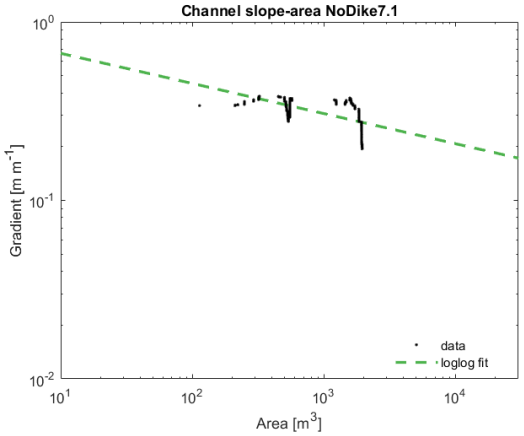

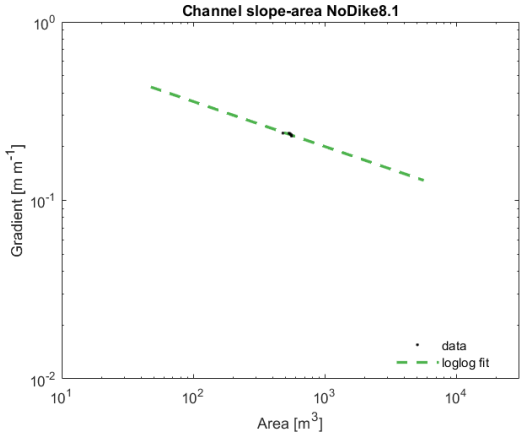

Slope-drainage area relationship with all smoothed points by K=500 with the CRS algorithm for the trunk channels in study area 1 without dikes.

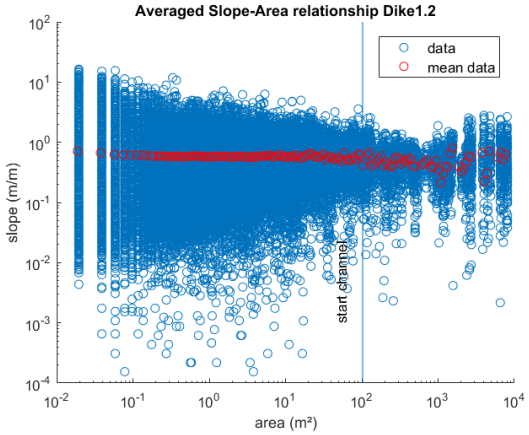

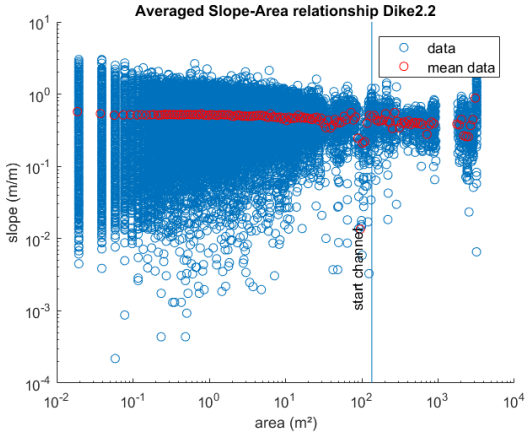

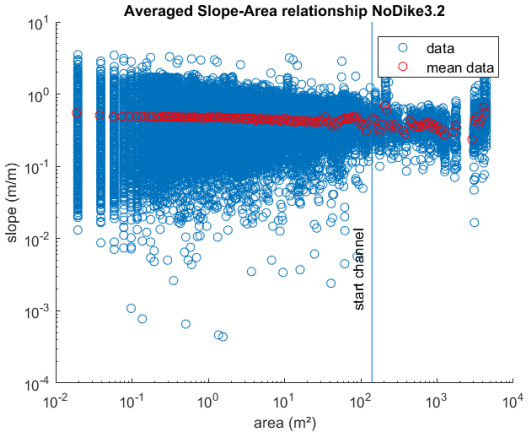

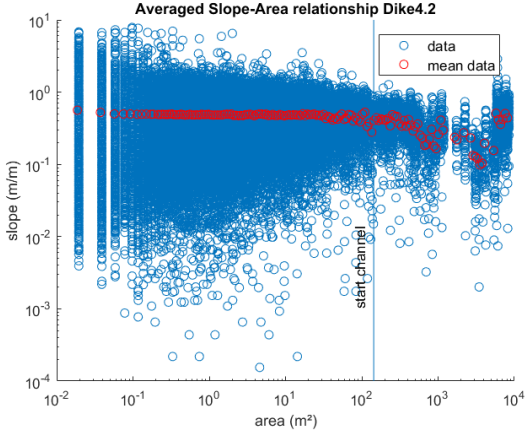

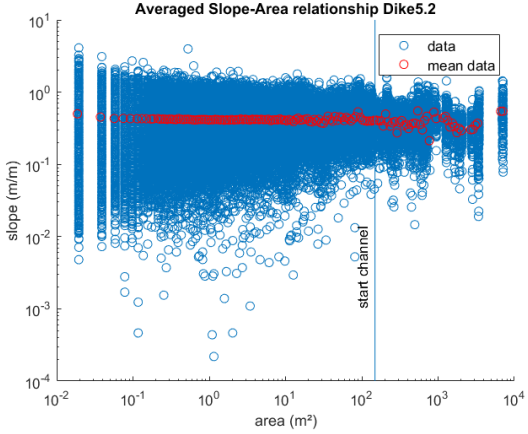

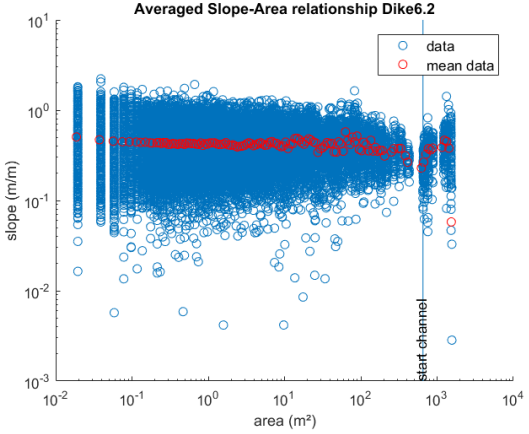

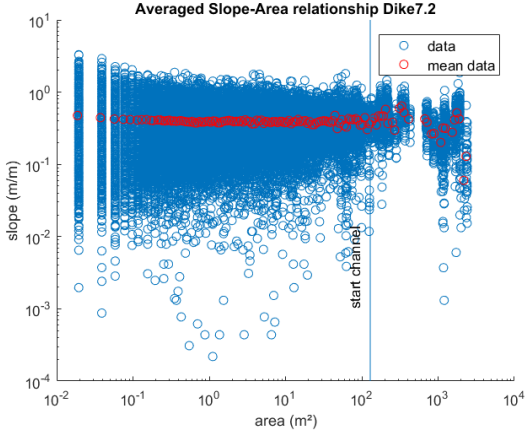

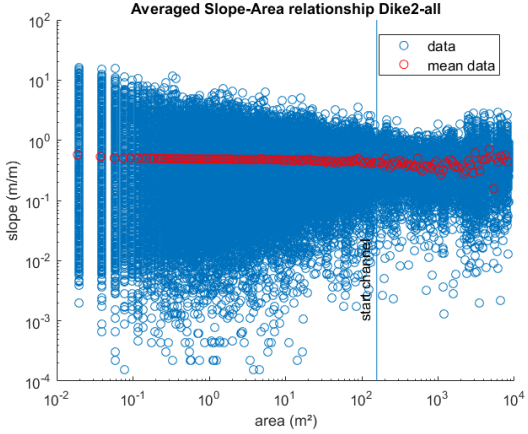

Slope-drainage area relationship with all points for the catchments in study area 2 with dikes.

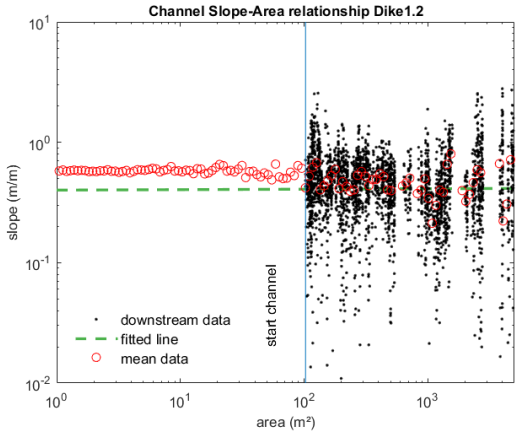

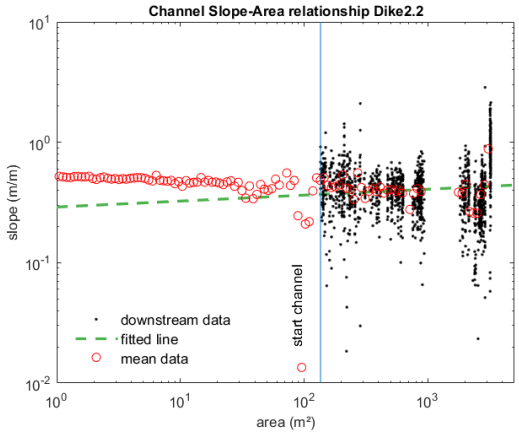

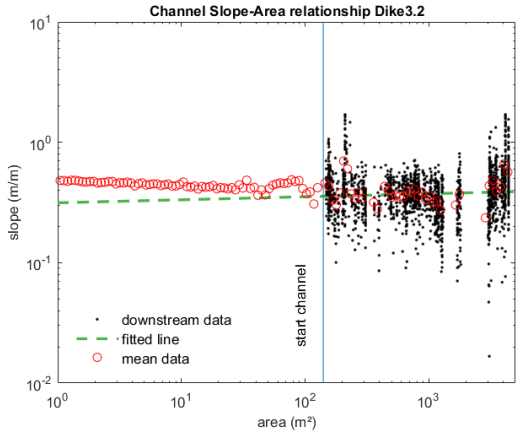

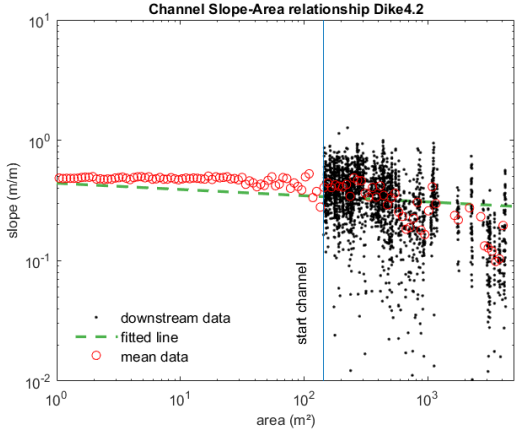

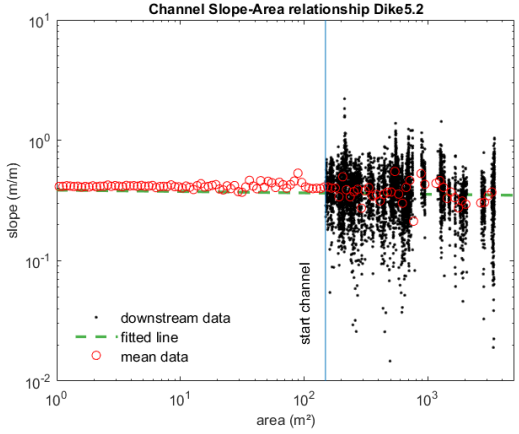

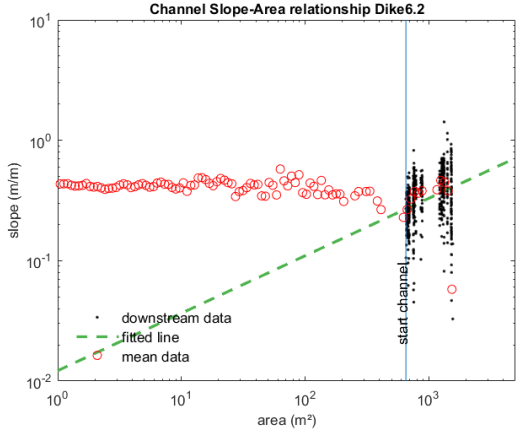

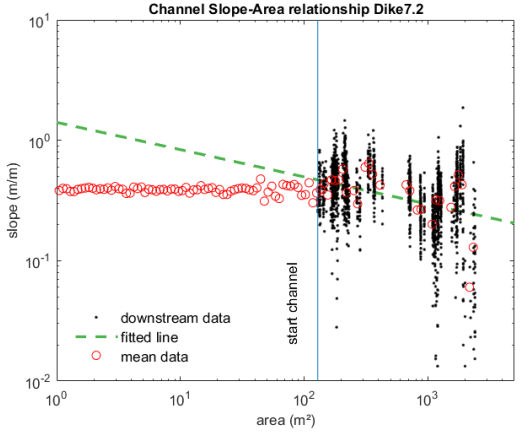

Slope-drainage area relationship with all points for the catchments in study area 2 with dikes when channels start to incise.

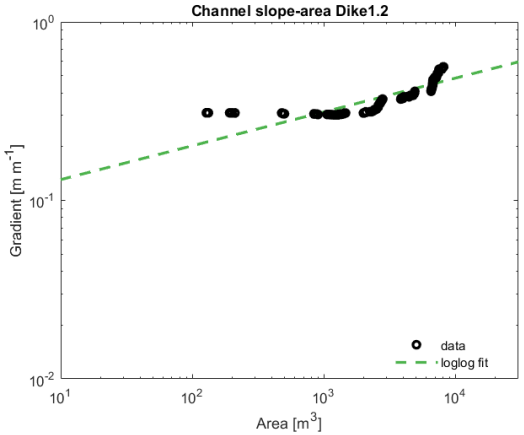

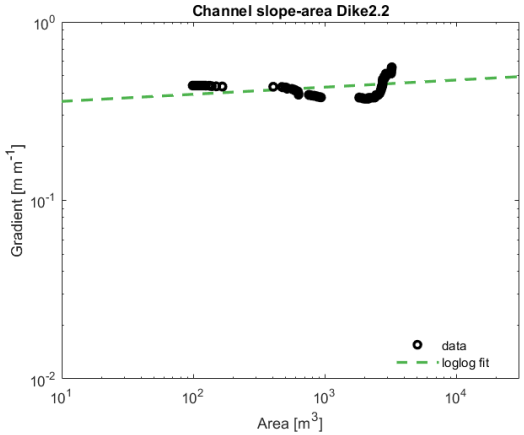

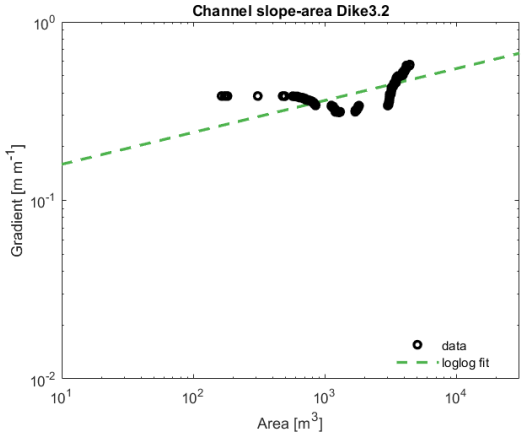

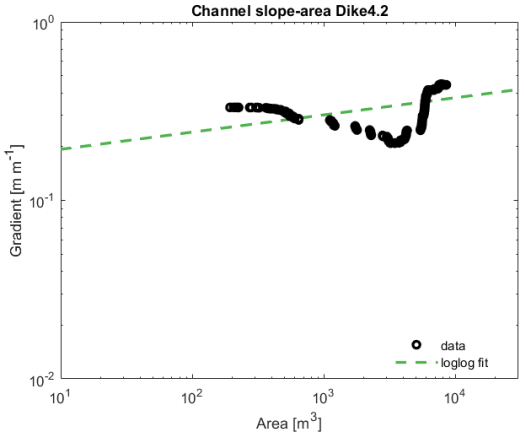

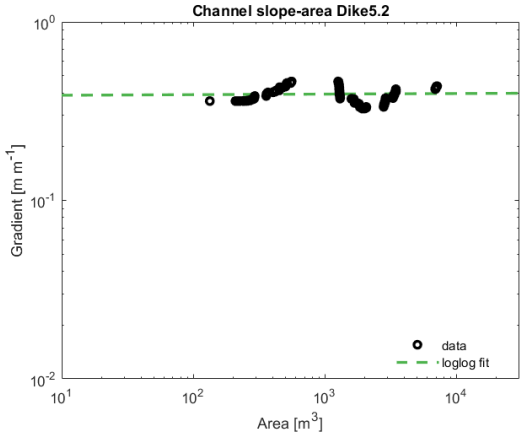

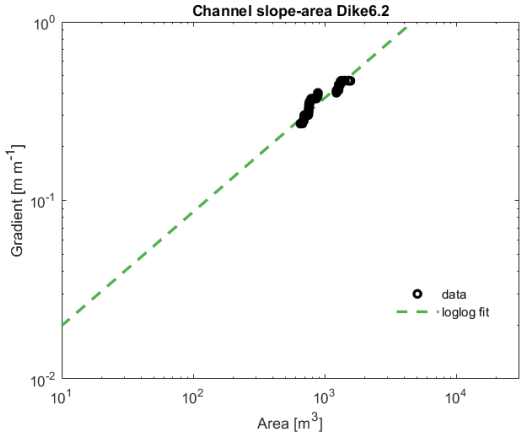

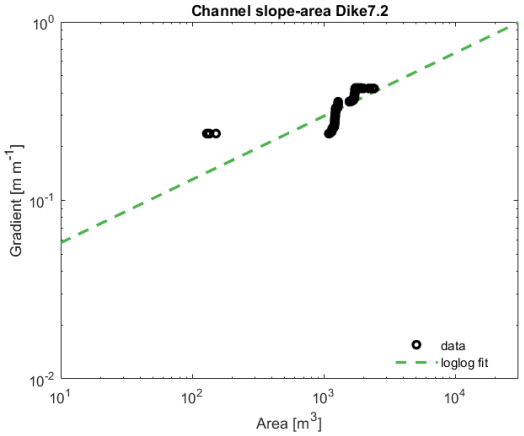

Slope-drainage area relationship with all smoothed data points by K = 10000 with the CRS algorithm for the trunk channels in study area 2 with dikes.

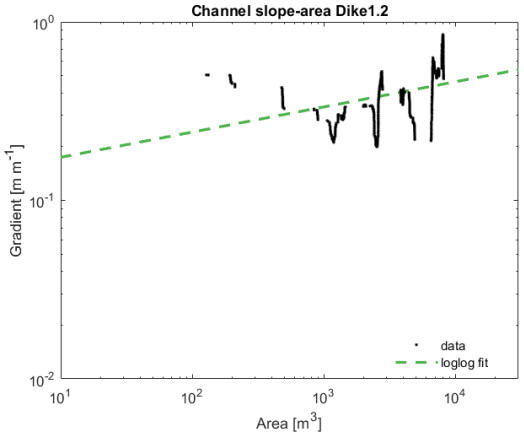

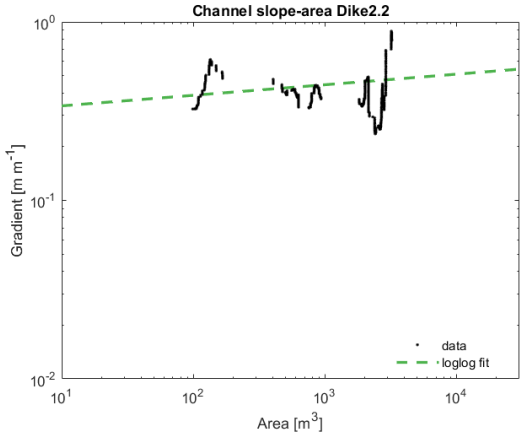

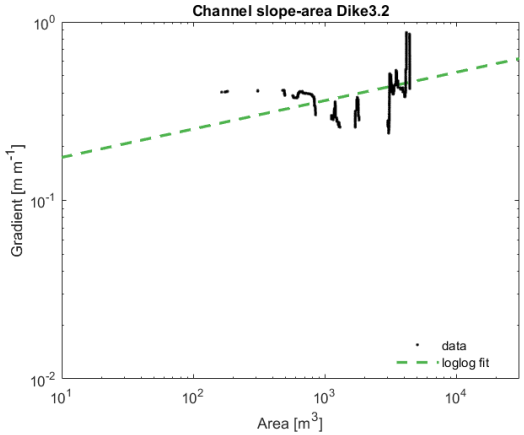

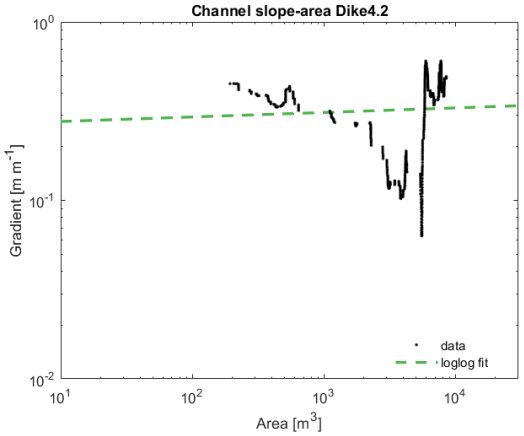

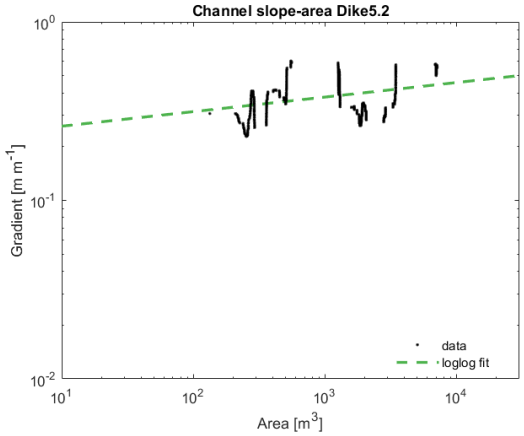

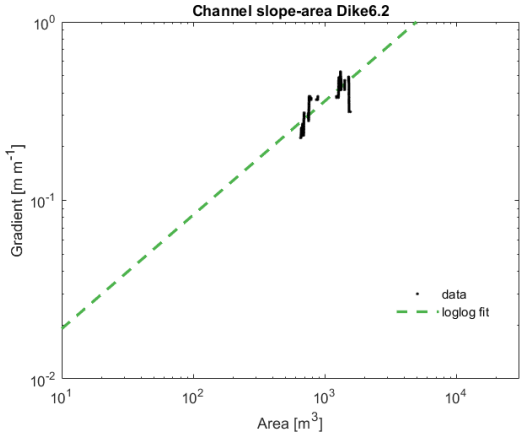

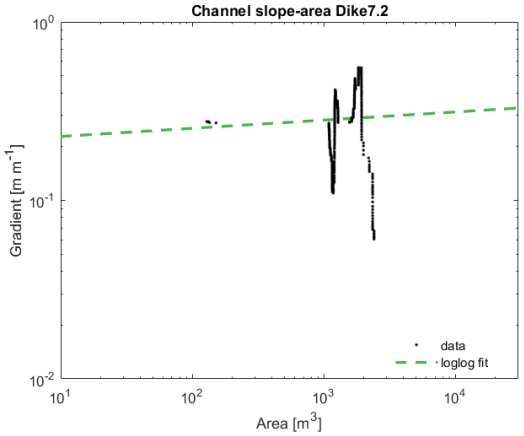

Slope-drainage area relationship with all smoothed data points by K=500 with the CRS algorithm for the trunk channels in study area 2 with dikes.

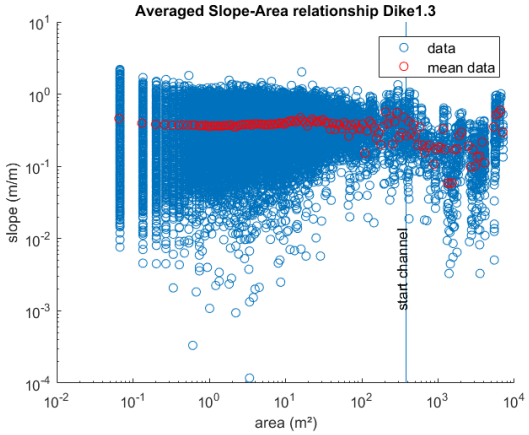

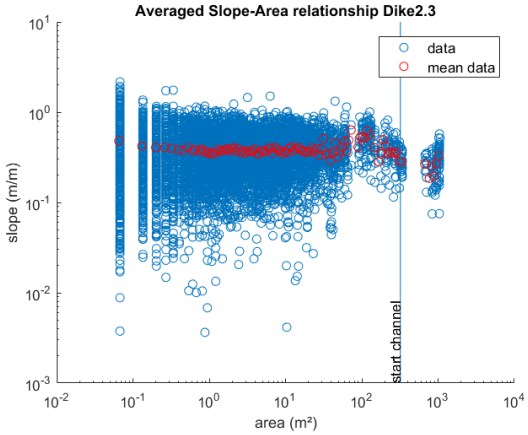

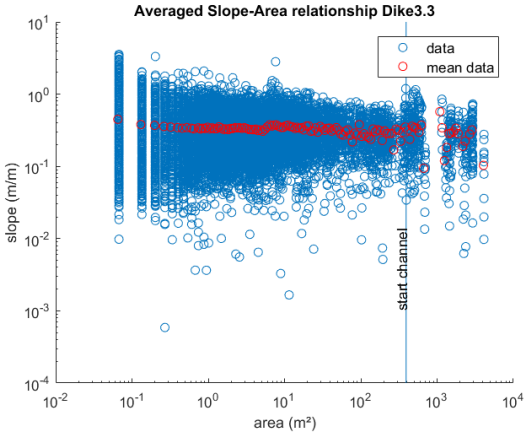

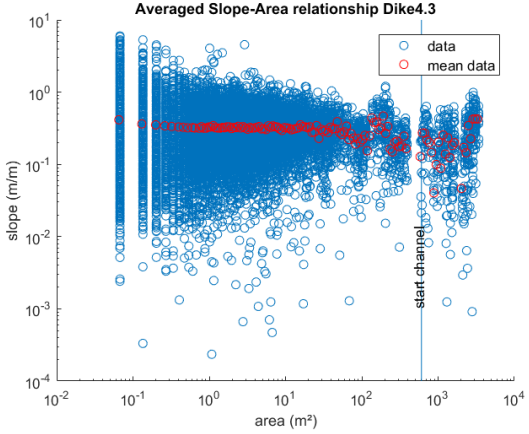

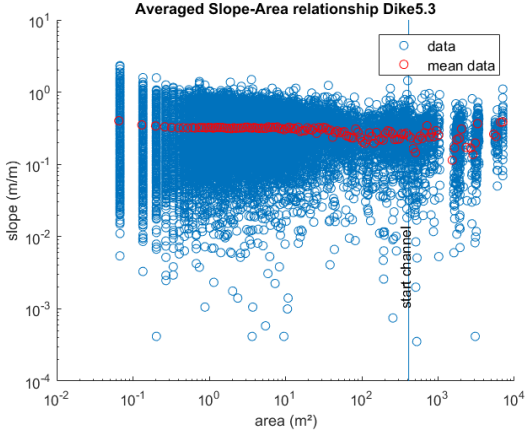

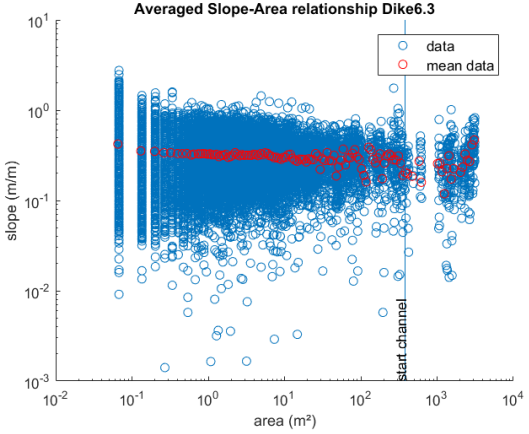

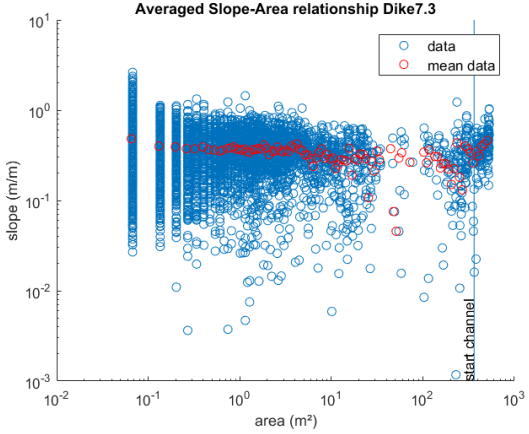

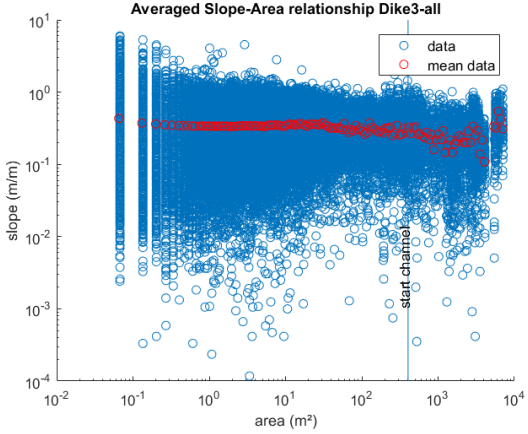

Slope-drainage area relationship with all points for the catchments in study area 3 with no dikes.

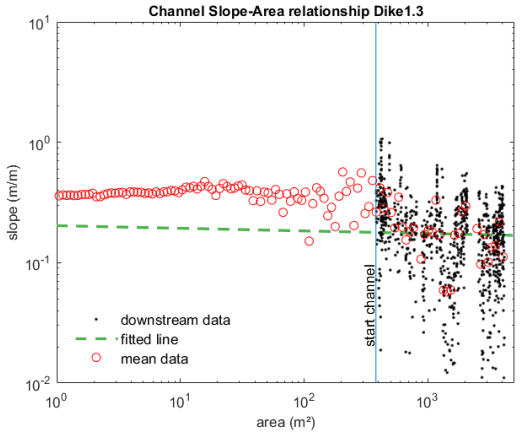

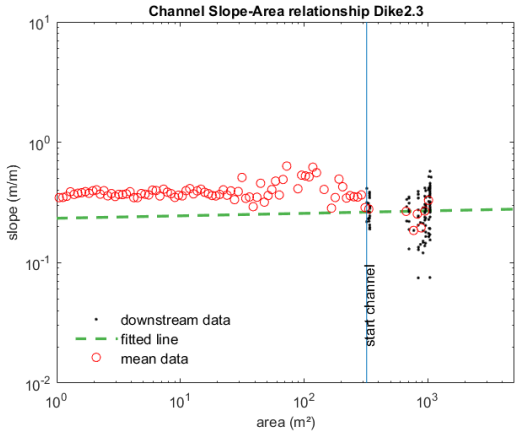

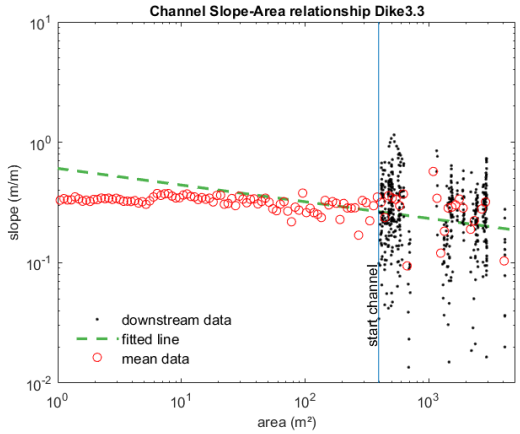

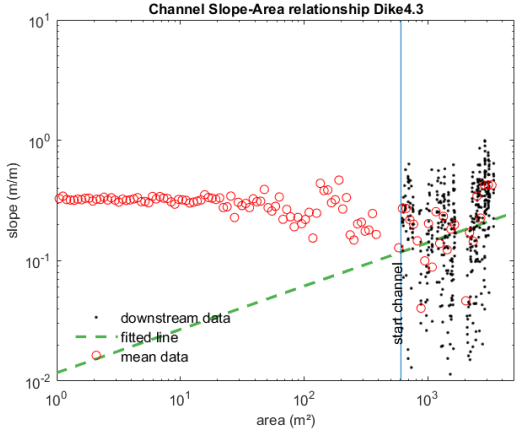

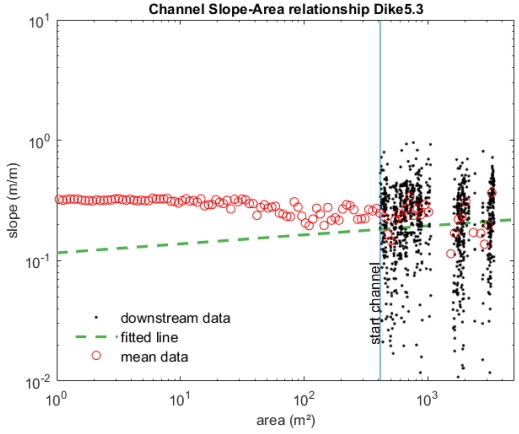

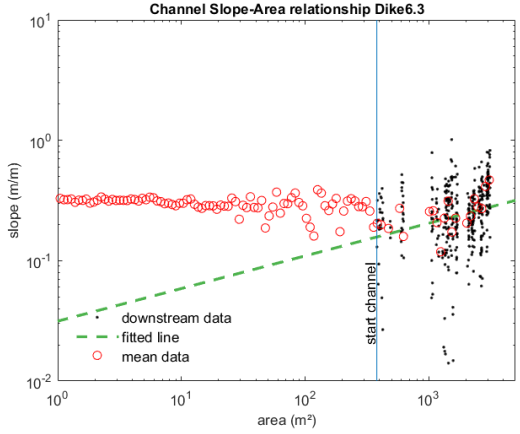

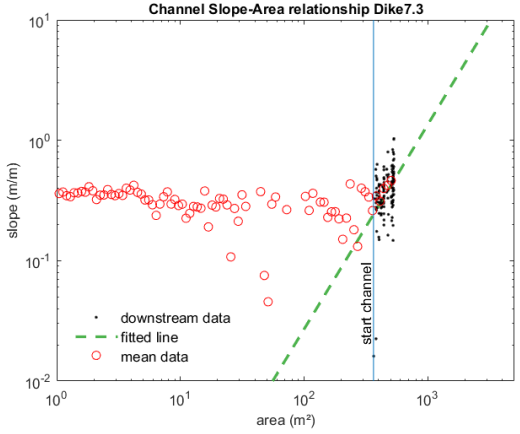

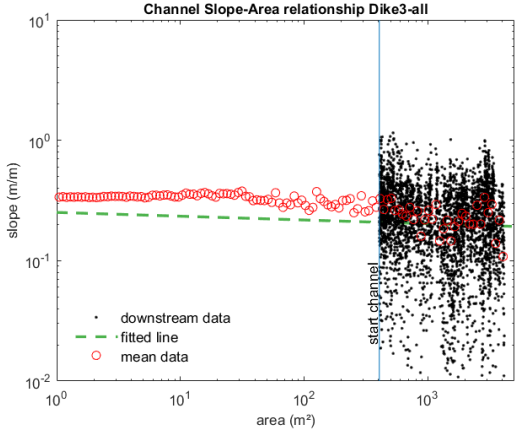

Slope-drainage area relationship with all points for the catchments in study area 3 with no dikes when channels start to incise.

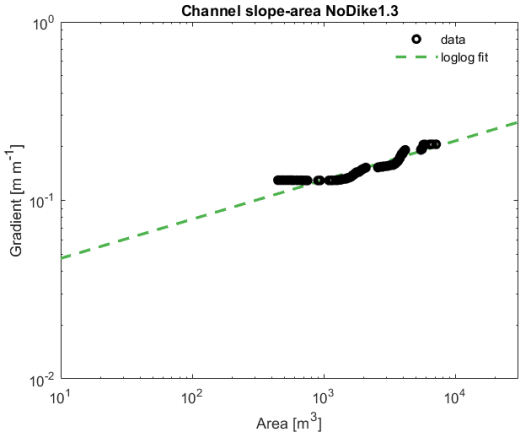

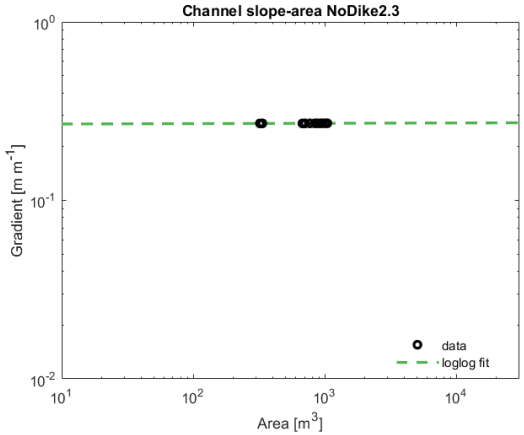

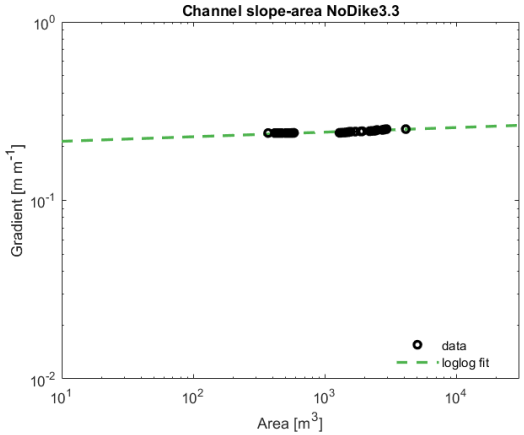

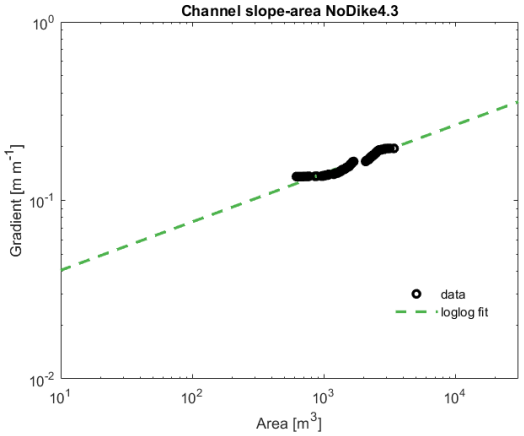

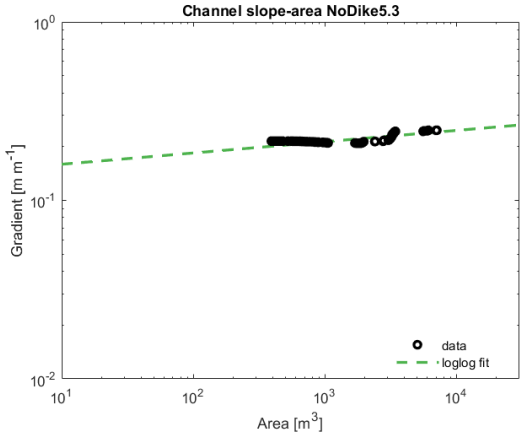

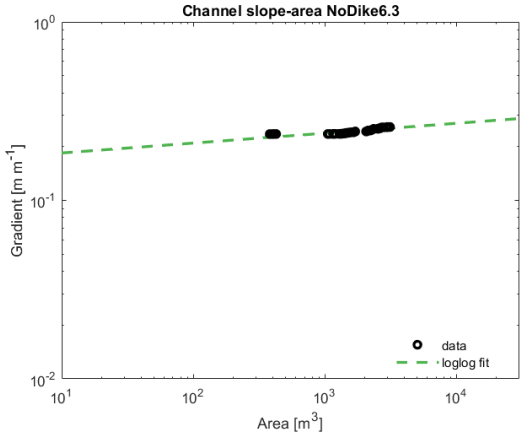

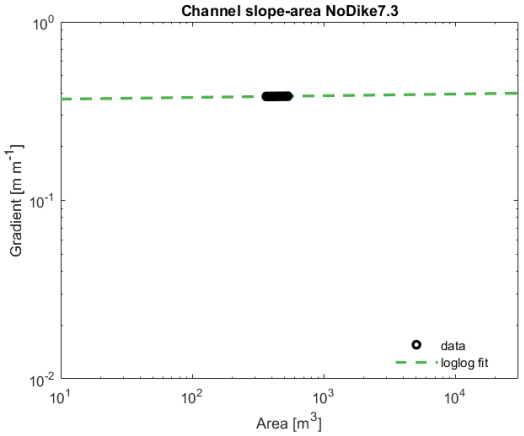

Slope-drainage area relationship with all smoothed data points by K = 10000 with the CRS algorithm for the trunk channels in study area 3 without dikes.

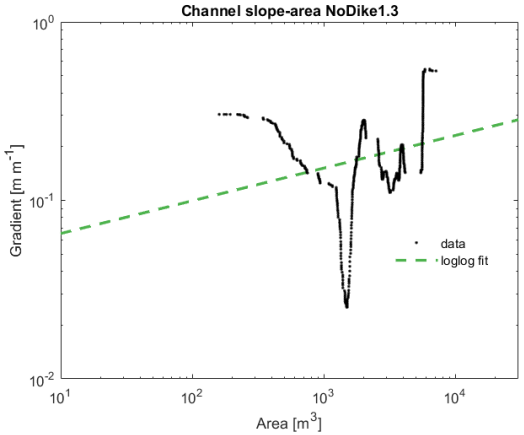

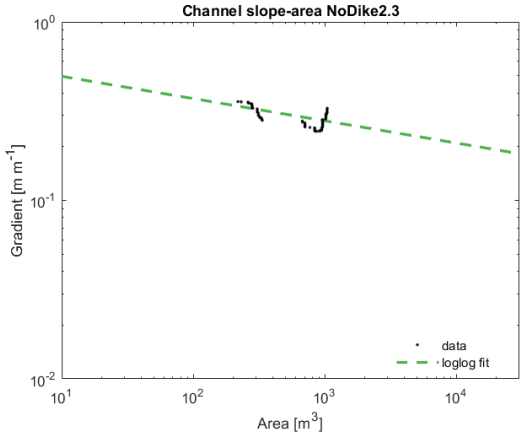

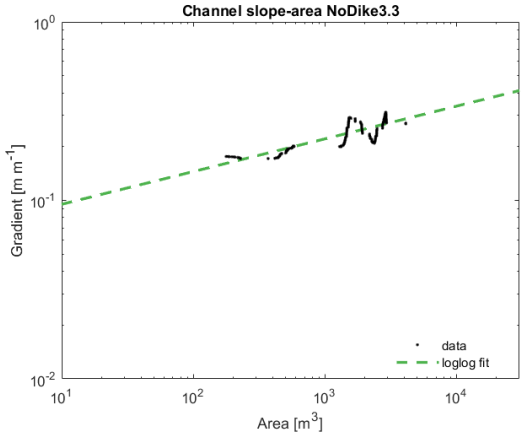

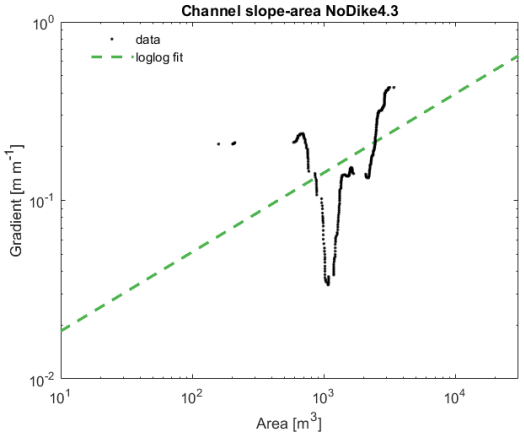

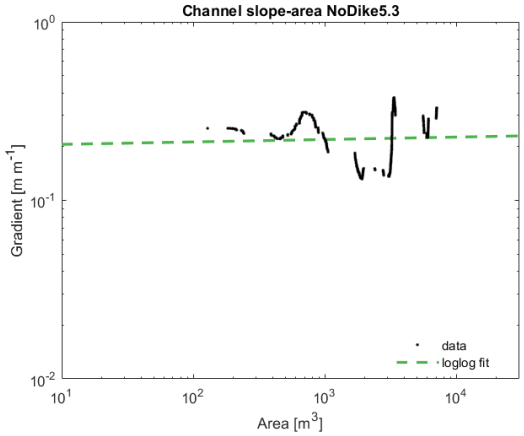

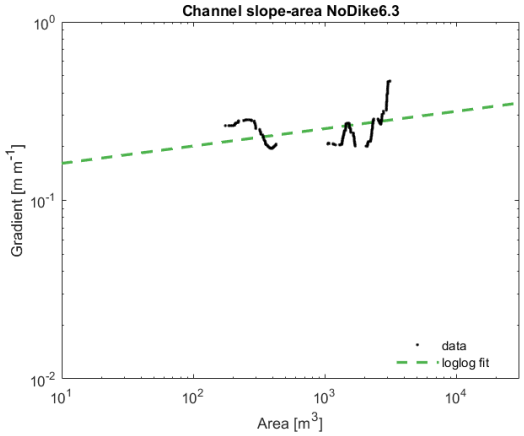

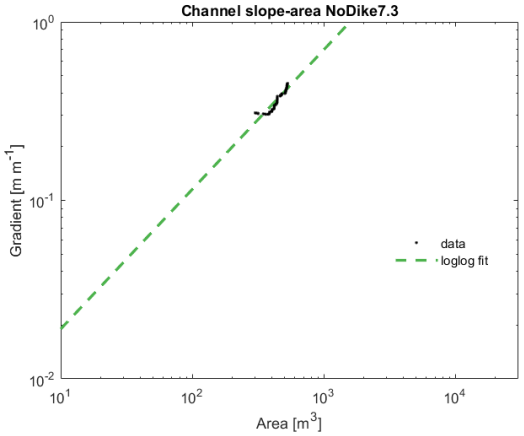

Slope-drainage area relationship with all smoothed data points by K=500 with the CRS algorithm for the trunk channels in study area 3 without dikes.

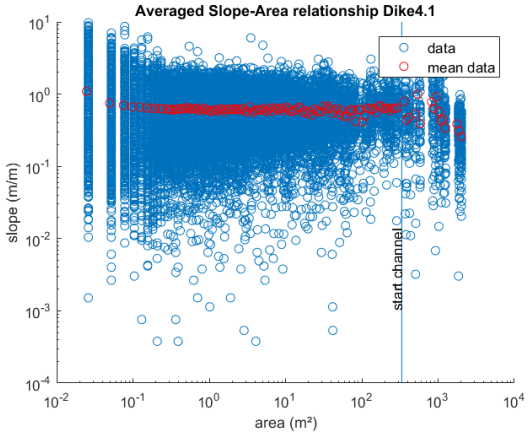

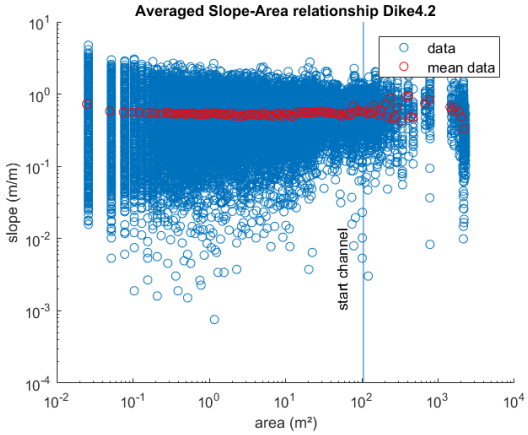

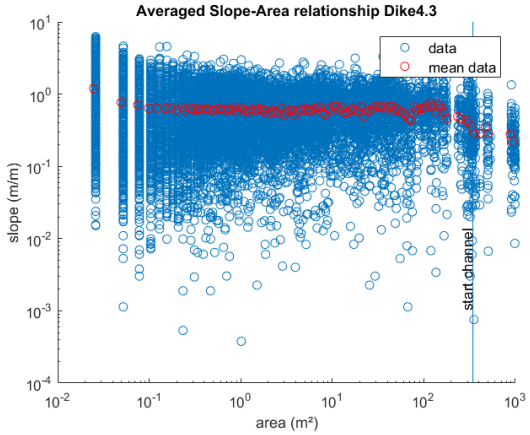

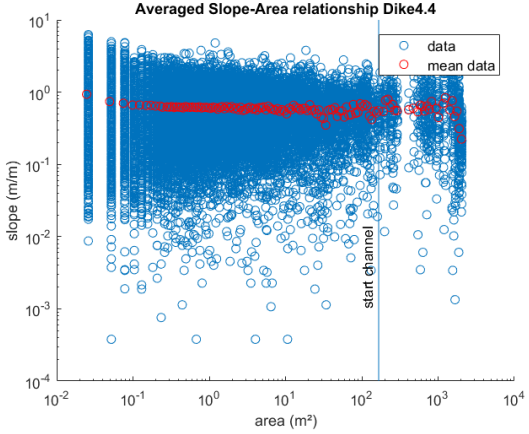

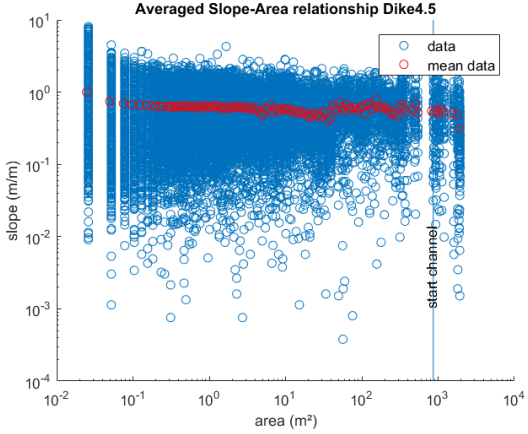

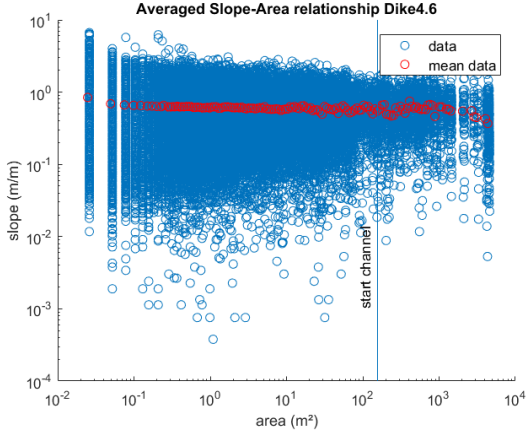

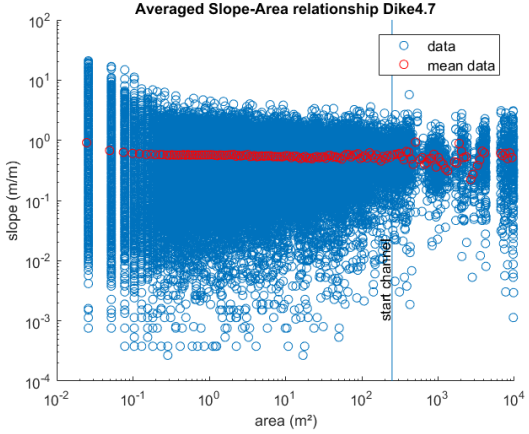

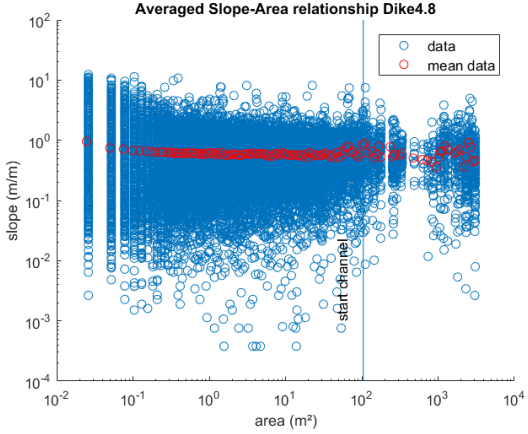

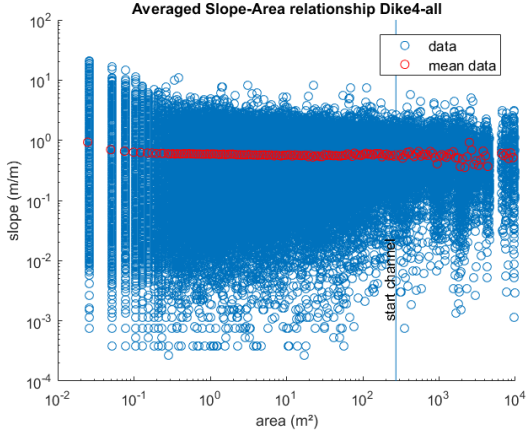

Slope-drainage area relationship with all points for the catchments in study area 4 with dikes.

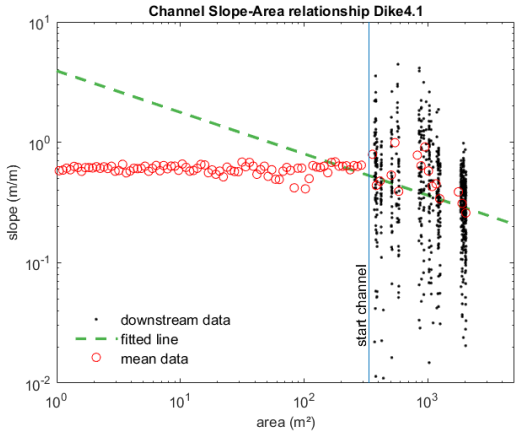

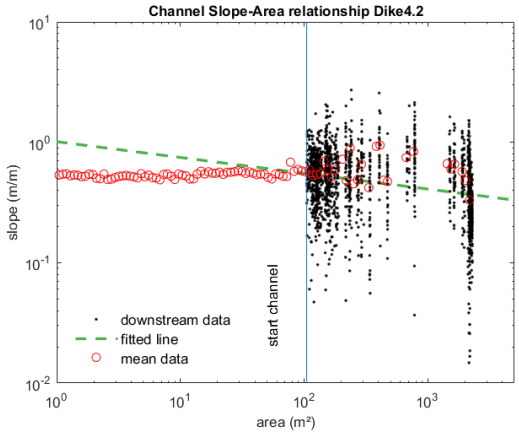

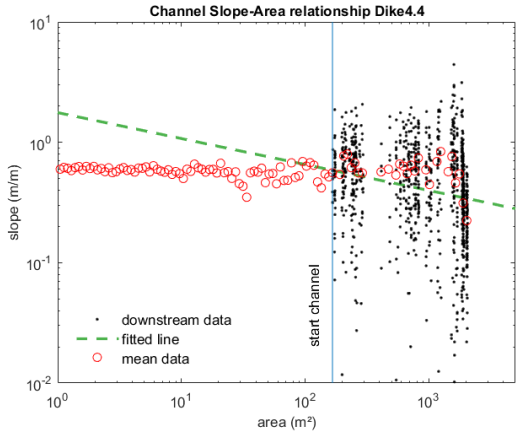

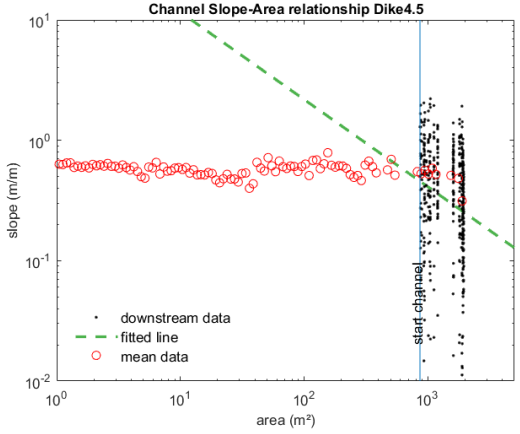

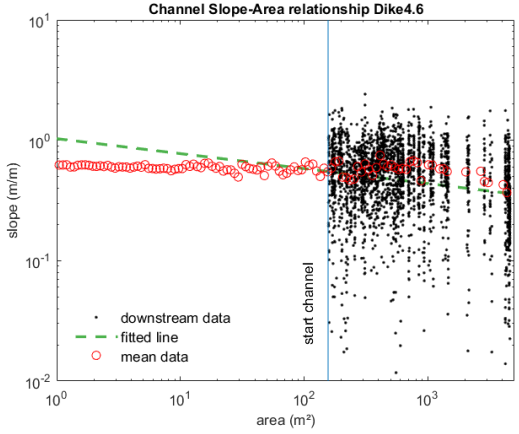

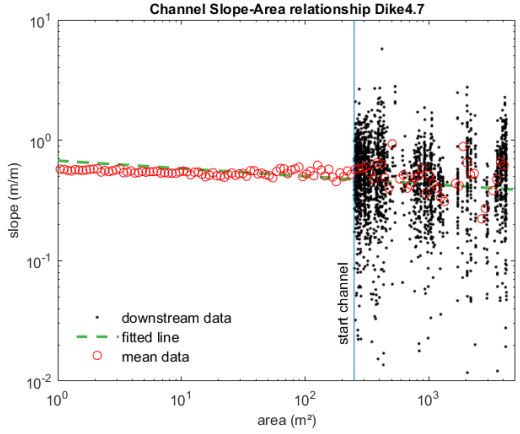

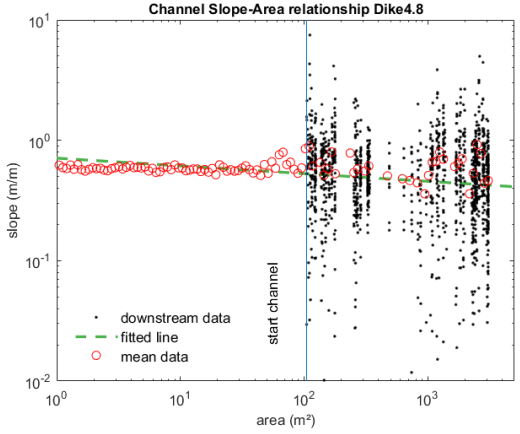

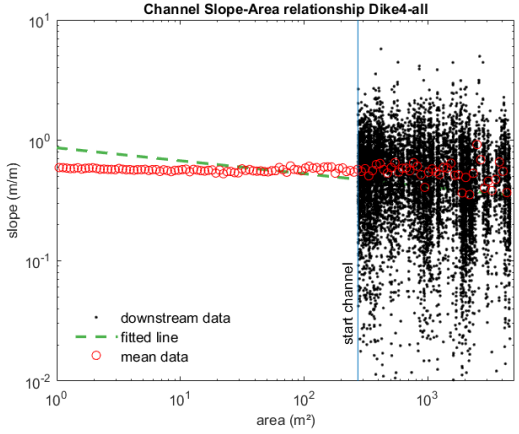

Slope-drainage area relationship with all points for the catchments in study area 4 with dikes when channels start to incise.

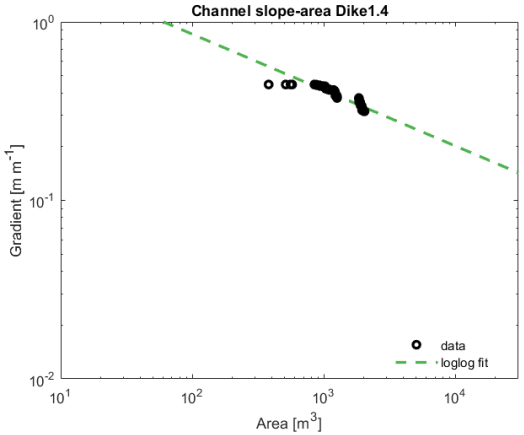

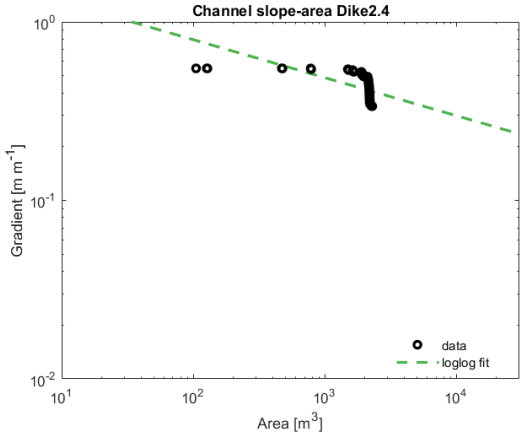

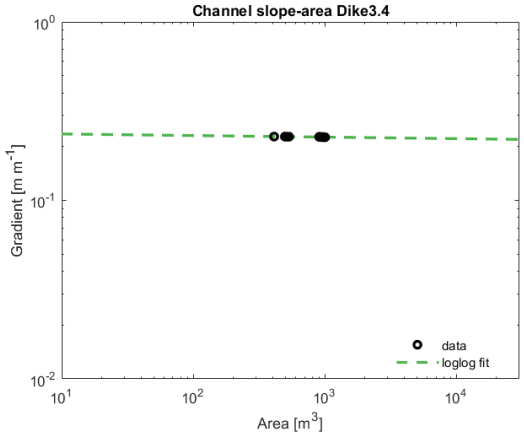

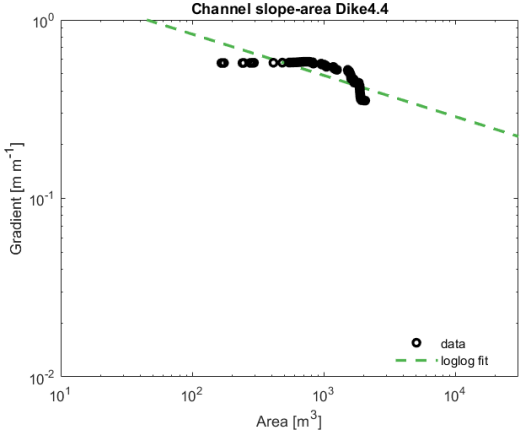

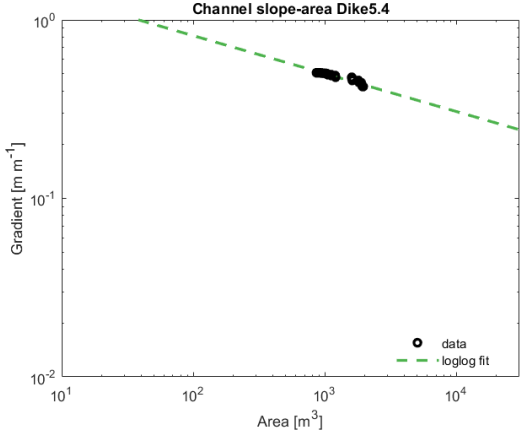

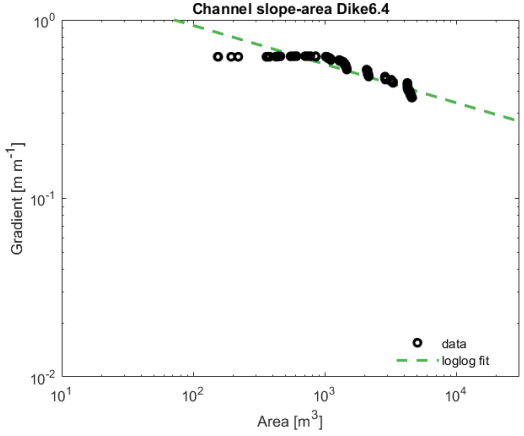

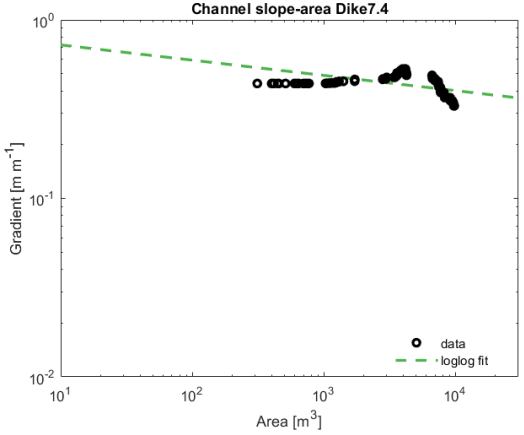

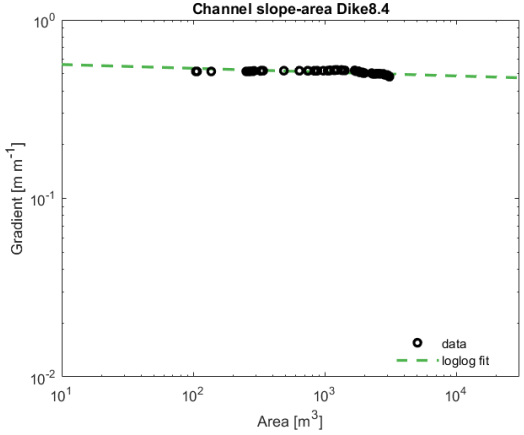

Slope-drainage area relationship with all smoothed data points by K = 10000 with the CRS algorithm for the trunk channels in study area 4 with dikes.

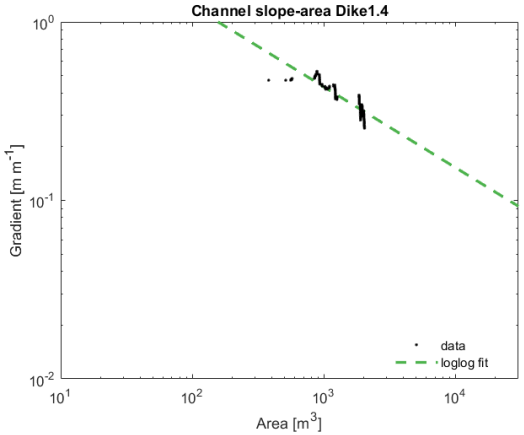

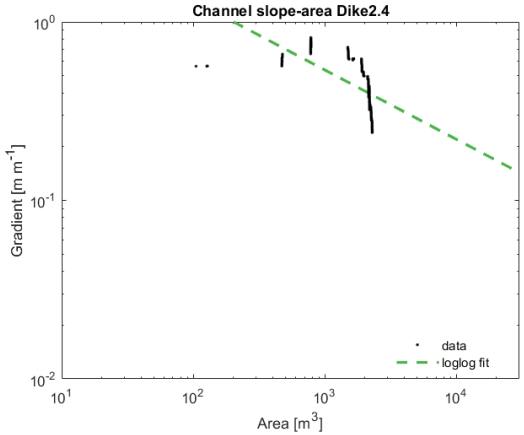

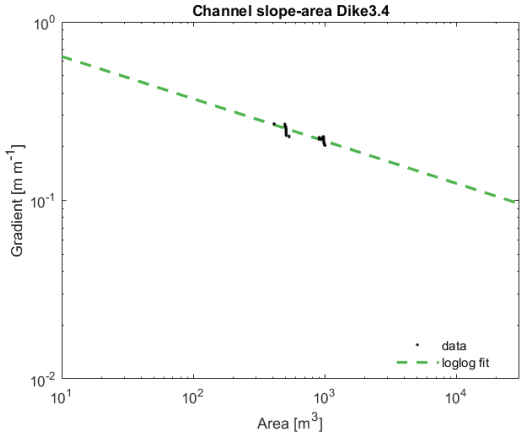

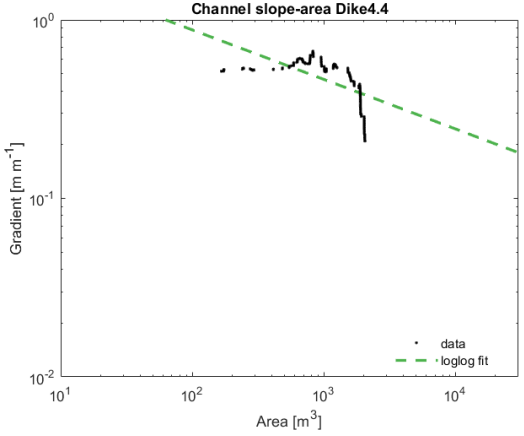

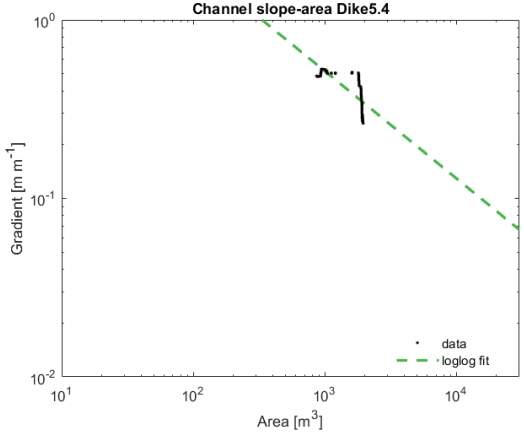

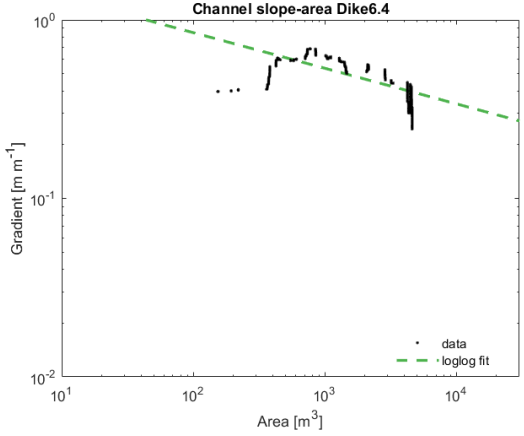

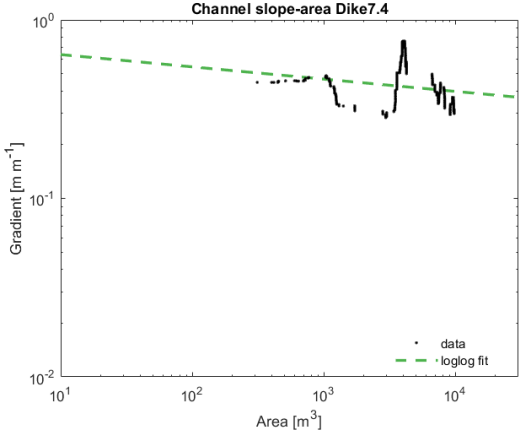

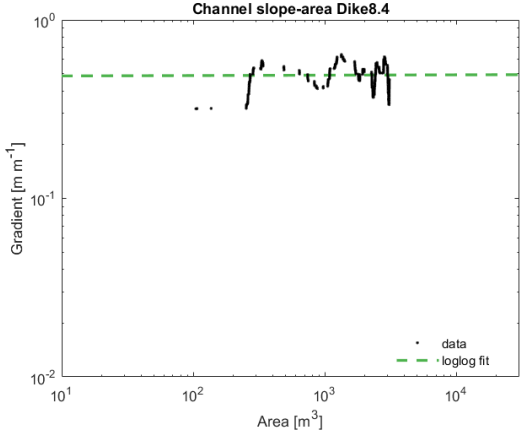

Slope-drainage area relationship with all smoothed data points by K=500 with the CRS algorithm for the trunk channels in study area 4 with dikes.

a.

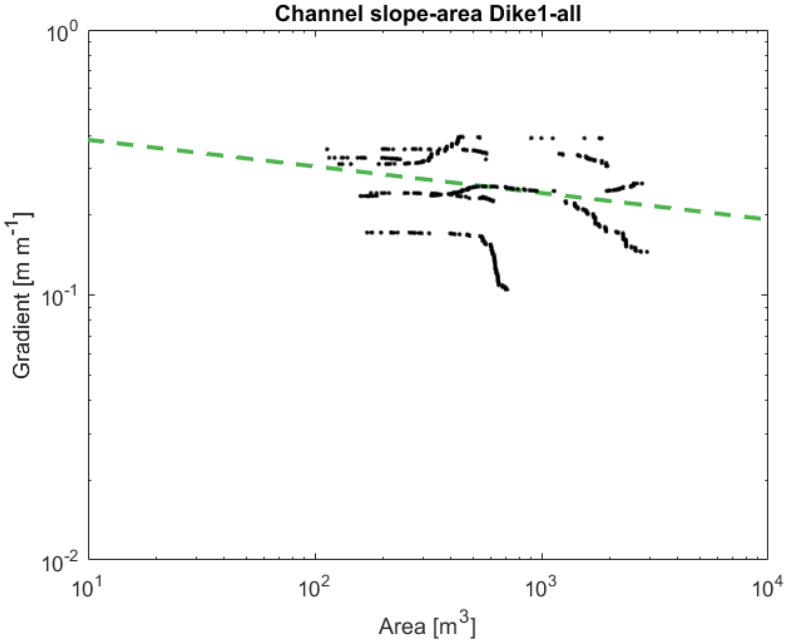
Channel slope-area Dike1-all
Gradient [m m^{-1}]
Area [m^3]

b.

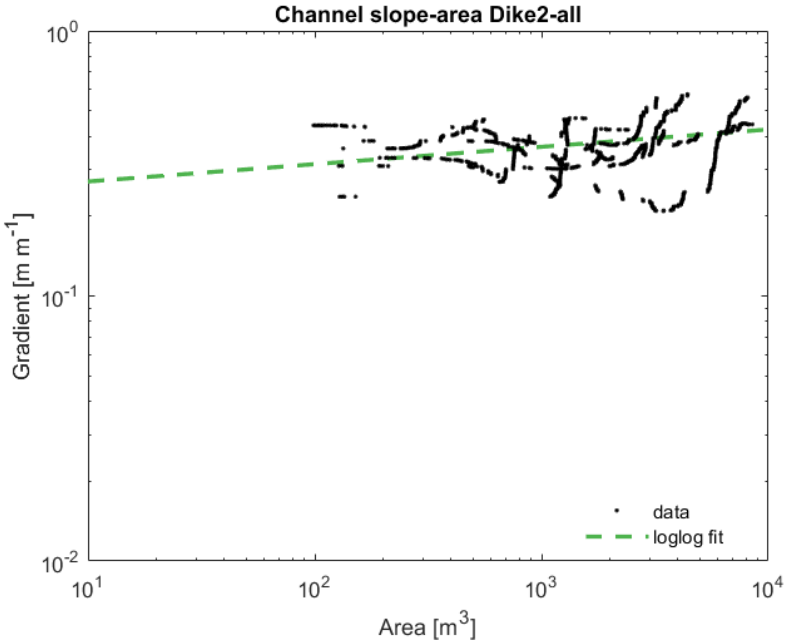
Channel slope-area Dike2-all
Gradient [m m^{-1}]
Area [m^3]
data
loglog fit

c.

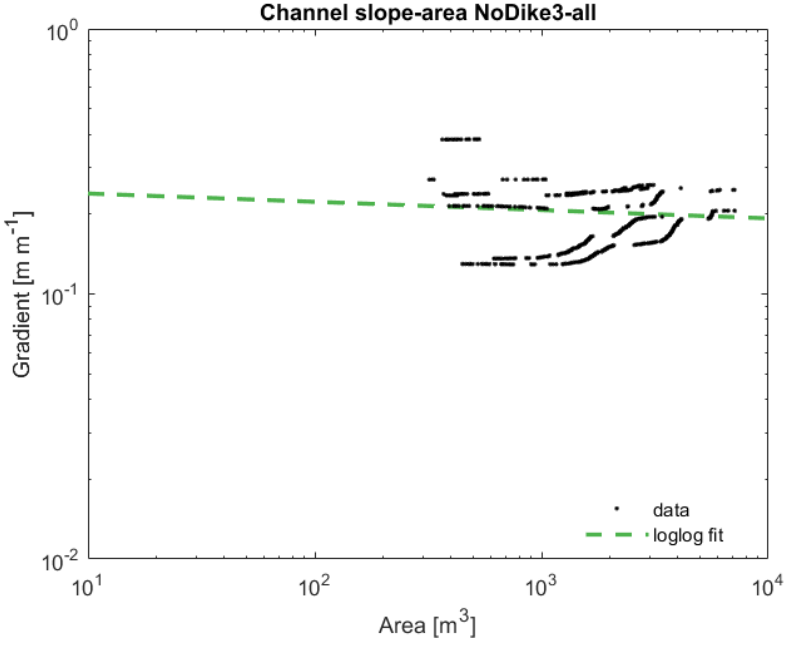
Channel slope-area NoDike3-all
Gradient [m m^{-1}]
Area [m^3]
data
loglog fit

d.

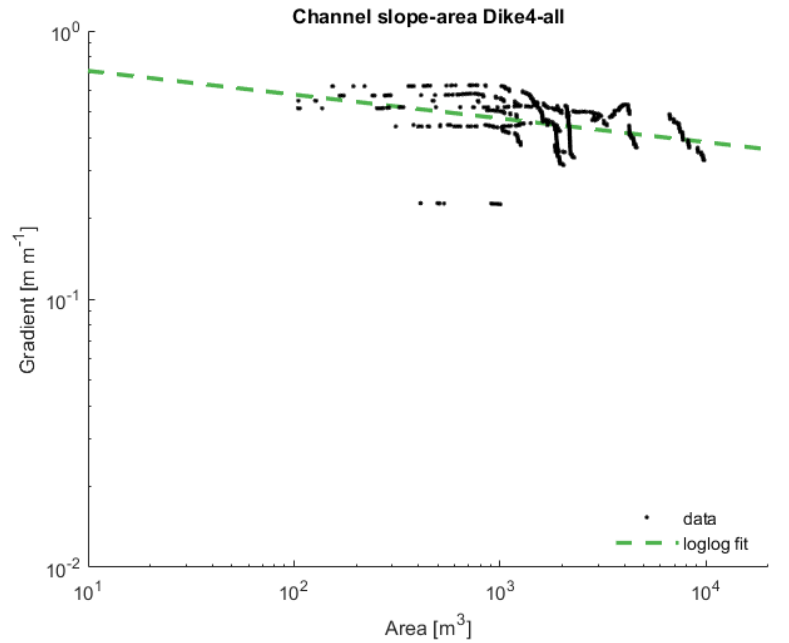
Channel slope-area Dike4-all
Gradient [m m^{-1}]
Area [m^3]
data
loglog fit

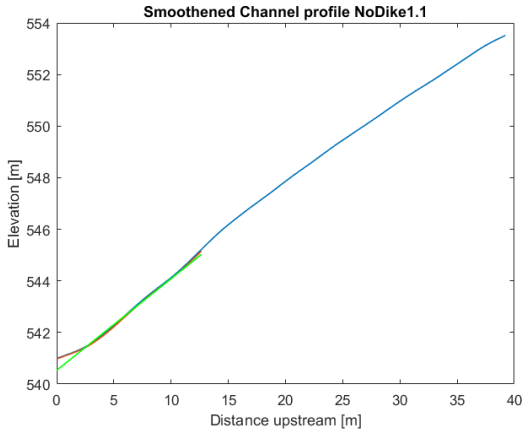

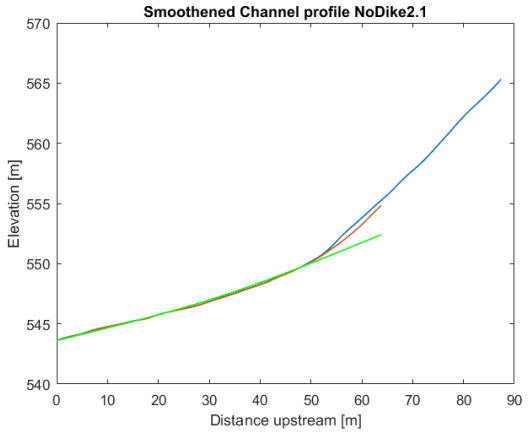

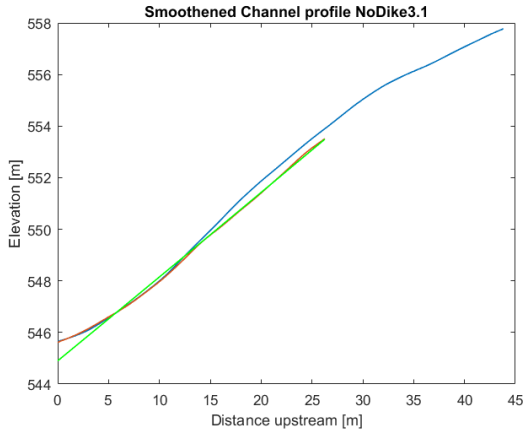

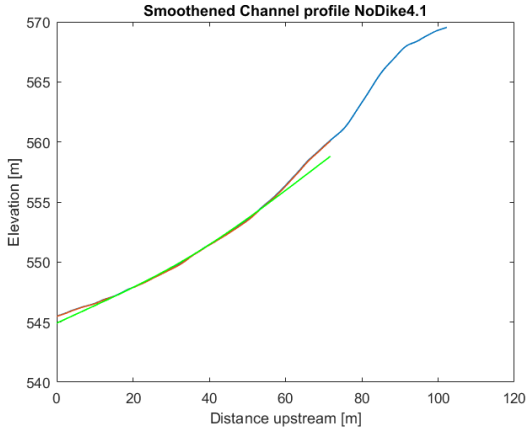

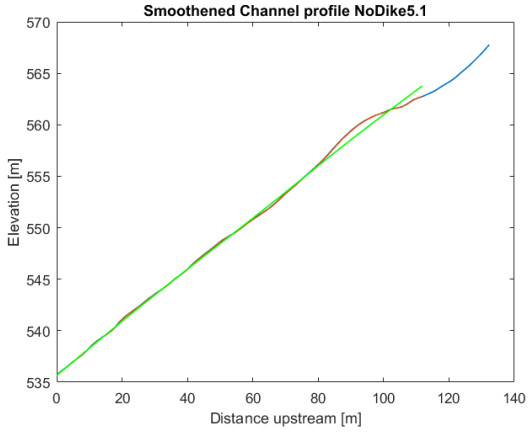

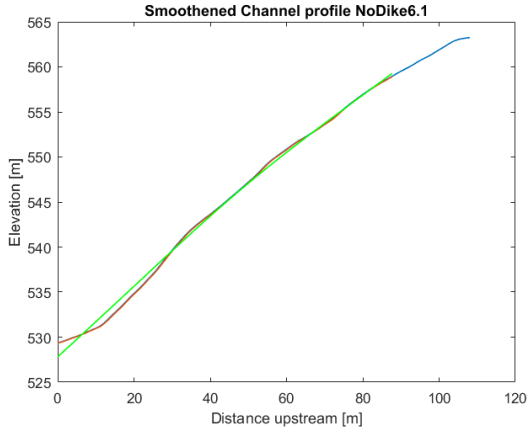

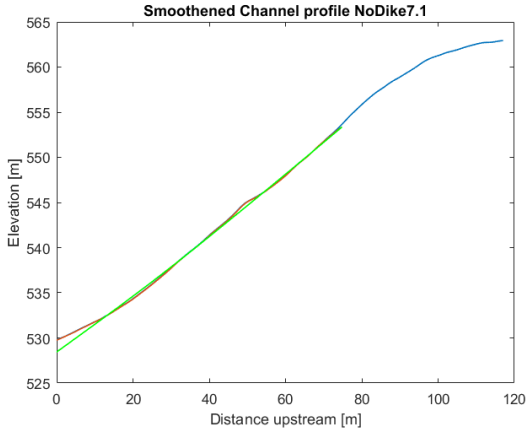

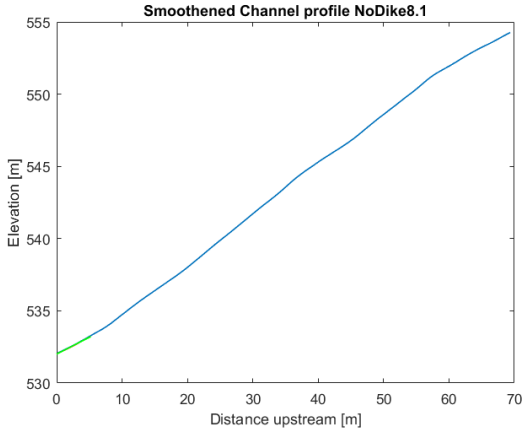

Trunk channel profiles for the catchments in study area 1.
Blue: Total profile from channel to hilltop
Red: Channel profile
Green: Smoothed channel profile (K=10000)

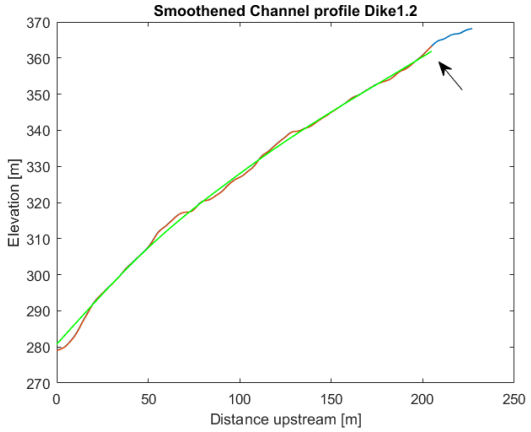

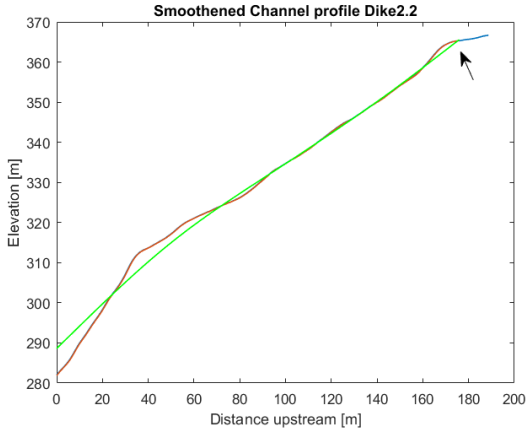

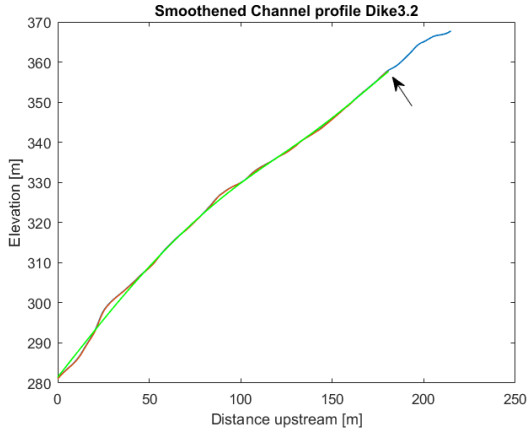

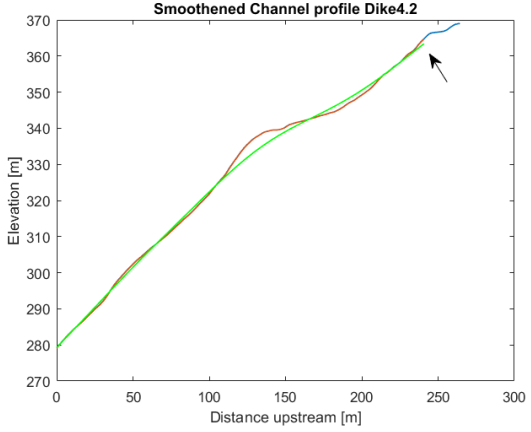

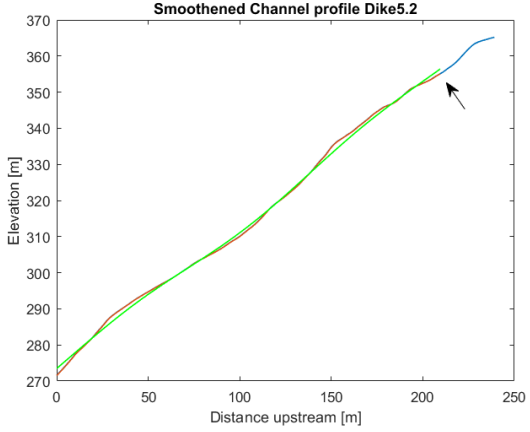

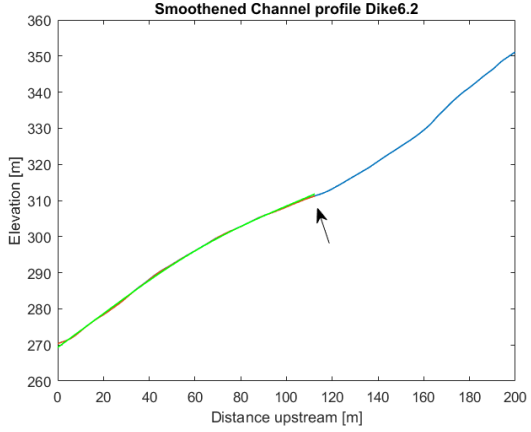

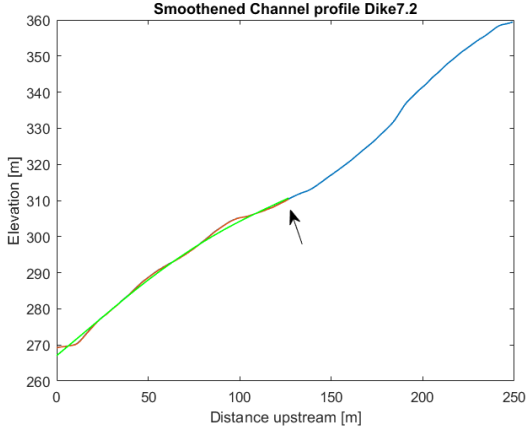

Trunk channel profiles for the catchments in study area 2.
Blue: Total profile from channel to hilltop
Red: Channel profile
Green: Smoothed channel profile (K=10000)

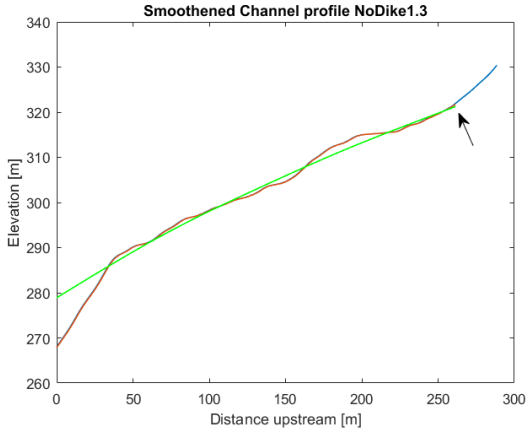

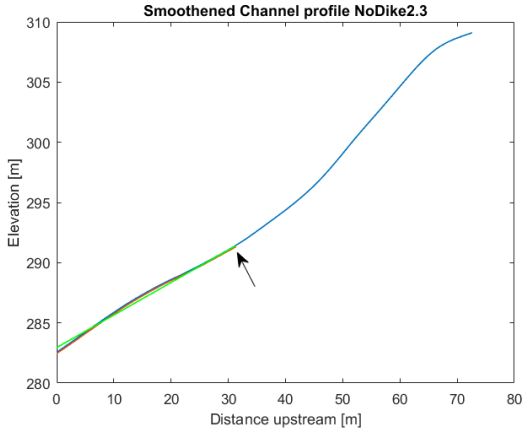

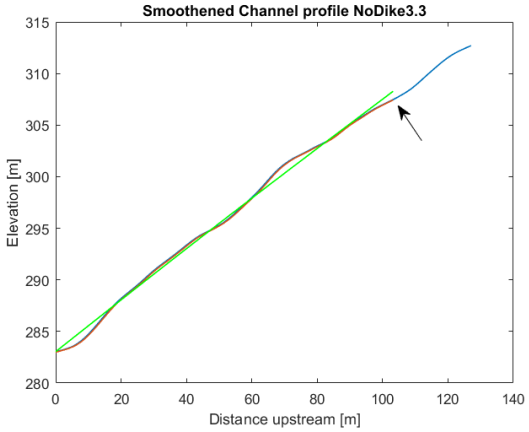

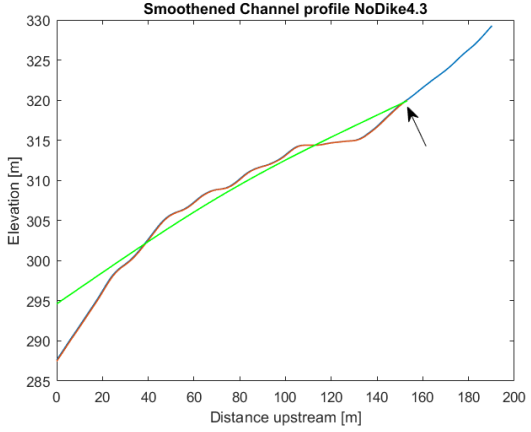

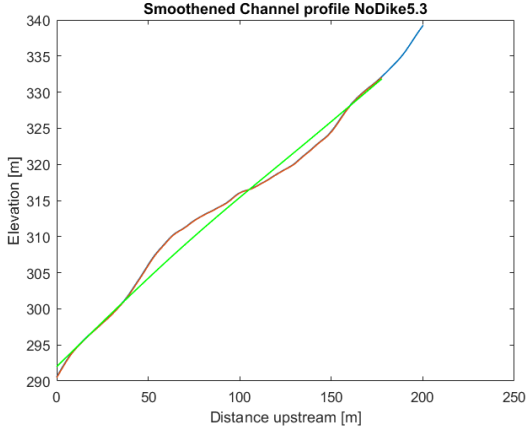

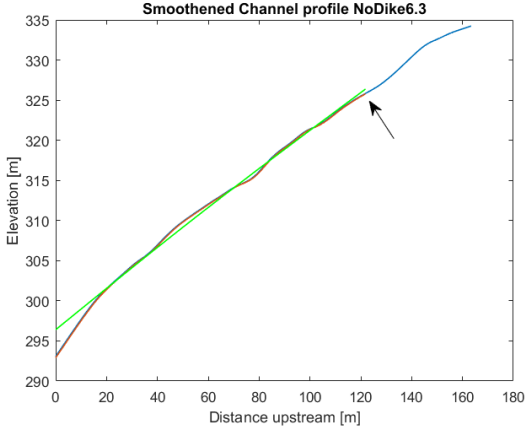

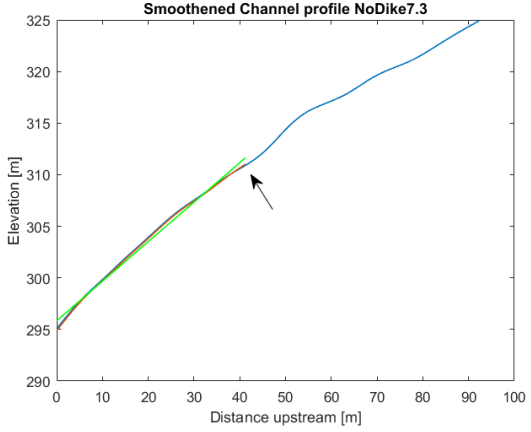

Trunk channel profiles for the catchments in study area 3.
Blue: Total profile from channel to hilltop
Red: Channel profile
Green: Smoothed channel profile

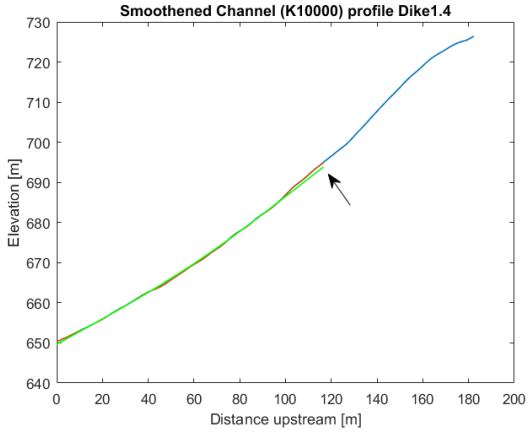

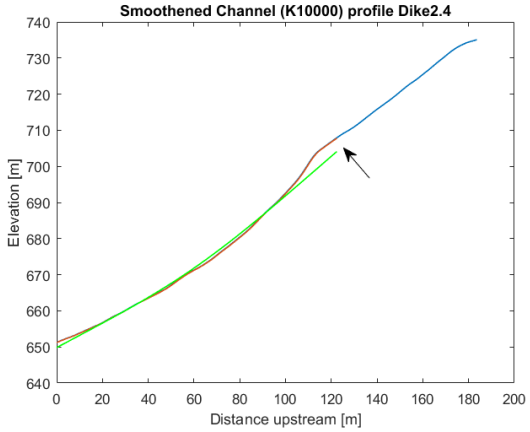

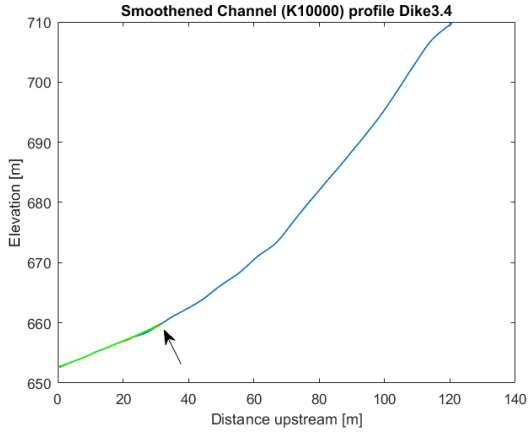

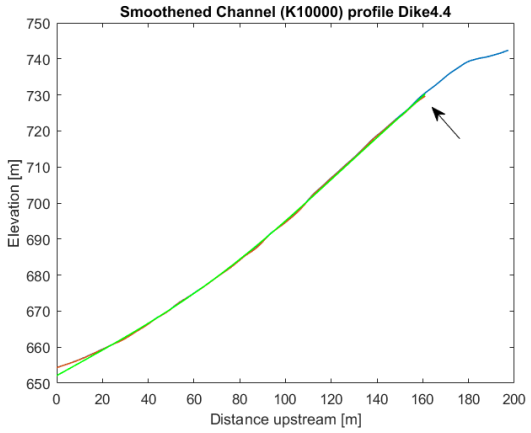

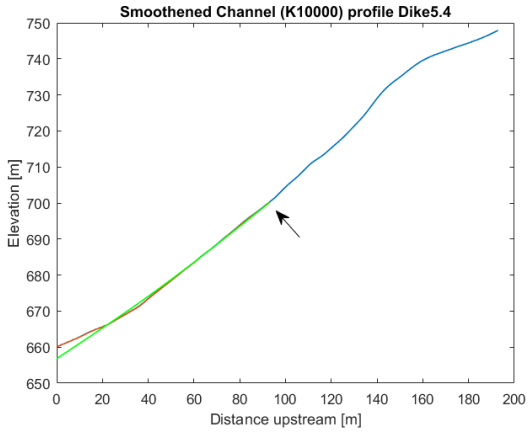

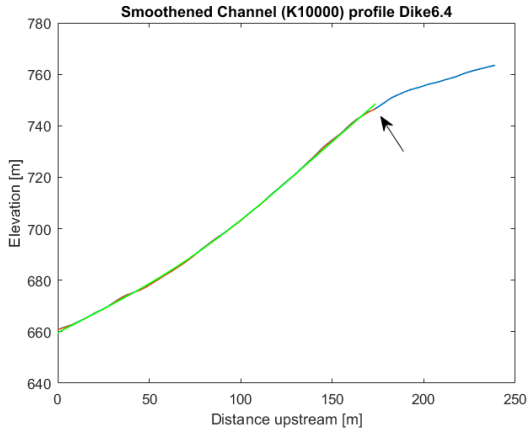

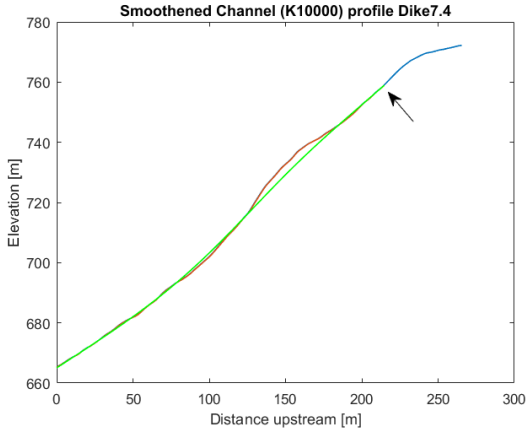

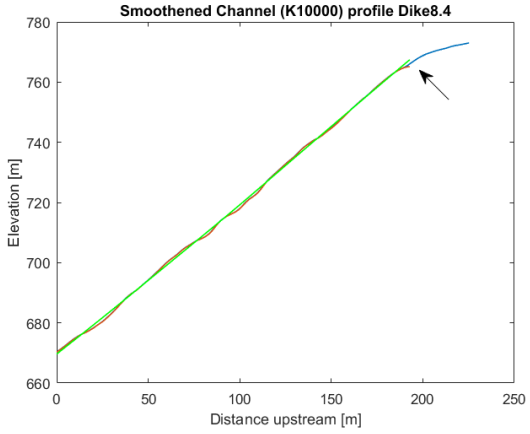

Trunk channel profiles for the catchments in study area 4.
Blue: Total profile from channel to hilltop
Red: Channel profile
Green: Smoothed channel profile

Left: for each height is determined what the area of dikes (Blue) is compared to the granite (red). Right: Original channel profiles with the channel head (arrow).

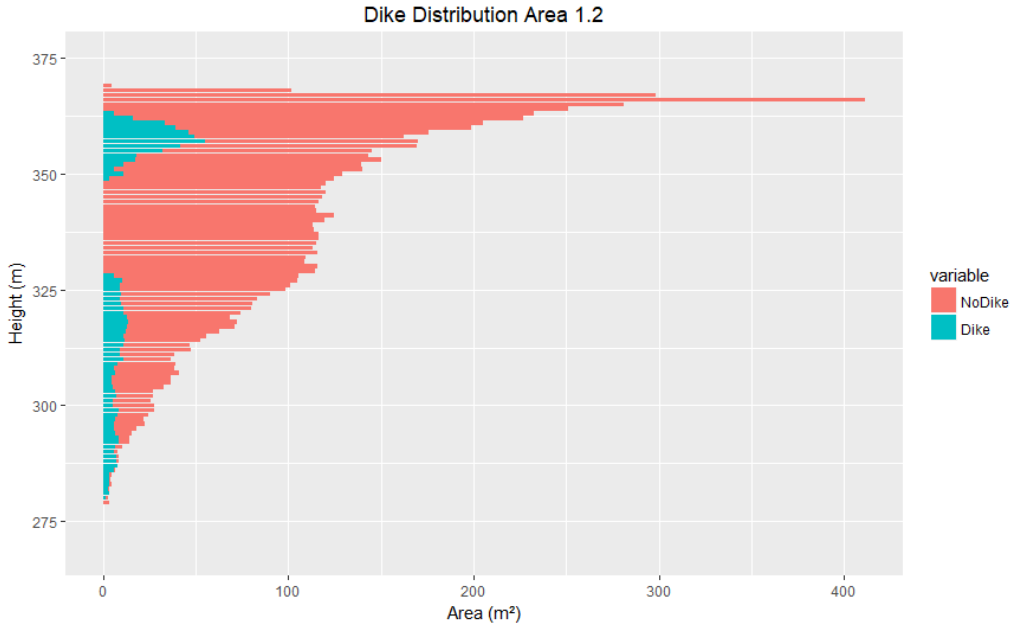

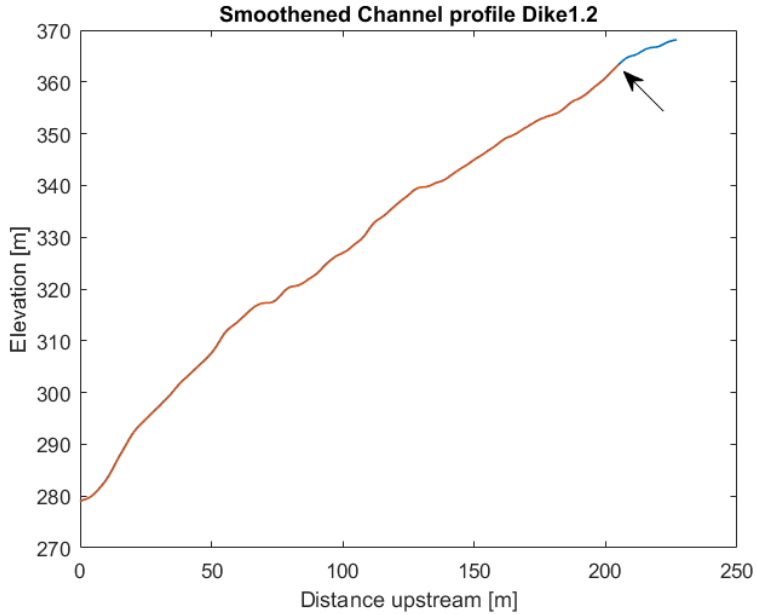

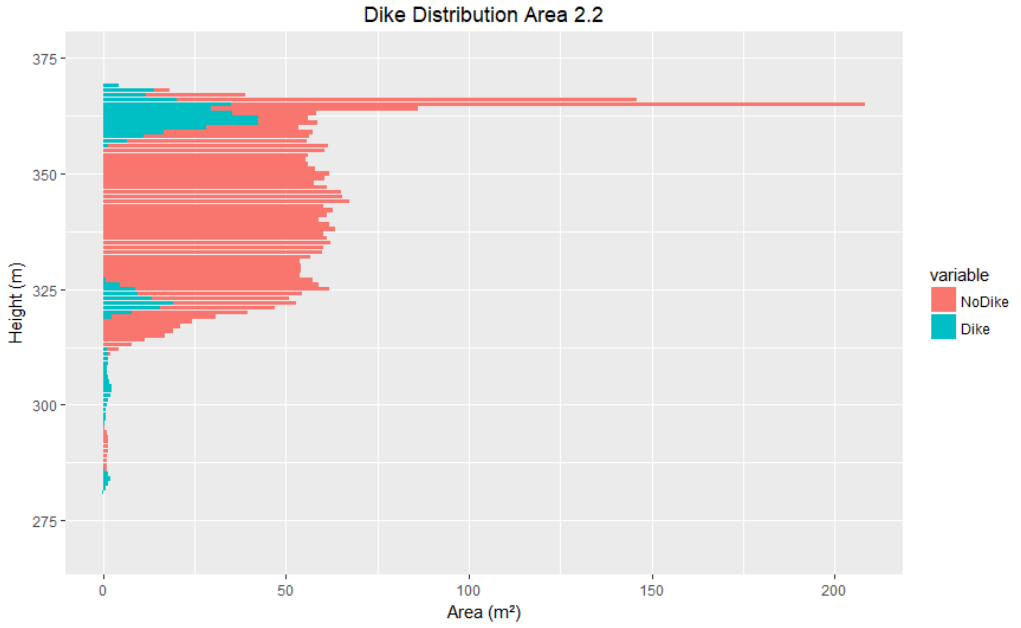

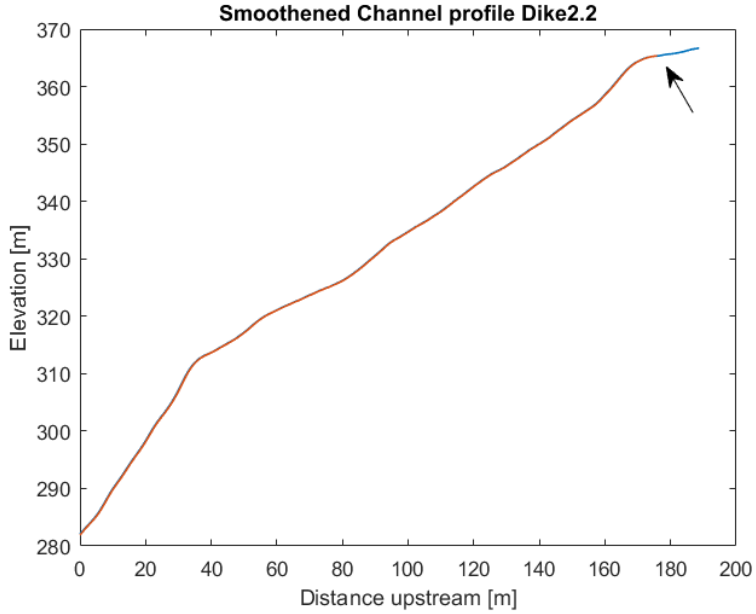

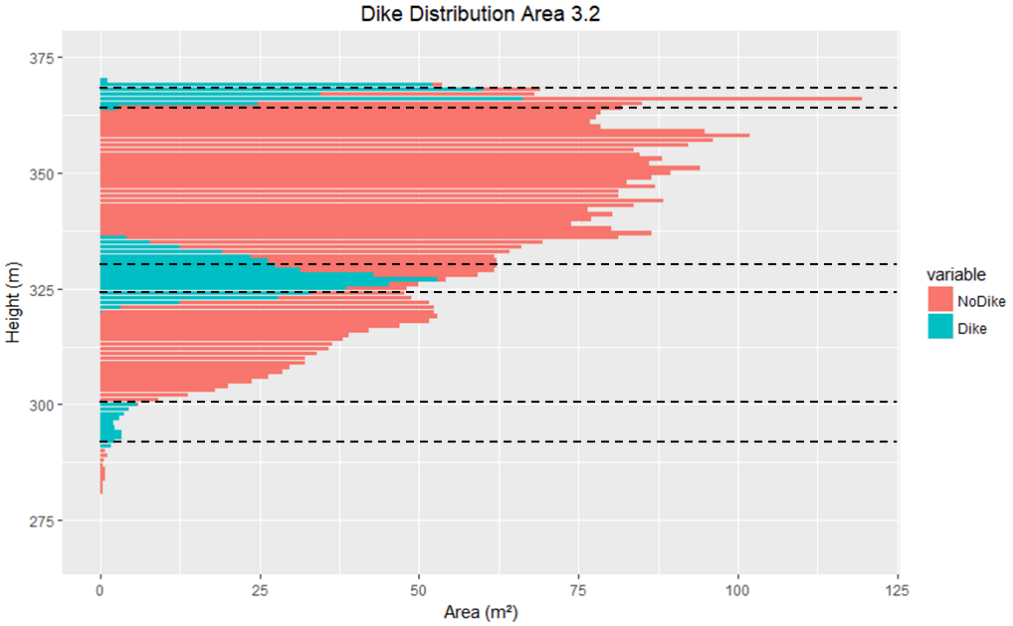
Dike Distribution Area 3.2
Height (m)
Area (m²)
variable
NoDike
Dike

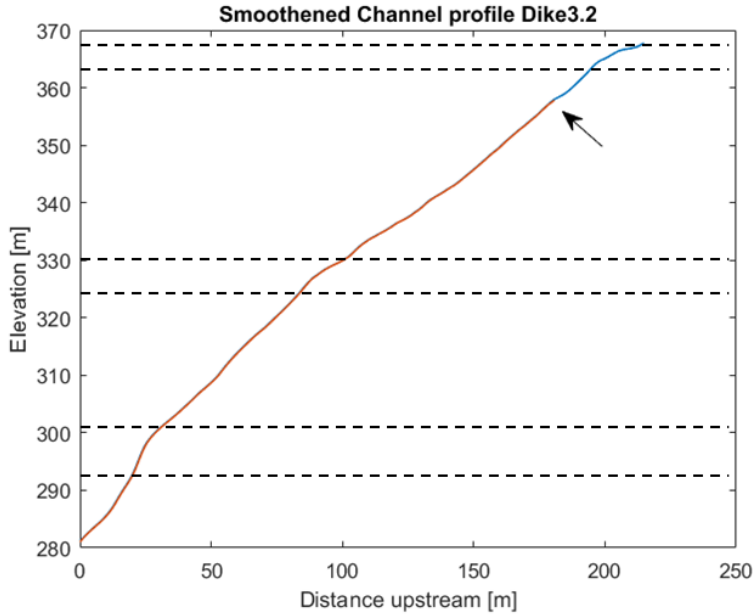
Smoothened Channel profile Dike3.2
Elevation [m]
Distance upstream [m]

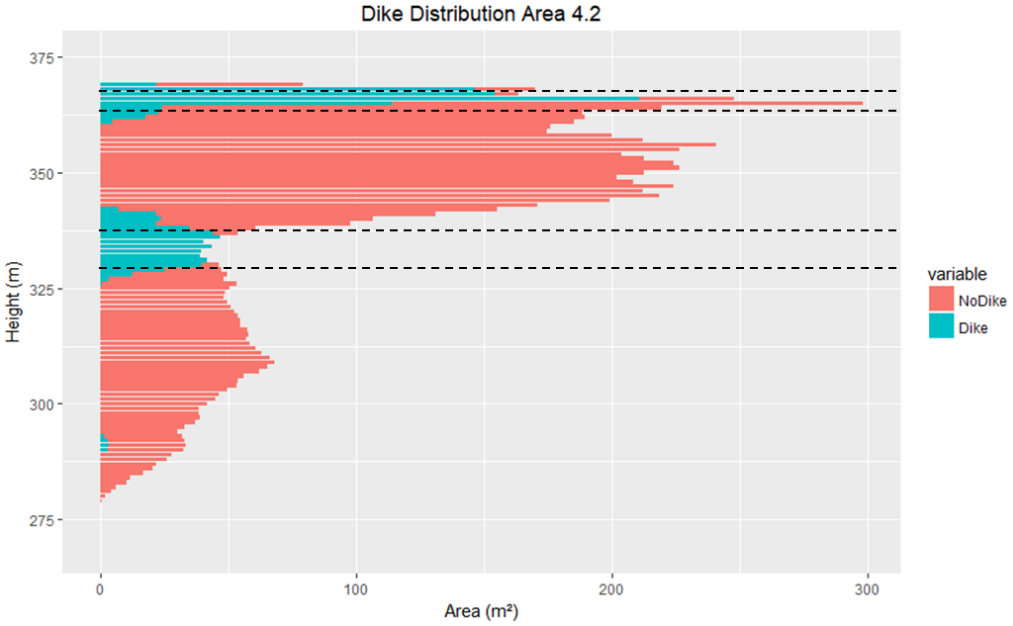
Dike Distribution Area 4.2
Height (m)
Area (m²)
variable
NoDike
Dike

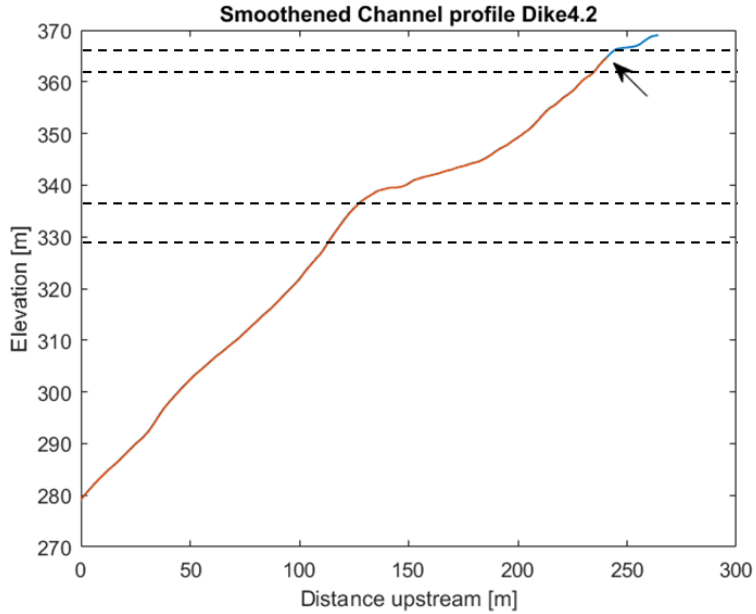
Smoothened Channel profile Dike4.2
Elevation [m]
Distance upstream [m]

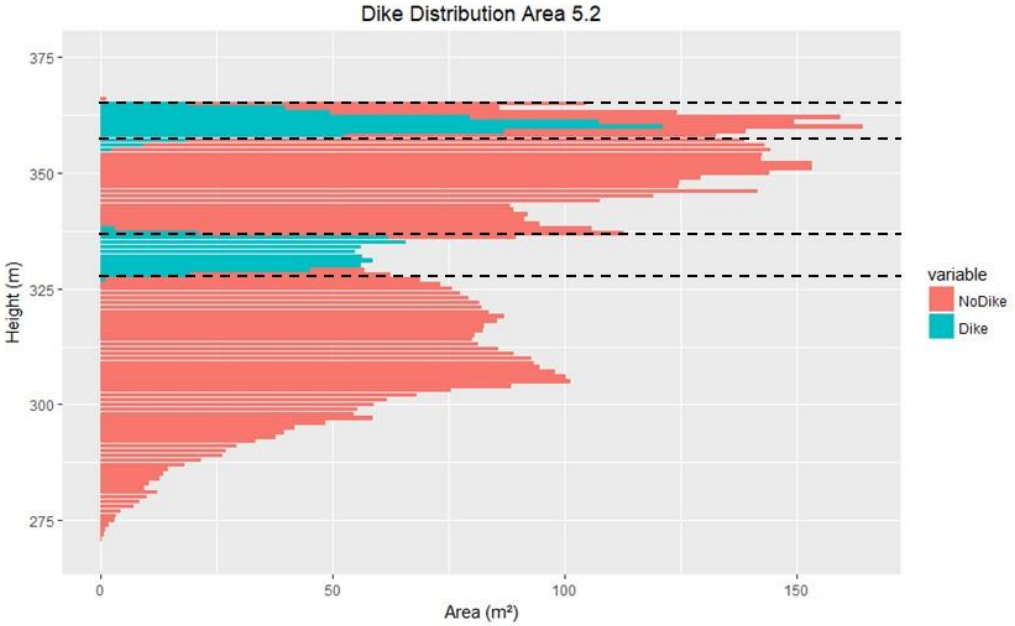
Dike Distribution Area 5.2
Height (m)
Area (m²)
variable
NoDike
Dike

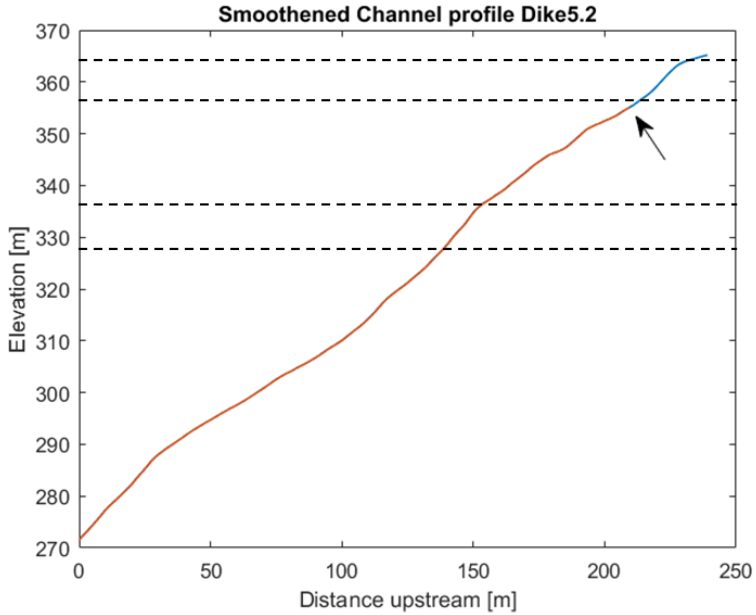
Smoothened Channel profile Dike5.2
Elevation [m]
Distance upstream [m]

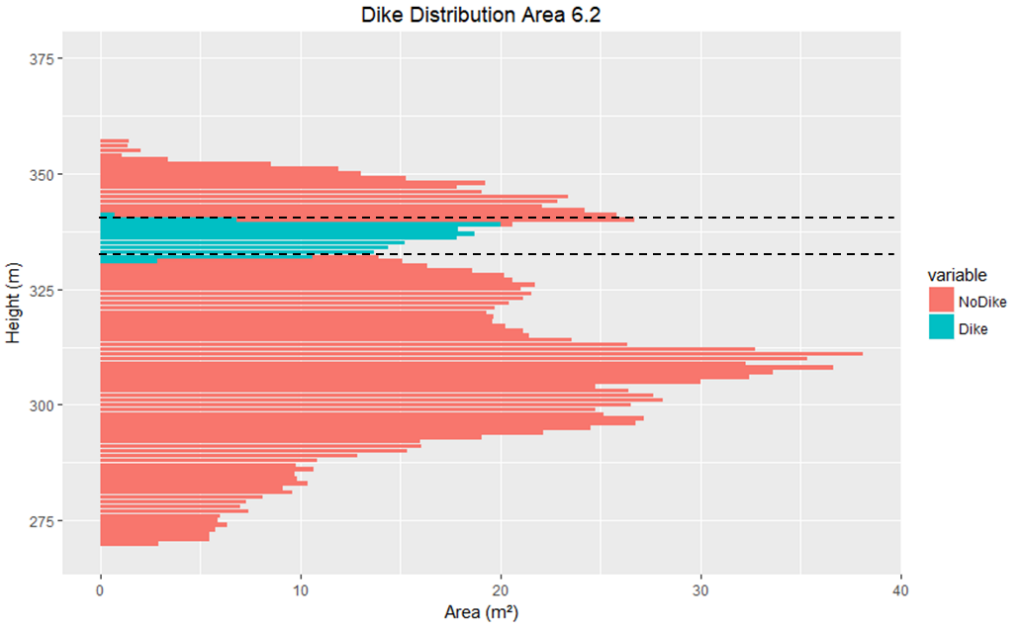
Dike Distribution Area 6.2
Height (m)
Area (m²)
variable
NoDike
Dike

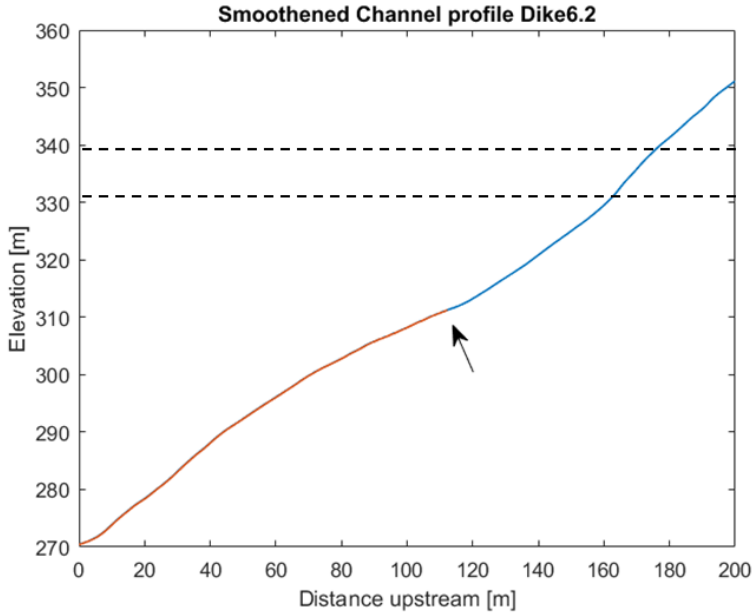
Smoothened Channel profile Dike6.2
Elevation [m]
Distance upstream [m]

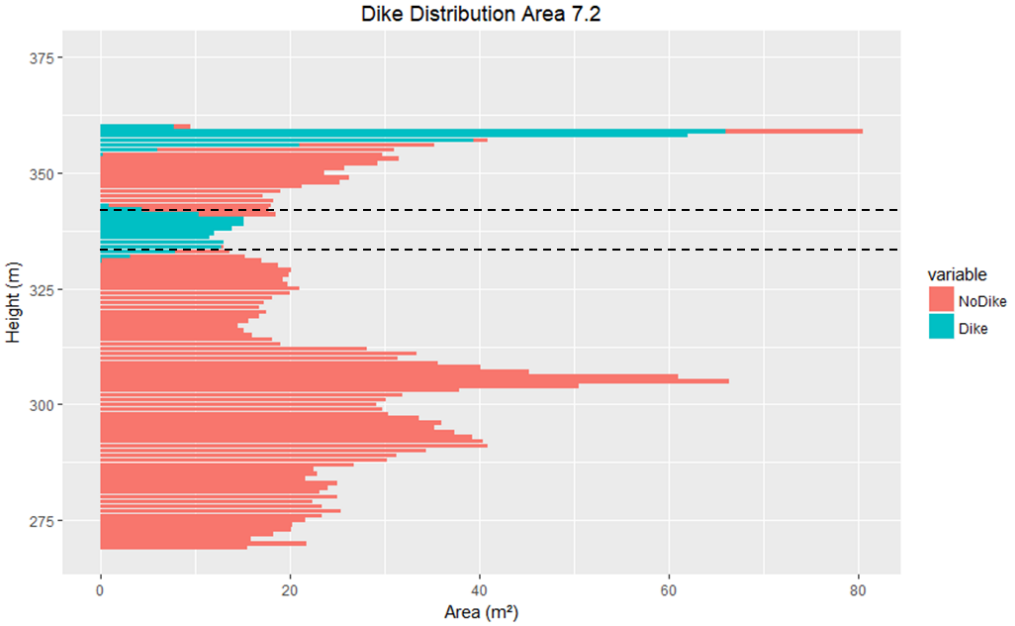
Dike Distribution Area 7.2
Height (m)
Area (m²)
variable
NoDike
Dike

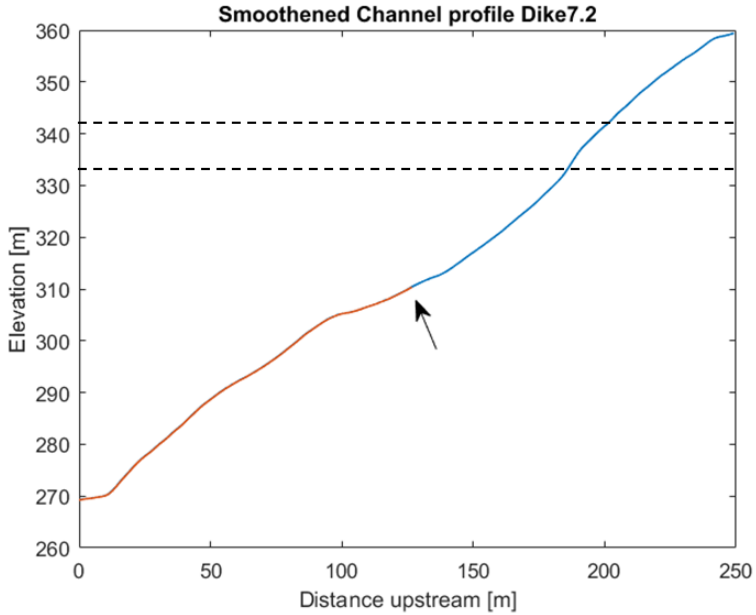
Smoothened Channel profile Dike7.2
Elevation [m]
Distance upstream [m]


Dike Distribution Area 1.4
Height (m)
Area (m²)
variable
NoDike
Dike

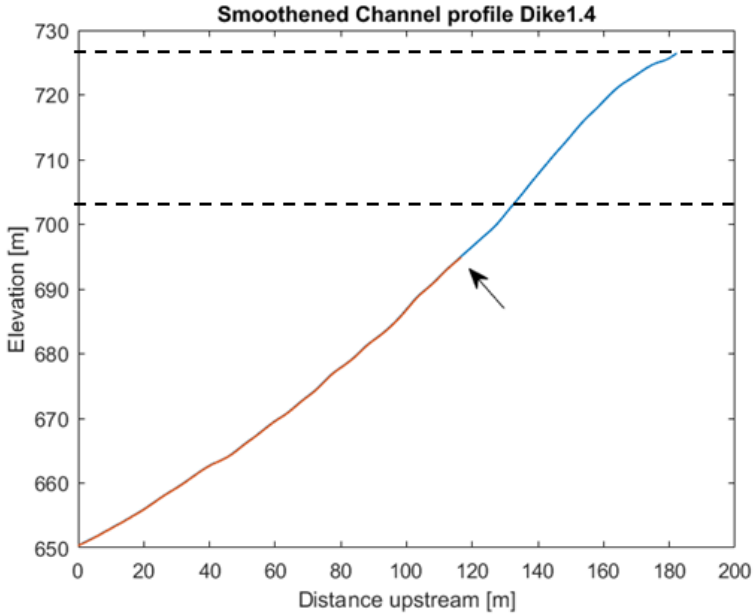
Smoothened Channel profile Dike1.4
Elevation [m]
Distance upstream [m]

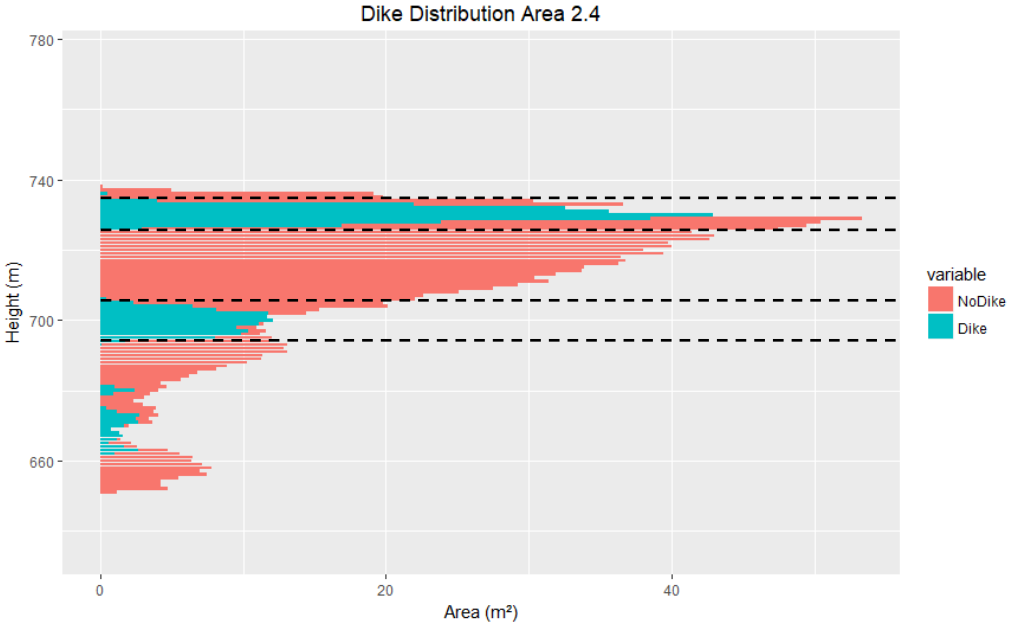
Dike Distribution Area 2.4
Height (m)
780
740
700
660
0
20
40
Area (m²)
variable
NoDike
Dike

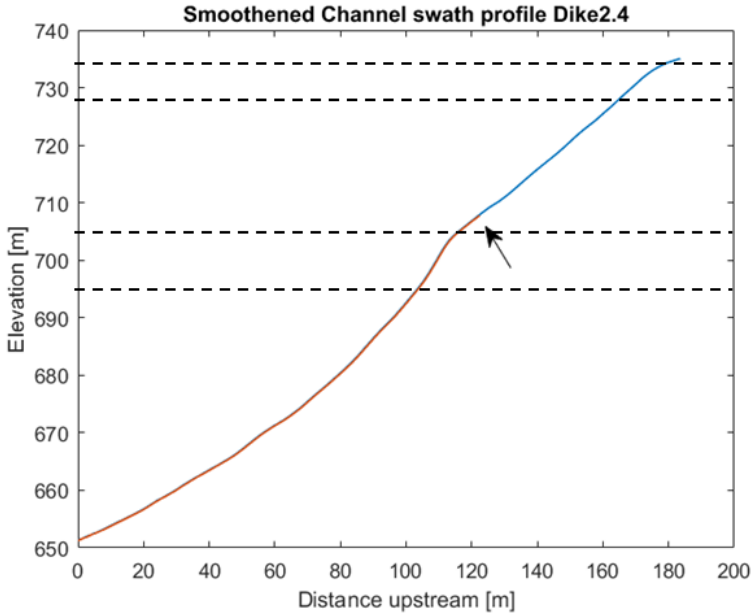
Smoothened Channel swath profile Dike2.4
Elevation [m]
740
730
720
710
700
690
680
670
660
650
0
20
40
60
80
100
120
140
160
180
200
Distance upstream [m]

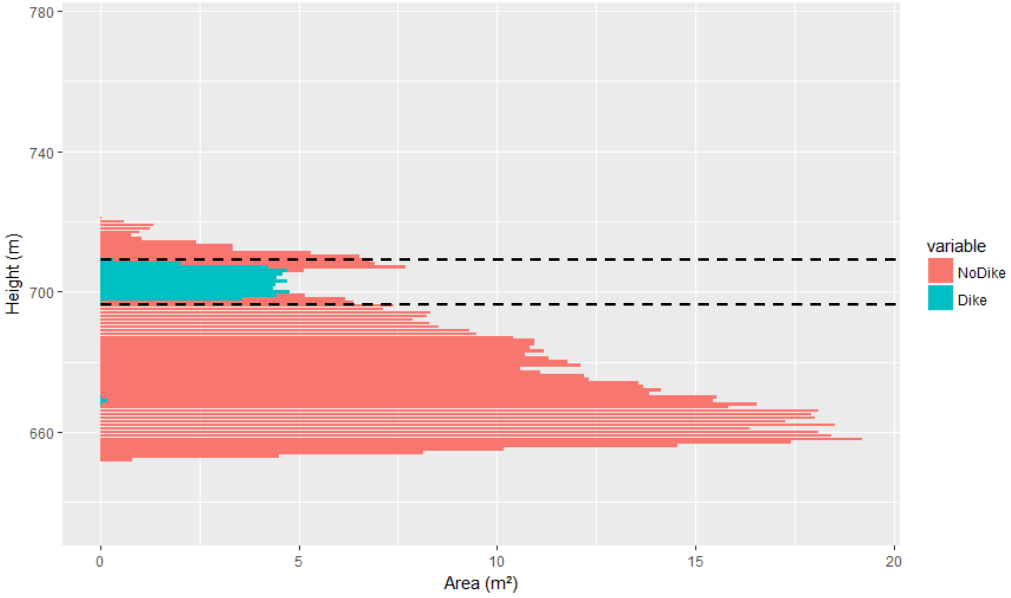
Dike Distribution Area 3.4
Height (m)
780
740
700
660
0
5
10
15
20
Area (m²)
variable
NoDike
Dike

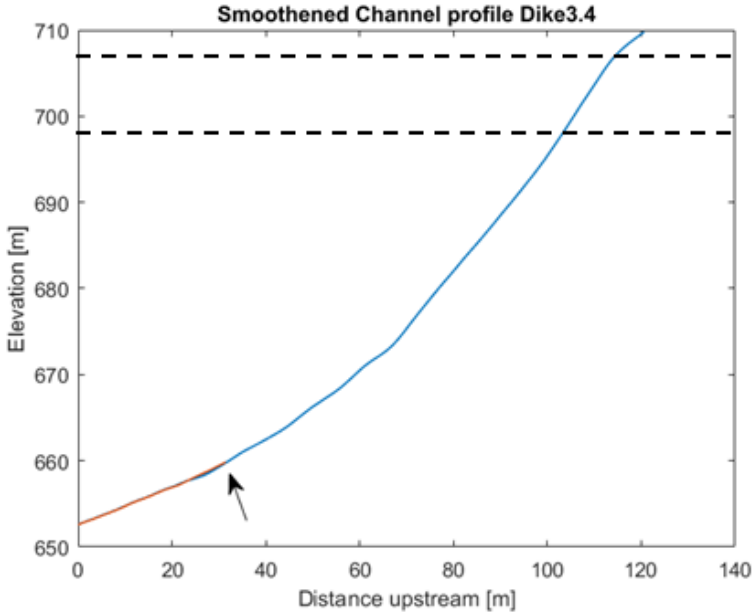
Smoothened Channel profile Dike3.4
Elevation [m]
710
700
690
680
670
660
650
0
20
40
60
80
100
120
140
Distance upstream [m]

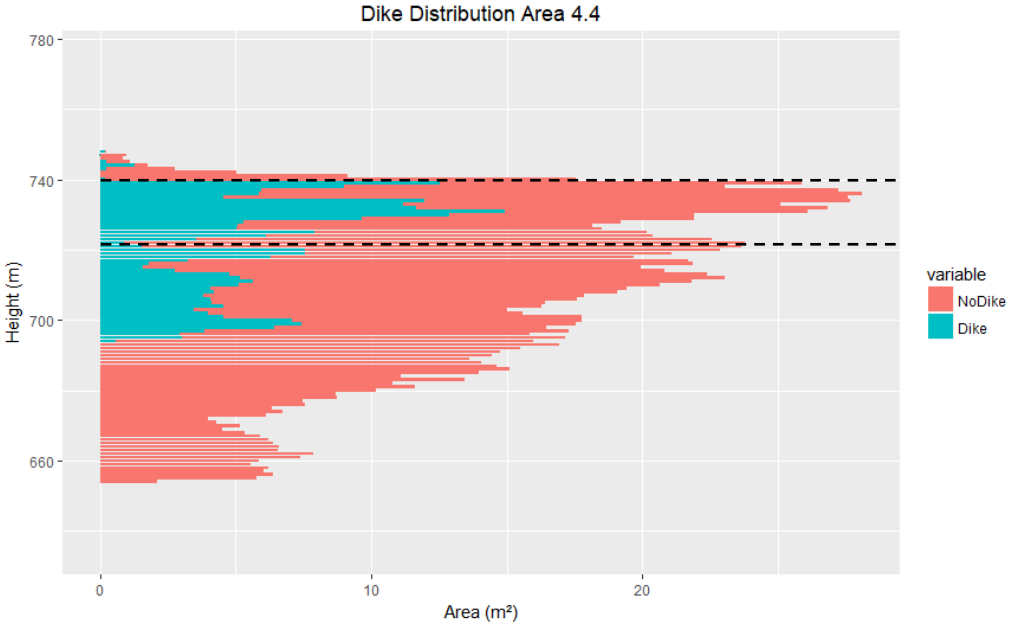
Dike Distribution Area 4.4
Height (m)
780
740
700
660
0
10
20
Area (m²)
variable
NoDike
Dike

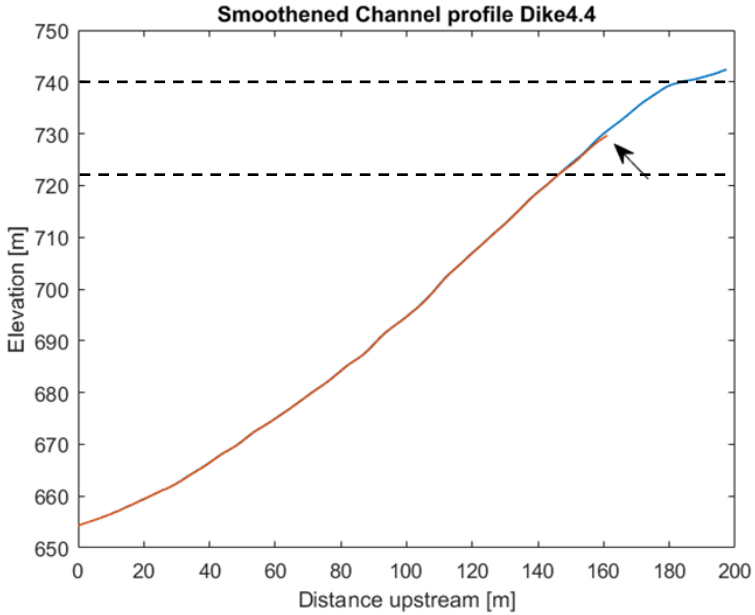
Smoothened Channel profile Dike4.4
Elevation [m]
750
740
730
720
710
700
690
680
670
660
650
0
20
40
60
80
100
120
140
160
180
200
Distance upstream [m]

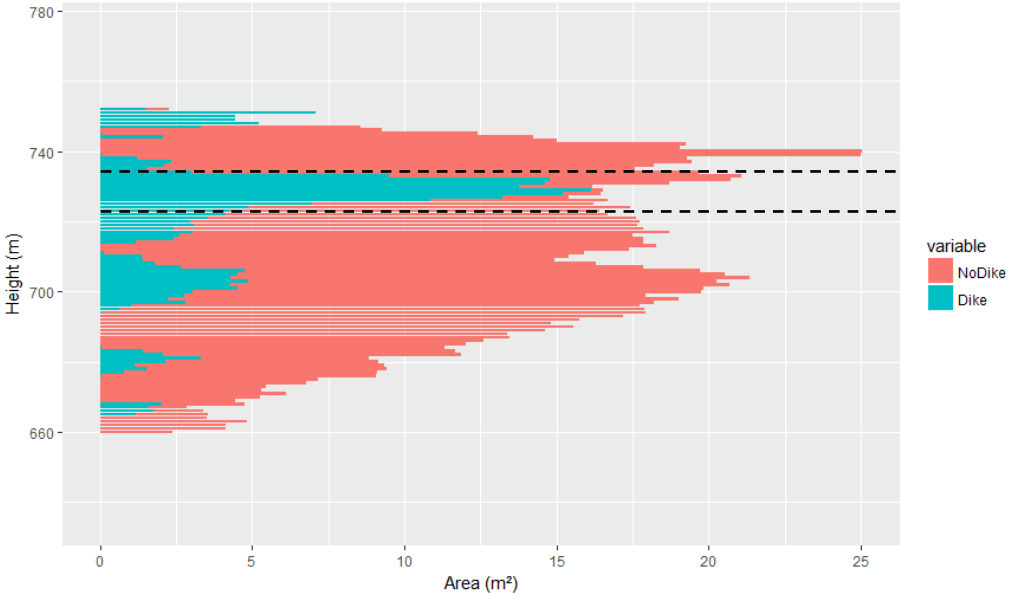
Dike Distribution Area 5.4
Height (m)
780
740
700
660
0
5
10
15
20
25
Area (m²)
variable
NoDike
Dike

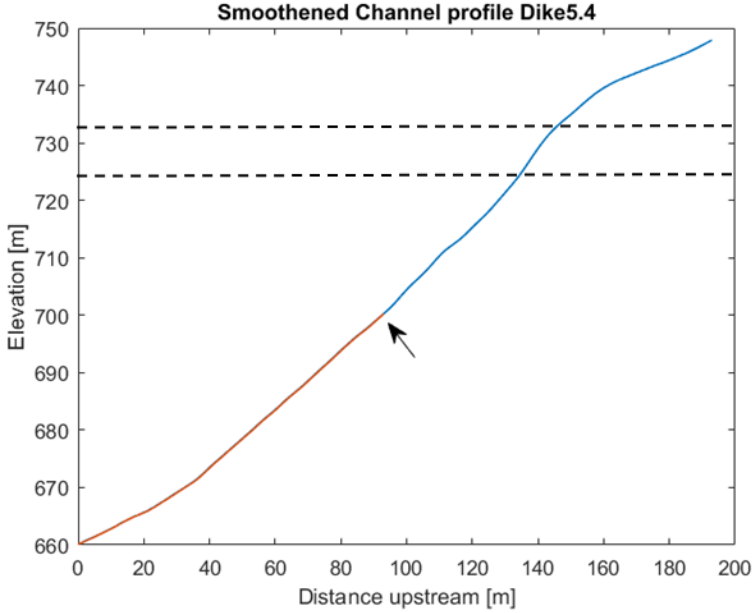
Smoothened Channel profile Dike5.4
Elevation [m]
750
740
730
720
710
700
690
680
670
660
0
20
40
60
80
100
120
140
160
180
200
Distance upstream [m]

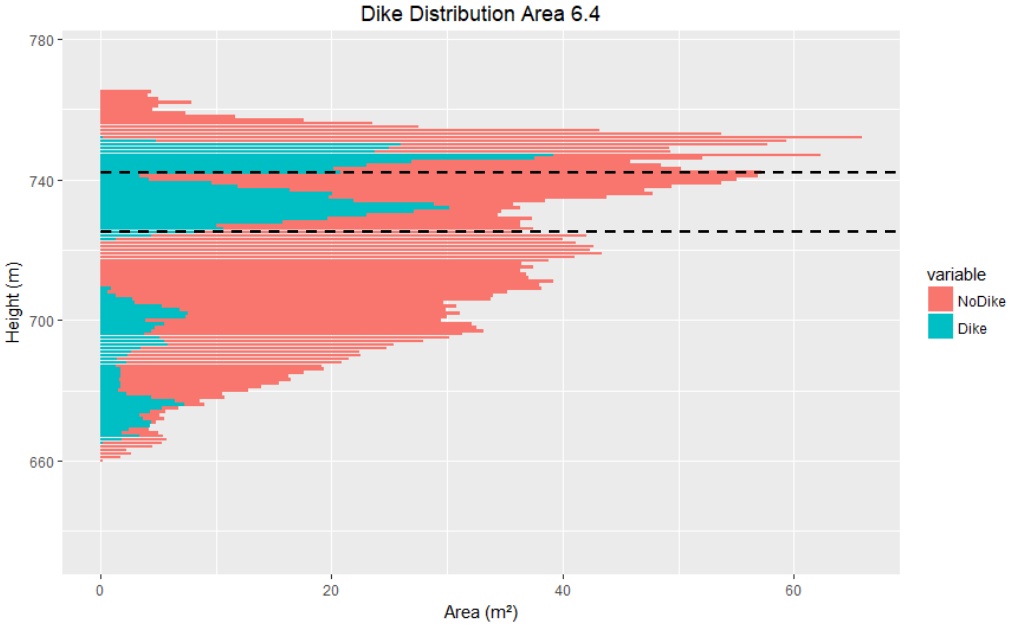
Dike Distribution Area 6.4
Height (m)
780
740
700
660
0
20
40
60
Area (m²)
variable
NoDike
Dike

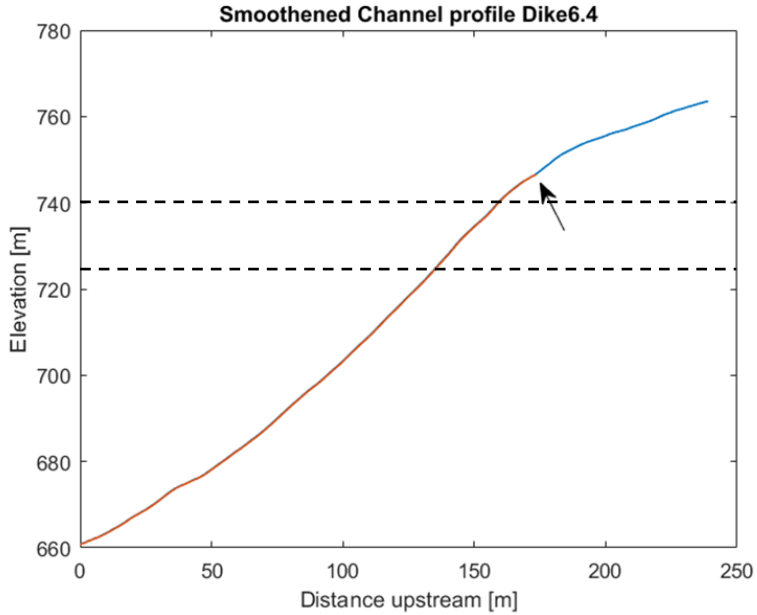
Smoothened Channel profile Dike6.4
Elevation [m]
780
760
740
720
700
680
660
0
50
100
150
200
250
Distance upstream [m]

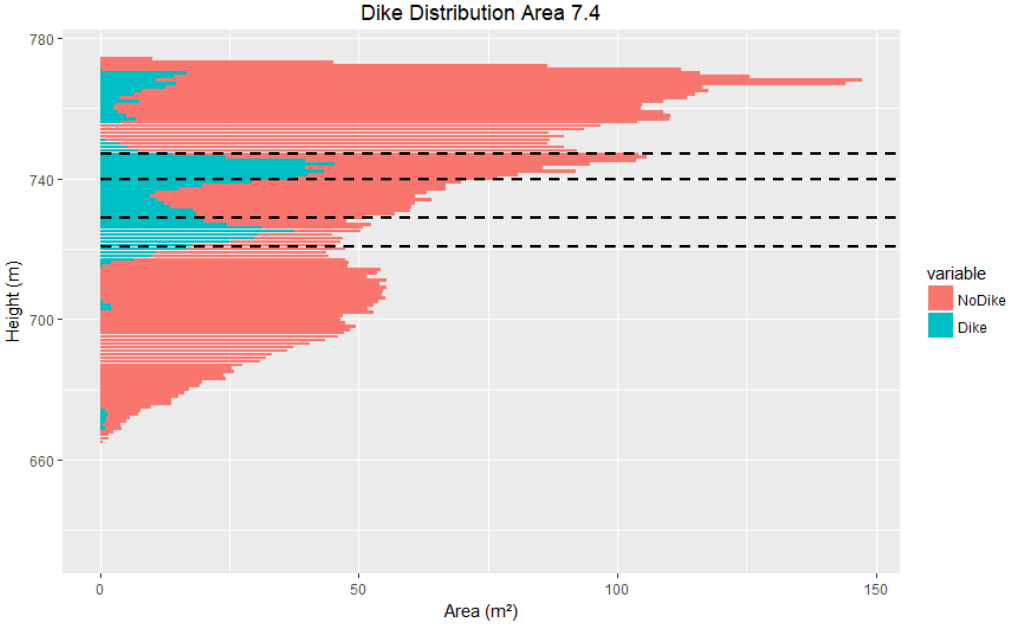
Dike Distribution Area 7.4
Height (m)
780
740
700
660
0
50
100
150
Area (m²)
variable
NoDike
Dike

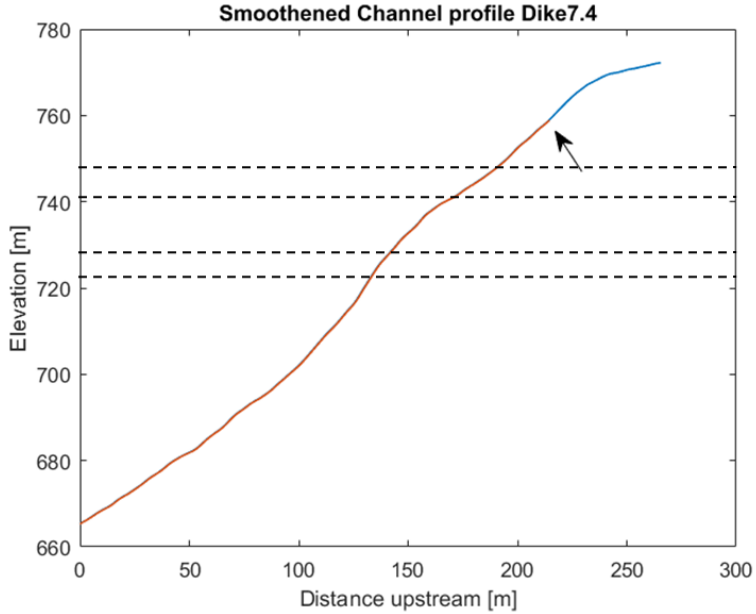
Smoothened Channel profile Dike7.4
Elevation [m]
780
760
740
720
700
680
660
0
50
100
150
200
250
300
Distance upstream [m]

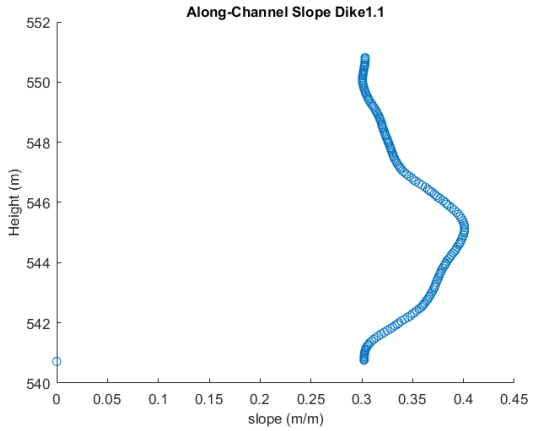

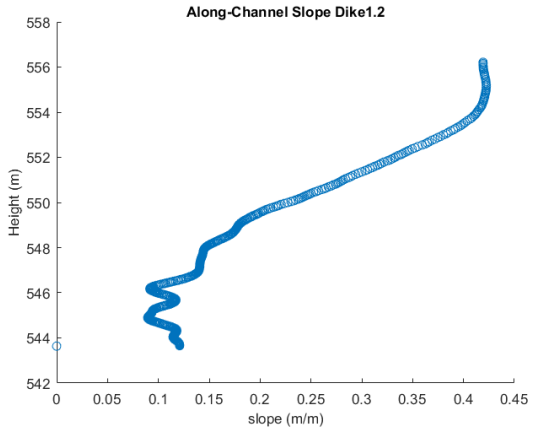

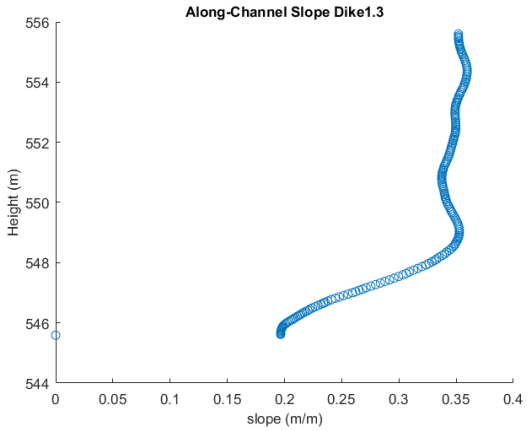

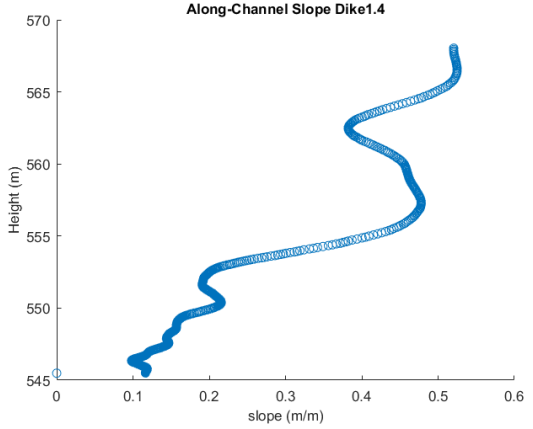

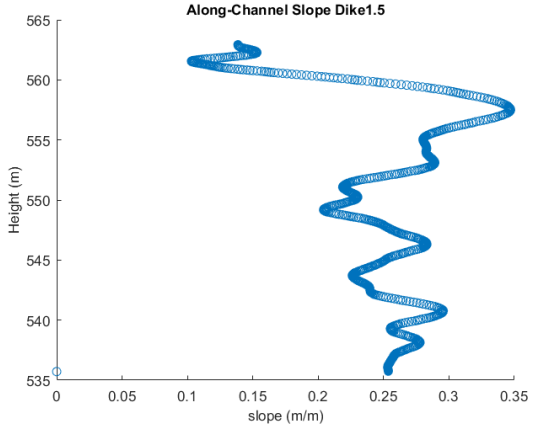

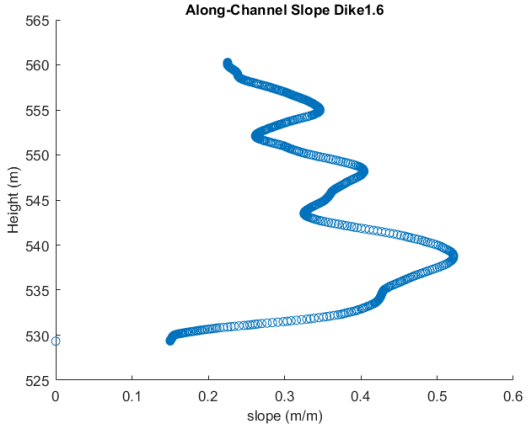

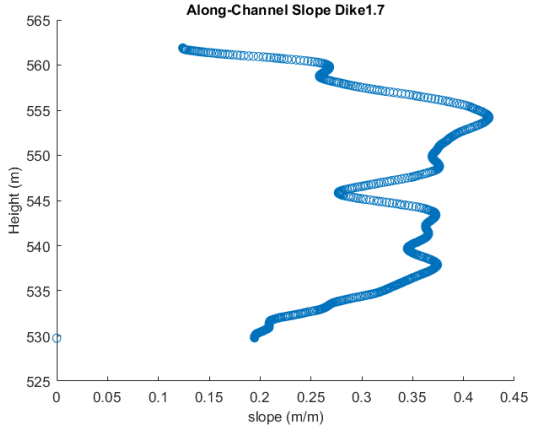

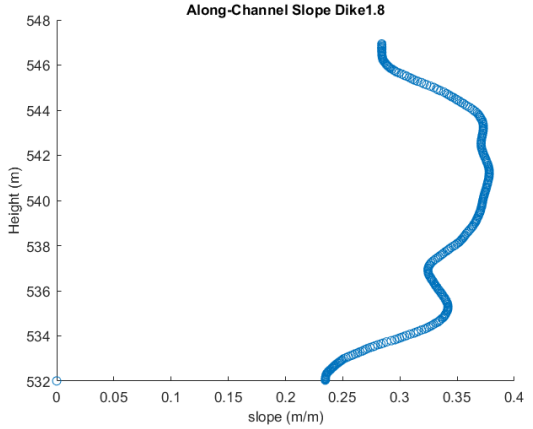

Slope along channel profiles for the catchments in study area 1. Compared to areas with dikes values on the x-axis are clearly lower.

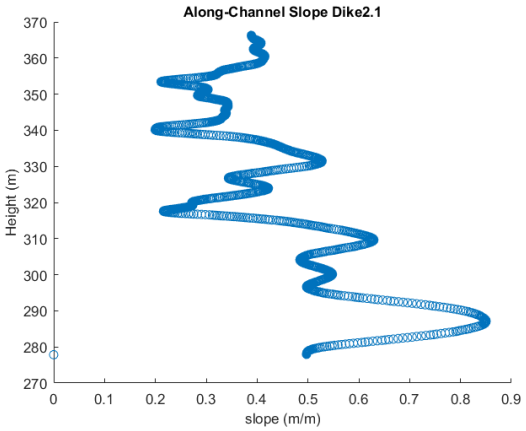

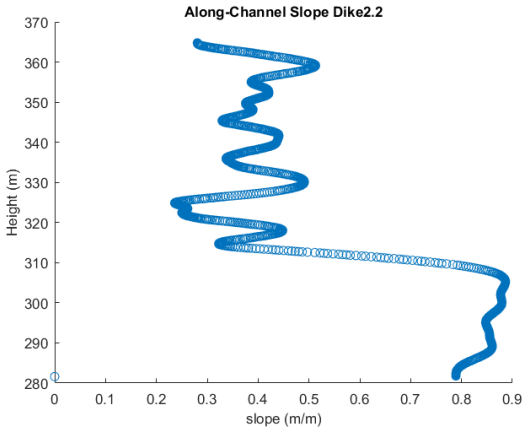

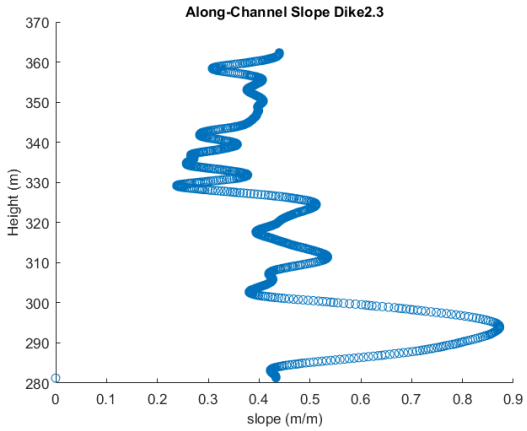

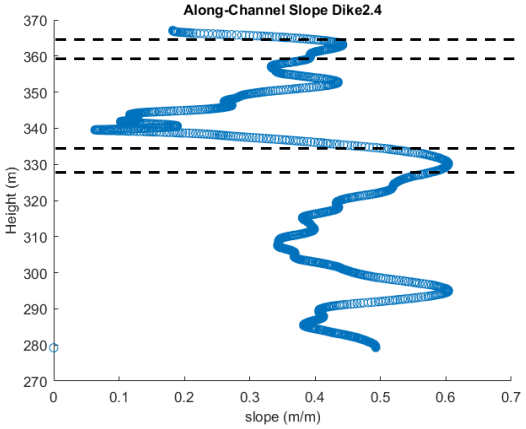

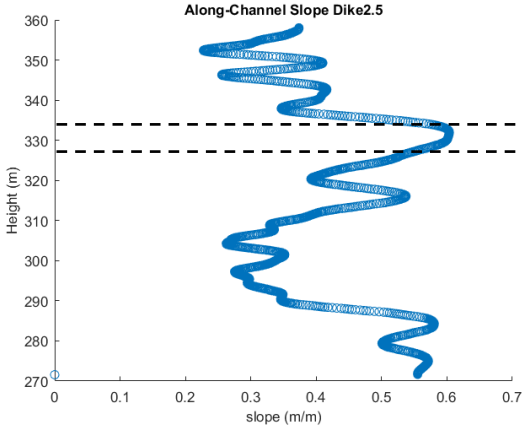

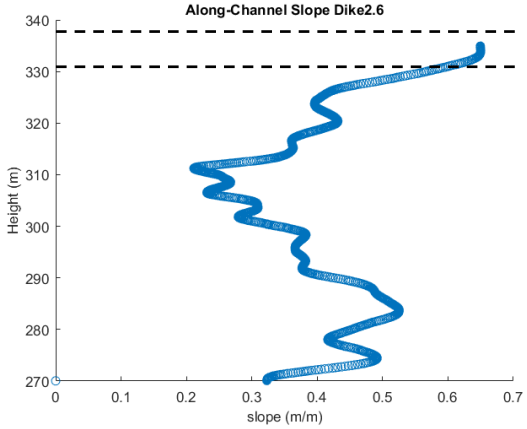

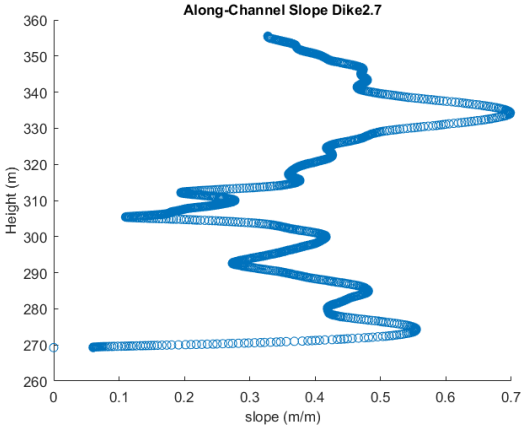

Slope along channel profiles for the catchments in study area 2. In between dotted lines are areas with dike intrusions. Slope values are clearly higher at these locations.

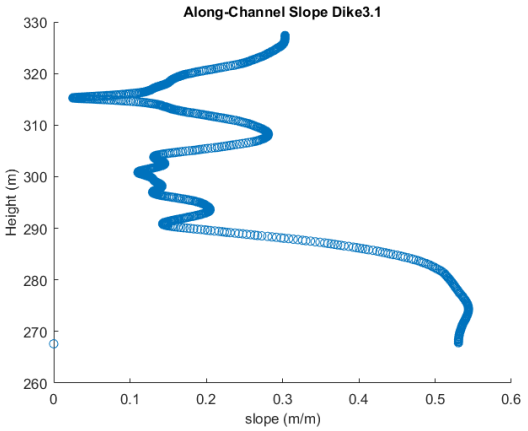

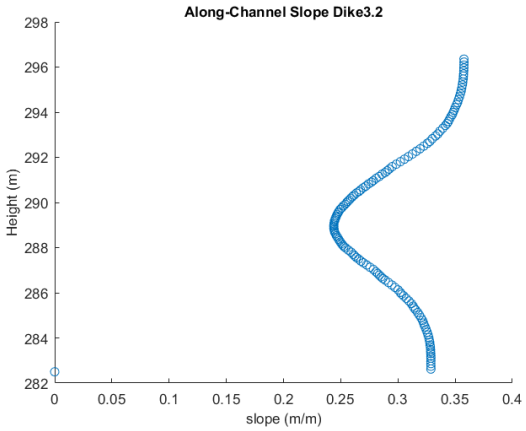

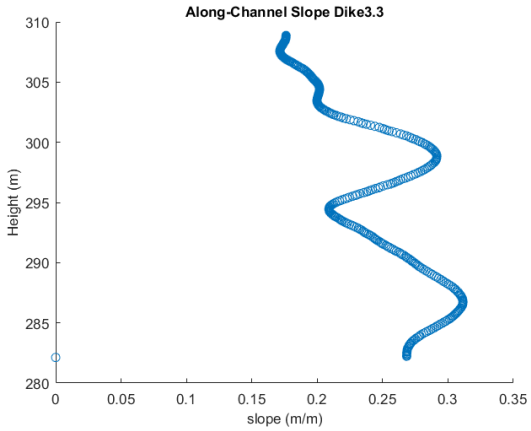

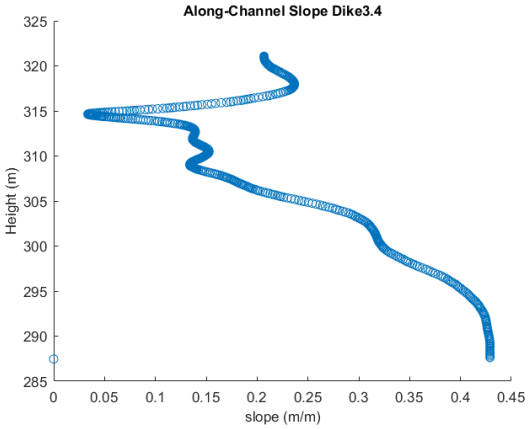

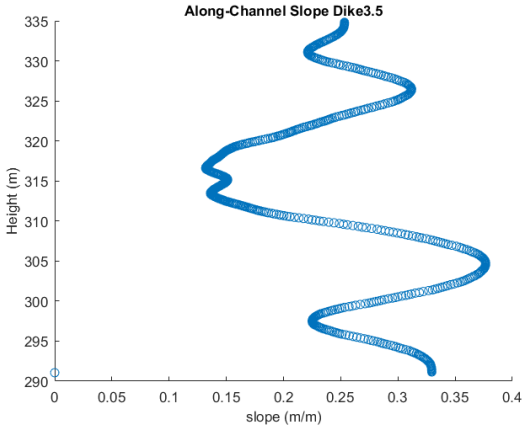

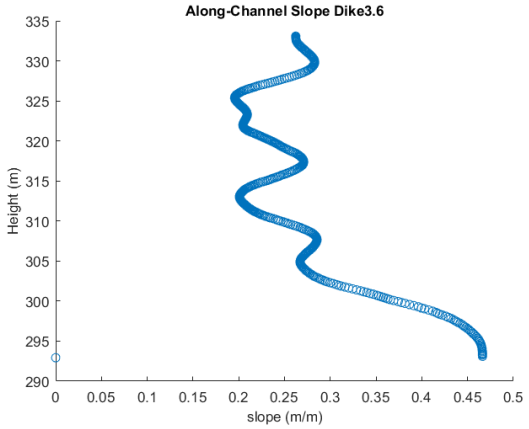

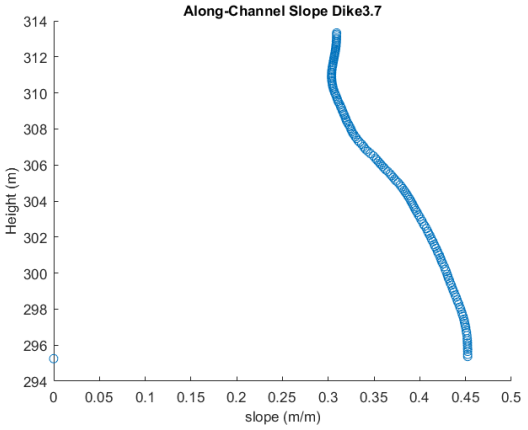

Slope along channel profiles for the catchments in study area 3. Compared to areas with dikes values on the x-axis are clearly lower.

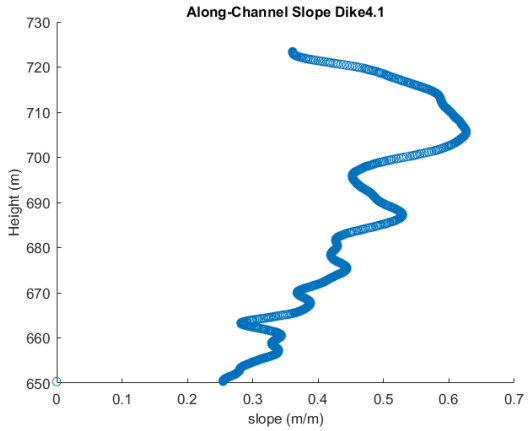

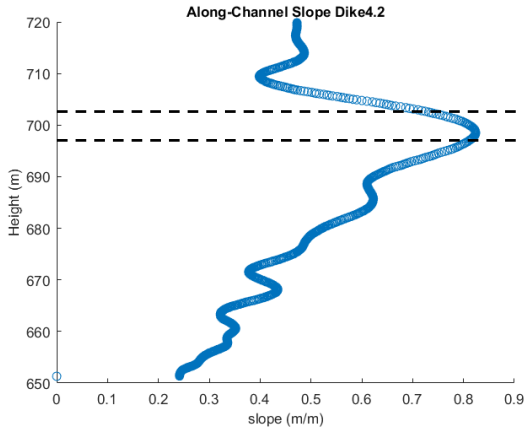

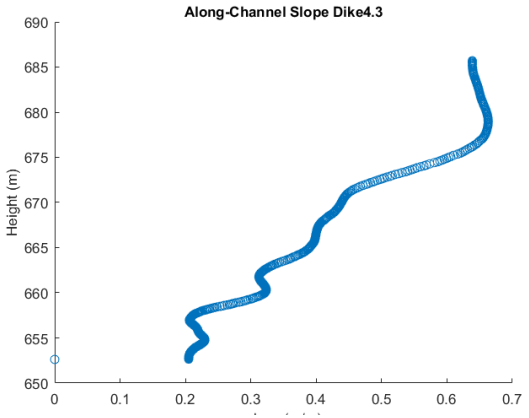

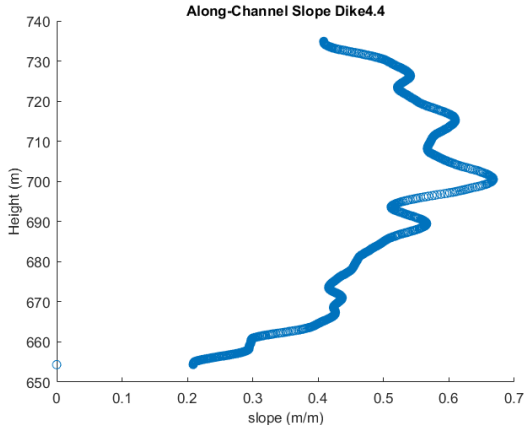

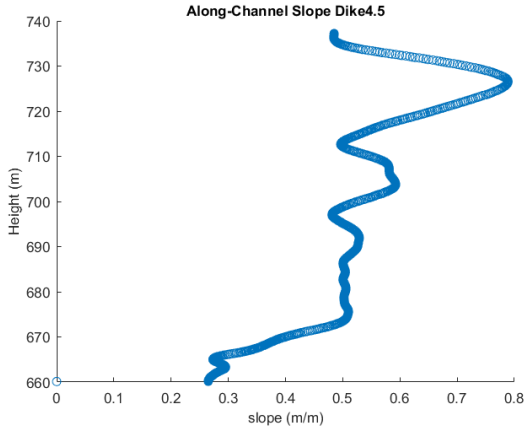

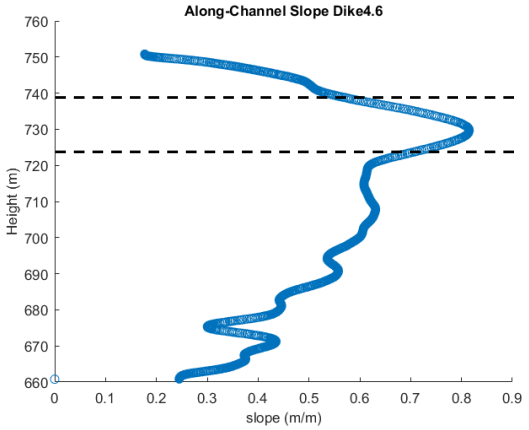

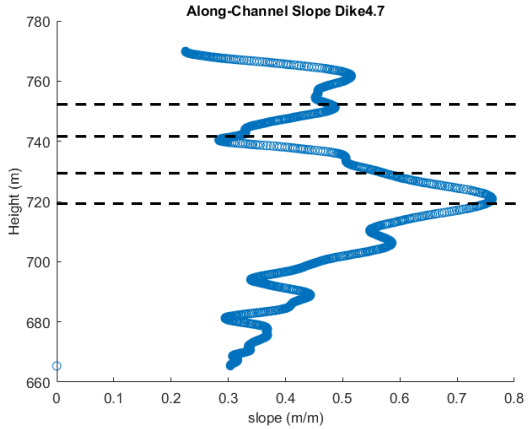

Slope along channel profiles for the catchments in study area 4. In between dotted lines are areas with dike intrusions. Slope values are clearly higher at these locations.

Appendix XIII – Histogram & QQ-plot Slope and k_{sn}

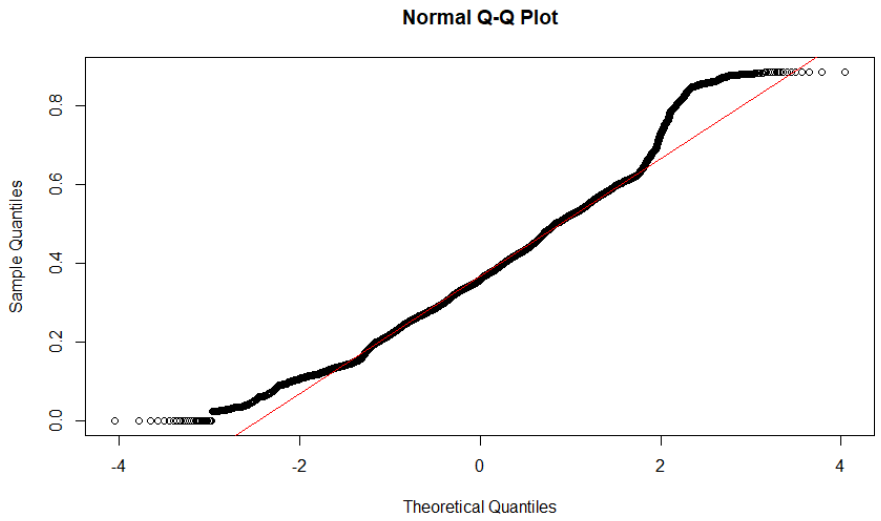

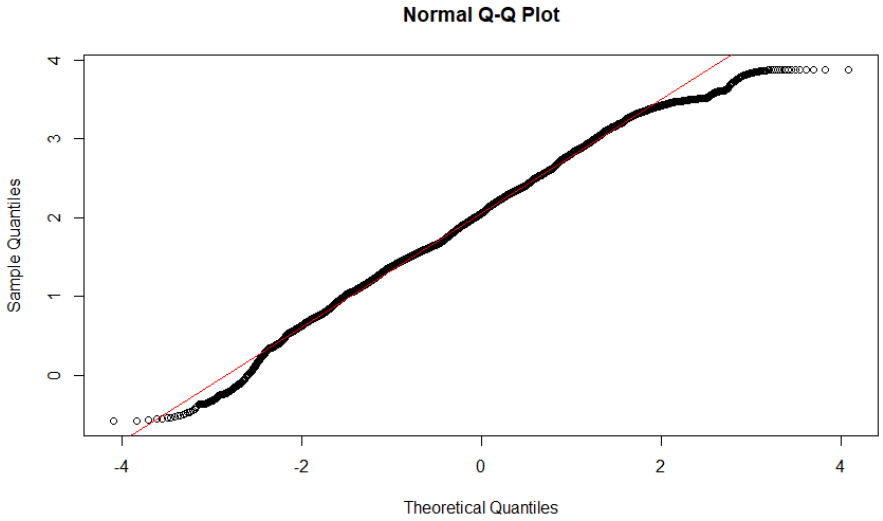

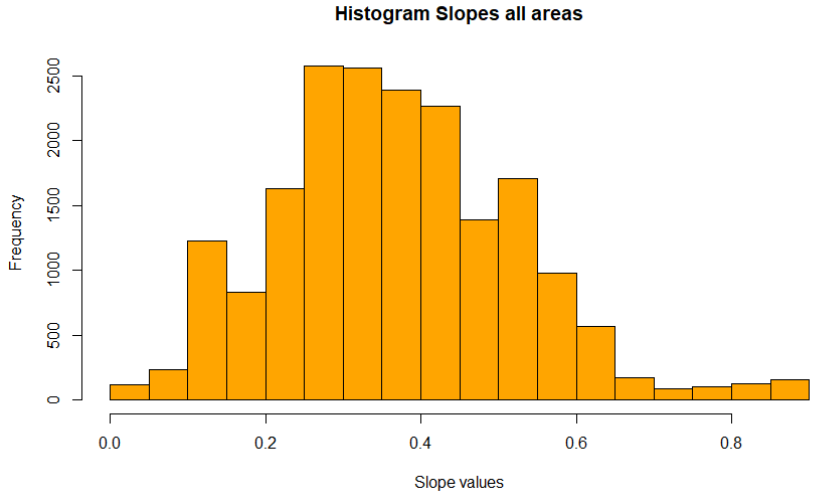

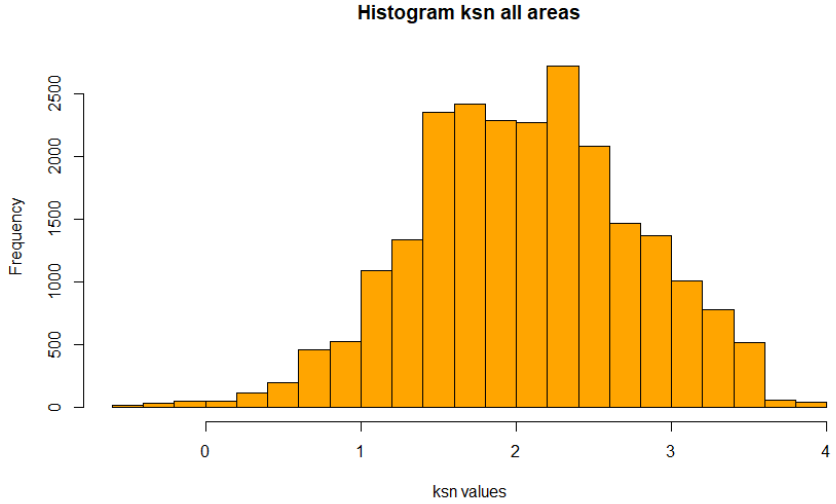

Appendix XIV – K_{sn}-values all areas on DEM